

Syntheses and Characterization of Biologically Active Gold Nanoparticles

Von der Fakultät für Mathematik, Informatik und Naturwissenschaften der
RWTH Aachen University zur Erlangung des akademischen Grades einer
Doktorin der Naturwissenschaften genehmigte Dissertation

vorgelegt von
Diplom-Chemikerin Annika Leifert
aus Münster

Berichter: Universitätsprofessor Dr. rer. nat. U. Simon
Universitätsprofessor Dr. rer. nat. W. Jahnen-Dechent

Tag der mündlichen Prüfung: 21.03.2012

Diese Dissertation ist auf den Internetseiten der Hochschulbibliothek online
verfügbar.

Meiner Familie.

Acknowledgments

I would like to thank my supervisor, Prof. Dr. rer. nat. Ulrich Simon, for giving me the opportunity to work on this very interesting topic, for many helpful and inspiring discussions and his great scientific support.

Further I would like to thank Prof. Dr. rer. nat. Willi Jahnen-Dechent for the excellent cooperation within the project, enabling that most cell tests described herein were performed in his group, and for the second assessment of my thesis.

It was a great pleasure to work together with Dr. rer. nat. Yu Pan-Bartneck, and I want to thank her for her hard work within the project.

I also would like to thank the other cooperation partners, Prof. Dr. rer. nat. Günter Schmid, Prof. Dr. rer. nat. Wolfgang Brandau and Prof. Dr. rer. nat. Wolfgang Wenzel, for interesting discussions during the project meetings and the altogether fruitful collaborations.

I am grateful for the help by Birgit Hahn concerning syntheses and STEM measurements.

Jan Timper also performed multitudinous STEM measurements and was always a very helpful colleague and good friend.

Further, I would like to thank the Simon group for the great time I had during my PhD thesis. Helpful and kind colleagues are so important for both scientific and personal well-being, and I appreciate that I could work together with them.

I thank my research students Michael Müller, Maryam Peymandar, Thorsten vom Stein, Dominik Schmitz, Michael Kather, Anna Clemens, and Katharina Wiemer, and Monika Krystof during her bachelor thesis, for their great work and that I could enjoy working with such motivated students.

I thank Prof. Dr. rer. nat. Paul Kögerler and Dr. rer. nat. Claire Besson for their help with the EPR measurements.

I am very thankful for the great support by Dr. rer. nat. Bryant Nelson and Dr. rer. nat. Elijah Petersen during my stay in Gaithersburg at the NIST, for the help with the GC/MS measurements and for conducting the LC/MS/MS measurements.

I thank Dr. rer. nat. Melanie Homberger and Dr. rer. nat. Corinna Kaulen for helpful discussions about NMR spectroscopy of gold nanoparticles, and Toni Gossen for performing the NMR measurements.

Furthermore I would like to thank Prof. Dr. rer. nat. Frank Haarmann and Oliver Pecher for performing the solid state NMR measurements and helpful discussions concerning the interpretation of the results.

I acknowledge the help of Dr. rer. nat. Olaf Scheel from Cytocentrics AG with the patch clamp experiments, very interesting discussions and the altogether nice time in Rostock.

I thank Dr. rer. nat. Klaus Beckerle for performing the DSC measurements.

Prof. Dr. rer. nat. Gerhard Müller-Newen is kindly acknowledged for the fluorescence microscopy experiments.

I would like to thank Ludwig Storck for performing the AAS measurements.

Further, I thank Brigitte Pütz for the MS measurements.

Last but not least I gratefully acknowledge corrections of the manuscript by Anna Clemens, Astrid Beyer, Dr. rer. nat. Corinna Kaulen and Oliver Pecher.

Contents

1	Introduction	1
2	Basic Knowledge	5
2.1	Gold Nanoparticles	5
2.1.1	Definitions and Nomenclature	5
2.1.2	Physical Properties	6
2.1.2.1	Electronic Structure of AuNPs	6
2.1.2.2	Optical Properties	7
2.1.2.3	Catalytic Activity of AuNPs	7
2.1.3	Syntheses	8
2.1.4	Ligands and Functionalization	10
2.1.5	Separation from Possible Impurities	12
2.2	Characterization	14
2.2.1	UV/Vis Spectroscopy	14
2.2.2	Electron Microscopy	15
2.2.3	X-ray Diffractometry	16
2.2.4	DLS and ζ Potential Measurement	17
2.2.5	Elemental Analysis	18
2.2.6	Nuclear Magnetic Resonance Spectroscopy	19
2.2.7	Infrared Spectroscopy	19
2.2.8	Fluorescence Spectroscopy	20
2.2.9	X-ray Photoelectron Spectroscopy	20
2.2.10	Electron Paramagnetic Resonance Spectroscopy	21
2.3	Biological Effects of Gold Nanoparticles	21
2.3.1	Methods	22
2.3.2	Uptake Mechanisms	23
2.3.3	Cytotoxicity	24
2.3.4	Oxidative Stress & Reactive Oxygen Species	26
2.3.5	Genotoxicity	27
2.3.6	Ion Channels & Patch Clamp Technique	28

2.4	Modification of AuNPs for Biomedical Applications	29
2.4.1	Targeting with Bombesin	30
2.4.2	Labeling with Fluorophores/Aminofluorescein	31
3	Results and Discussion	33
3.1	Syntheses of AuNPs	33
3.2	Size-Dependent Cytotoxicity	34
3.3	Ligand-Dependent Cytotoxicity: Phosphine vs. Thiol	39
3.4	Cellular Response Reactions	42
3.4.1	Necrosis vs. Apoptosis	42
3.4.2	Gene Regulation	44
3.4.3	Oxidative Stress	45
3.5	EPR Spectroscopy with AuNPs	50
3.6	Genotoxicity Studies	55
3.7	The Au(I) Question	61
3.8	Patch Clamp Experiments	70
3.9	Other Monophosphine Ligands	80
3.10	Diphosphine Ligands	85
3.11	Labeling Au1.4 with (Lys ³)-bombesin	98
3.12	Labeling Au1.4 with 5-Aminofluorescein	107
4	Summary and Outlook	113
5	Experimental Part	119
5.1	Chemicals and Solvents	119
5.1.1	Precursor Chemicals	119
5.1.2	Commercially Purchased or Provided AuNPs	121
5.2	General Comments on Preparative Work	122
5.3	General Comments on Analytics	122
5.3.1	UV/Vis Spectroscopy	122
5.3.2	Scanning Transmission Electron Microscopy (STEM)	122
5.3.3	Scanning Electron Microscopy (SEM) and Energy-Dispersive X-Ray Spectroscopy (EDX)	123
5.3.4	Elemental Analysis (EA)	123
5.3.5	Atomic Absorption Spectroscopy (AAS)	123
5.3.6	Electron Paramagnetic Resonance (EPR)	124
5.3.7	Gas chromatography / mass spectrometry (GC/MS)	124
5.3.8	Nuclear Magnetic Resonance Spectroscopy (NMR)	124

5.3.8.1	Solution NMR	124
5.3.8.2	Solid State NMR	124
5.3.9	Patch Clamp Experiments	125
5.3.10	Differential Scanning Calorimetry (DSC)	125
5.3.11	Dynamic light scattering (DLS) and ζ potential measurements	126
5.3.12	Mass Spectrometry (MS)	126
5.3.13	Infrared Spectroscopy (IR)	126
5.3.14	Fluorescence Spectroscopy	126
5.3.15	Cell Experiments	126
5.4	Syntheses	127
5.4.1	Ligands	127
5.4.1.1	TPPMS	127
5.4.1.2	Diphenylphosphine (precursor)	127
5.4.1.3	<i>p</i> TPPMA, <i>m</i> TPPMA	127
5.4.1.4	TPPMCMA	128
5.4.1.5	TPPMC	128
5.4.1.6	DPPETS	128
5.4.1.7	DPPPTS, DPPBTS	129
5.4.2	Gold Nanoparticles	129
5.4.2.1	Au1.4TPP	129
5.4.2.2	Au1.4MS	130
5.4.2.3	Au5.6MS	130
5.4.2.4	Au15MS	131
5.4.2.5	Au1.1GSH, Au1.5GSH	131
5.4.2.6	Au1.4GSH by Ligand Exchange	132
5.4.2.7	Au1.4TS	132
5.4.2.8	Au1.4TPPMCMA	132
5.4.2.9	Au1.4TPPMC	133
5.4.2.10	Au1.4DPPETS	133
5.4.2.11	Au1.4DPPPTS	133
5.4.2.12	Au1.4DPPBTS	134
5.4.2.13	Au13DPPETS	134
5.4.2.14	Au11DPPPTS	134
5.4.2.15	Au12DPPBTS	134
5.4.2.16	Degradation of Diphosphine-Stab. AuNPs with KCN	135
5.4.2.17	DTT Exchange with Au1.4DPPBTS	135
5.4.2.18	Au1.4MS/MC	135

5.4.2.19	Au1.4MS/MC-(Lys ³)-bombesin	136
5.4.2.20	Au1.4MC-bombesin	136
5.4.2.21	DTT Exchange with Au1.4MC-bombesin	136
5.4.2.22	Au1.4MS/MC-Aminofluorescein	136
5.5	Measurements with AuNPs	137
5.5.1	EPR Measurements	137
5.5.2	GC/MS Measurements	137
5.5.3	NMR and EDX Experiments	138
5.5.3.1	Au1.4MS + TPPMS	138
5.5.3.2	Solid State NMR of Au1.4MS	139
5.5.3.3	Dialysis and EDX of Au1.4MS	139
5.5.4	Patch Clamp Experiments	139
5.5.5	Cell Experiments	141
6	Abbreviations	143
	Bibliography	147
	List of Figures	159
	List of Tables	163
	Curriculum Vitae	165

1 Introduction

Nanoscience, the investigation of objects in the nanometer regime, has greatly emerged within the last decades, due to new synthesis routes to nanomaterials and also further developed analytical tools to characterize them. Along with this, the field of nanotechnology where nanomaterials with new, size-dependent properties are brought to application is growing steadily.[1]

Among these, diverse applications in the biomedical field are envisioned.[2, 3] Nanomaterials might help to answer fundamental questions in cell biology to understand molecular mechanisms of natural nanostructures.[4] They might also find their way to applications in medicinal diagnosis, imaging and therapy techniques, the latter both in the form of drug carrier systems or as active compounds in magnetically or photometrically based thermotherapy.

Furthermore, the enhanced production and use of nanomaterials in other than biomedical applications such as electronic devices and in materials science leads to increased potential exposition to public and the environment during production, usage and even after disposal.[5]

For these reasons, the investigation of biological effects of nanomaterials is of great importance. There is already a huge number of nanomaterials of different materials, sizes and shapes available, and this number is still growing, yet data of biological effects are sparse and far from being fully understood.[6]

Based on the information gained so far, there are some first general assumptions. Firstly, there are size-dependent effects, i. e. a non-toxic bulk material might be toxic in the nanometer size range. Nanomaterials with dimensions of smaller than approximately 2nm are in the same size regime as cellular structures and can thus potentially mimic biologically active compounds, such as peptide hormones, cytokines or antigens, thereby causing adverse

effects to living organisms. Secondly, these phenomena are not only determined by size, but the chemical composition, which might be crucial as well.[7] It would therefore be important to conduct systematic investigations concerning these parameters to potentially find some fundamental mechanisms and conclusions about the manifold interactions of nanomaterials with biological entities.

Exemplary for unexpected toxic behavior are gold nanoparticles (AuNPs) for which conflicting data were presented. While in its bulk form being biologically inert, small phosphine-stabilized AuNPs of the chemical formula $\text{Au}_{55}[(\text{C}_6\text{H}_5)_2\text{P}(\text{C}_6\text{H}_4\text{SO}_3\text{Na})]_{12}\text{Cl}_6$ were found to be highly cytotoxic in different cell lines. A potential mechanism based on an interaction of these AuNPs with the major groove of DNA was proposed, supported by molecular dynamics simulations.[8, 9]

Pernodet et al. reported of 14 nm sized citrate-stabilized AuNPs that induced a disturbed actin structure in human dermal fibroblasts, accompanied by a decrease in cell proliferation, adhesion, and motility.[10] On the other hand it was found that 18 nm sized AuNPs, stabilized by either citrate or biotin, do not cause acute cytotoxicity in K562 leukemia cells despite being taken up in cells.[11]

Against this background, a DFG funded cooperation project of the groups Simon and Jahnen-Dechent (Aachen), Schmid and Brandau (Duisburg-Essen) and, in a second funding phase, Wenzel (Karlsruhe), was initiated concerning the "Control of the physiological impact of noble metal nanoparticles by size and chemical modification", including a project part for "Size-selective synthesis of new, water-soluble noble metal nanoparticles" that was the basis for this work.

In this, the synthesis and characterization of a series of ligand-stabilized water-soluble spherical AuNPs was sought by modifying known synthesis routes as well as generating new ones for systematic cytotoxicity studies. The parameters of variation include AuNP size as well as the gold-ligand stability and the outer functional groups of ligands, thus the introduction of new, AuNP-stabilizing ligands (see fig. 1.1). While this work focuses on synthesis and chemical characterization of the AuNPs, the cell experiments were conducted by Dr. Yu Pan-Bartneck and are described in detail in the respective dissertation.[12]

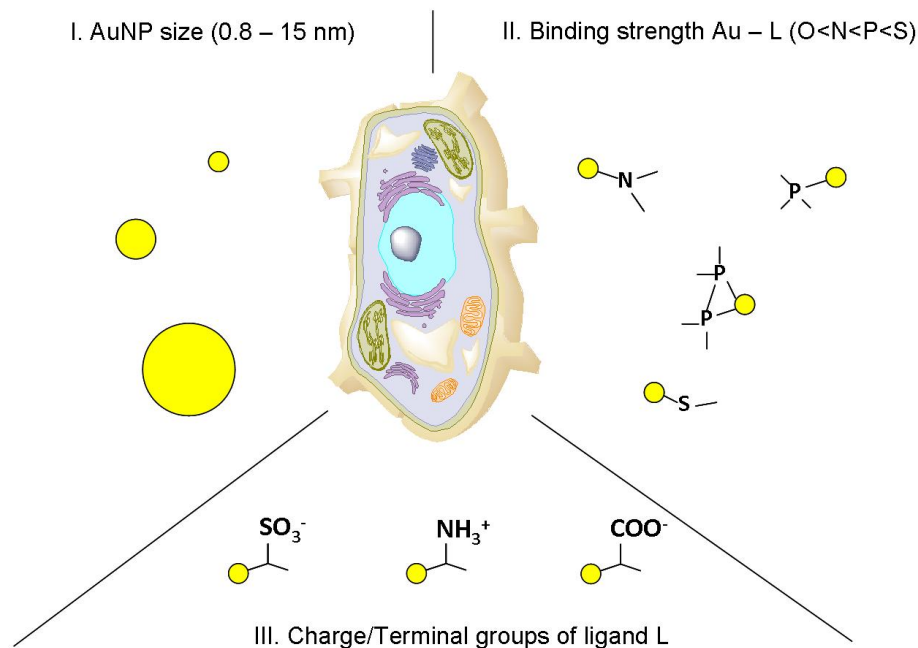


Figure 1.1: Control parameters for the cytotoxicity evaluation of AuNPs.

Further, the subjacent mechanisms of biological activity of AuNPs were investigated by a variety of methods. The generation of reactive oxygen species (ROS) and resulting oxidative stress has been related to nanomaterial toxicity before[13] and was therefore investigated in detail. This was, amongst other tests, done by EPR spectroscopy.

Besides cytotoxicity evaluation, genotoxicity was also examined by sophisticated GC/MS measurements in cooperation with Dr. Bryant Nelson at the National Institute of Standards and Technology (NIST, Gaithersburg, MD, USA).

An approach to identify the toxicity mechanism of AuNPs was an investigation concerning possibly released Au(I) species, and the analysis of the equilibrium between AuNPs, a Au(I) complex and the phosphine ligand 3-(diphenylphosphino)benzenesulfonic acid sodium salt (TPPMS) by ^{31}P -NMR spectroscopy.

As another potential biological effect, the interaction of AuNPs with ion channel expressing cells was determined by electrophysiological patch clamp experiments. This was done at CytoCentrics AG in Rostock. Parts of these results are already described in the dissertation of Dr. Yu Pan-Bartneck.[12]

Besides these mechanistic investigations, a species with application potential in cancer therapy was synthesized. This was sought by functionalization of toxic AuNPs with (Lys³)-bombesin, an oligopeptide, to induce cancer cell specificity for a conceivable application as an anticancer drug. By a similar route it was also attempted to functionalize AuNPs with a fluorophore as a probe for potential ligand release in contact to cells.

2 Basic Knowledge

2.1 Gold Nanoparticles

2.1.1 Definitions and Nomenclature

The term "nanotechnology" describes the field of developments in which size-dependent properties of materials in the nanometer regime play a dominant role, and where these properties can be used to generate new techniques and devices.[14] The materials can include nanoparticles with dimensions of less than 100 nm as well as patterned surfaces and more sophisticated assemblies. Nanotechnology is an interdisciplinary field with contributions from physics, chemistry, biology, materials science, medicine and other disciplines. A typical example of a nanomaterial with distinct properties and a broad variety of potential and already realized applications are gold nanoparticles.[15]

Gold nanoparticles (AuNPs) are spherical particles with a diameter of less than 100 nm and, in solution, typically consist of a gold metal core and a stabilizing ligand shell that prevents the particles either sterically or electrostatically from aggregation.[16] The term "nanoparticles" (NPs) includes clusters as well as colloids. The term "cluster" is used for very small NPs with a well defined number of metal atoms, i.e. molecular species. The term "colloid" describes larger particles. Hence, colloidal materials do not have a precise molecular formula any more and are not monodisperse. However, particles with a size distribution of less than 10 % deviation are typically regarded as systems with sufficiently low polydispersity, and it is reasonable to describe such samples by their mean diameter. In this work, the term "ligand" is used for organic molecules that have the ability to bind to NPs *via* electron donating functional groups. For AuNPs, the most commonly used

molecules for this purpose are thiols that form a thiolate bond on the gold surface. Other molecules are for example phosphines, amines, carboxylates and polymers. For a more detailed discussion about ligands for AuNPs, see chapter 2.1.4.

The nomenclature for the AuNPs used in this work includes the element, the mean diameter of the particles in nm and an abbreviation for the ligand. For example, Au1.4MS is a NP of gold with a mean diameter of 1.4 nm and a ligand shell of TPPMS (MS).

2.1.2 Physical Properties

This work focuses on biological effects of AuNPs. However, to fully understand the discussion of the observed effects and the proposed mechanisms, an introduction into the main size-related physical properties of AuNPs is requisite.

2.1.2.1 Electronic Structure of AuNPs

As metal NPs have atom numbers between molecular species and the bulk material, their electronic structure differs from these both boundary states and thus they have several unique size-dependent properties.[16] Small gold clusters exhibit distinct energy gaps in their electronic structure, whereas for larger colloids no energy gaps exist in the 6sp band. A cluster can be described as a zero-dimensional entity in which the electrons occupy discrete energy levels and quantum mechanical properties become dominant.[17] The valence electrons in clusters are therefore in quantized states, but also highly delocalized within the cluster.[18] With increasing NP size, the orbital density increases and quasi-continuous electron bands as in the bulk state arise. These size-dependent electronic states have an impact on intrinsic features such as optical or electronic properties and on application relevant characteristics, for example in metal NP catalysis (see chapter 2.1.2.3).

2.1.2.2 Optical Properties

In small gold clusters with energetically separated orbitals, discrete electron excitations occur. UV/Vis spectra show narrow peaks in the short-wave length range, reflecting such single electron excitations, as for example shown for the cluster $[\text{Au}_9[(\text{C}_6\text{H}_5)_3\text{P}]_8](\text{NO}_3)_3$.^[19] AuNPs above a size of approximately 3 nm show a plasmon resonance peak in their UV/Vis spectra. This phenomenon arises from the electron gas of delocalized 6s electrons of the individual particles. The plasmons of the electron gas are excited with energies in the range of visible light. In the case of resonance of the electromagnetic wave of light and the plasmon frequency, the latter is stimulated to oscillate and the light is absorbed. A full theoretical description of this was already given by Mie in 1908.^[20]

The plasmon oscillation frequency depends on the restoring force between electrons and nuclei. The UV/Vis spectrum of a certain AuNP species therefore depends e. g. on the size and shape of the particles and on the environment (i. e. the ligand shell and the solvent). This can be used for AuNP analysis (see 2.2.1).^[21]

AuNPs can also display fluorescence. This phenomenon is clearly dependent from size and ligand functionalization. Huang and Murray investigated tiopronin-stabilized AuNPs with a diameter of 1.8 nm and found fluorescence at 700-800 nm. They hypothesize a mechanism of interband transitions between the filled $5d^{10}$ band and $6(sp)^1$ conduction band.^[22]

2.1.2.3 Catalytic Activity of AuNPs

The electronic structure also has an impact on the catalytic activity of AuNPs. In general, NPs often have high catalytic activity due to their large number of surface atoms relative to their mass. Surface atoms are energetically in an activated state and can catalyze reactions of molecules that adsorb on the surface. For example, O_2 can be activated by AuNPs through partial electron transfer from the gold clusters to the antibonding π^* orbital of O_2 and generation of highly active peroxo-like species.^[23] Thus, the catalysis of oxidation reactions by AuNPs has recently been investigated by different groups.^[24, 25]

For small gold clusters, it was found that the activity varies with changes in the gold atom number, already with the alteration of single atoms.^[26] The observed size dependence

is, on the one hand, related to the surface to volume ratio and the enlarged number of energetically activated surface atoms. The energy levels of gold clusters, which are very sensitive to changes in single atom numbers, are on the other hand of great importance as well, as they influence the ability to activate adsorbed molecules. The activation of adsorbed substrates is a key issue in NP catalysis.

AuNPs on supporting metal oxides such as TiO_2 or MgO show significantly enhanced activity and selectivity.[27] This is explained by charge transfer between gold clusters and metal oxide support. Ligands on the other hand may hinder catalytic reactivity of AuNPs as they shield the surface against adsorption of the substrate. In some examples however, certain ligands such as poly(vinylpyrrolidone) (PVP) can enhance catalytic activity. A mechanism similar to the one proposed for support materials is expected.[28]

Turner et al. reported high activity and selectivity for the oxidation of styrene to benzaldehyde by $\text{Au}_{55}[(\text{C}_6\text{H}_5)_3\text{P}]_{12}\text{Cl}_6$ on different support materials at relatively mild conditions of 100°C in toluene. AuNPs of larger sizes were less active to completely inactive.[29] The ability of AuNPs to catalyze oxidation reactions will be relevant in the following discussion of AuNP cytotoxicity.

AuNPs can also catalyze other reactions. For example, the hydrogenation of α , β -unsaturated ketones and aldehydes by a $\text{Au}_{25}(\text{SR})_{18}$ cluster was published. Here, a catalytic cycle was proposed, in which the active sites on the Au_{25} structure could be spatially located.[30]

2.1.3 Syntheses

Metal NPs can generally be synthesized either in gas or in solution phase. In this work, only wet chemical synthesis routes are discussed. Gas phase syntheses are described elsewhere.[31] Due to the great interest of AuNPs for applications in different fields, there is a huge and still increasing number of different synthesis routes.[15] Some of these are exemplary described here in more detail.

The bottom-up synthesis of AuNPs is typically conducted by the reduction of a dissolved Au(III) salt or Au(I) complex to Au(0) in presence of a ligand. Typical reducing agents

are for example trisodium citrate, $\text{Na}_3\text{C}_6\text{H}_5\text{O}_7$, sodium borohydride, NaBH_4 , and diborane, B_2H_6 .

One of the most commonly used synthesis routes is the one of Turkevitch et al. from 1951.[32] Here, $[\text{AuCl}_4]^-$ is reduced by trisodium citrate in boiling water. The citrate which is added in excess also acts as ligand for the formed AuNPs. Depending on the synthesis conditions, i.e. the concentrations of the components as well as temperature and reaction time, different AuNP sizes in the range from 15 nm up to 150 nm can be generated.

Very small clusters with the chemical formula $\text{Au}_{55}[(\text{C}_6\text{H}_5)_3\text{P}]_{12}\text{Cl}_6$ and a gold core diameter of 1.4 nm can be synthesized by the method developed by Schmid et al. in 1981.[33] The Au(I) complex $[(\text{C}_6\text{H}_5)_3\text{P}]\text{AuCl}$ is dissolved in benzene and reduced with diborane at moderate heat.

Schmid et al. also developed a method to transfer these AuNPs into the aqueous phase.[34] For this purpose, a dichloromethane dispersion of the clusters is covered with an aqueous solution of TPPMS and stirred at room temperature for three days. An equilibrium of AuNPs in both phases is reached after this time. To improve the yield of water soluble clusters, the volume of the water phase is larger and TPPMS is added in excess. Furthermore, the ability to stabilize AuNPs is slightly higher for TPPMS compared to triphenylphosphine. They are not only stabilized by steric repulsion but also by an electrostatic stabilization of the charged TPPMS which has a negative sulfonate group when it is in solution. This further shifts the equilibrium.

Another break-through in AuNP synthesis was achieved in 1994 when Brust et al. developed the so-called Brust-Schiffrin synthesis.[35] In this two-phase system, HAuCl_4 is dissolved in H_2O , covered with an organic solvent (e.g. toluene) containing an alkylthiol, and reduced with an aqueous solution of sodium borohydride. AuNPs with sizes between 1.5 and 5.2 nm with different alkylthiol ligands were obtained. One year later, they expanded this route to a one-phase method by using methanol as solvent for all compounds.[36]

Leff et al. described a synthesis route to amine-stabilized AuNPs in a size range from 2.5 to 7.0 nm, depending on the synthesis conditions.[37] As amines are weakly binding ligands, these AuNPs are of special interest for subsequent ligand exchange reactions with more strongly binding ligands.

An approach to thiol-stabilized, water soluble AuNPs was performed by Whetten et al. and refined by Negishi et al..[38, 39] HAuCl_4 is reduced by sodium borohydride in the presence of glutathione, a biogenic tripeptide consisting of L-cysteine, L-glutamic acid and glycine. The resulting AuNPs have a mean diameter of approximately 1 nm.

2.1.4 Ligands and Functionalization

AuNPs need a stabilizing surfactant shell to prevent them from aggregation.[40] Molecules which are electron donors can act as ligands for AuNPs. The interaction between ligand and AuNP surface depends on the functional group which binds to the particle and ranges from coordinative chemisorption of strong ligands to electrostatic attraction of weaker ones. The binding strength has influence on several properties of the particles, the most prominent one being the AuNP stability.

AuNP stability in media further depends on the character of the end group (the part of the ligand molecule that points away from the particle surface). The stabilization is achieved either by steric (e.g. alkylthiols) or by electrostatic repulsion (e.g. phosphine sulfonates). The nature of the ligand not only determines the AuNP stabilization, but also influences their properties, such as solubility in apolar or polar solvents and the ζ potential. With respect to biological effects of AuNPs, it is reasonable to expect the ligand shell to play a crucial role, as this is the first entity the cell gets in contact with.

Thiols have the highest affinity to gold and are therefore the most frequently used class of ligands. For self-assembled monolayers (SAM) consisting of thiols on a flat gold surface, a binding energy of approximately 200 kJ/mol ($\cong 2.07$ eV) was determined.[41] However, this value may be different for AuNPs as the surface of NPs differs from a plain surface because of its curvature and the resulting edge and vertex atoms. Other sulfur containing molecules are e.g. disulfides and thioethers, both forming considerably weaker bonds towards AuNPs.[42, 43]

Phosphines are another class of widely used AuNP ligands. Compared to thiols, the binding energy is lower, as DFT calculations on Au_{38} and Au_{39} clusters showed. Here, binding energies of 0.93 eV for the $\text{Au}-\text{PH}_3$ bond compared to 2.45 eV for $\text{Au}-\text{SCH}_3$ were found.[44]

Typically, aryl phosphines like triphenyl phosphine (TPP) and its derivatives are used, as their phenyl rings provide high AuNP stability due to sterical bulkiness as well as oxidation resistance of the phosphine itself.

Amines, such as alkylamines or the amino acid lysine, have also been used as ligands.[45] Compared to thiols and phosphines, their affinity is only moderate, but stable AuNP dispersions can be obtained.

Carboxylates like trisodium citrate can also act as AuNP ligands. As they are mainly electrostatically bound to the surface, the stability strongly depends on factors such as salt concentration and pH of the solution. It is not possible to dry and redisperse such AuNPs. Dendrimers and polymers such as PVP and PEG are also used as ligands to stabilize AuNPs. Such AuNPs are often synthesized by reducing a gold salt in presence of the respective polymer, so that the polymer matrix determines the particle growth.[15]

Furthermore, a chelate effect can play a role in ligand binding. Multivalent ligands show higher affinity to NP surfaces. This is based on a higher probability of recombination if one functional group desorbed from the nanoparticle surface. A multivalent molecule remains in the proximity of the particle, as opposed to monovalent ligands which will desorb completely. Also, entropic effects play a role.

Perumal et al. investigated binding kinetics of mono-, di- and trithiols on differently sized AuNPs (2.2, 3.2 and 4.4 nm) *via* time resolved fluorescence spectroscopy of the leaving ligand (a pyrene).[46] They found that divalent ligands show highest exchange velocity and explain this by a cooperative activation model of vicinal atoms. The lower velocity of trithiols is explained by enhanced sterical hindrance. They also find a particle size dependence, as the ligand exchange rate increases with increasing particle size.

The chemical stability of mono-, di- and trithiol-stabilized AuNPs (2 nm diameter) was also investigated by Srisombat et al. by UV/Vis spectroscopic monitoring of cyanide degradation.[47] They found the same trend that dithiols stabilize AuNPs best.

Diphosphines can also act as AuNP ligands. An example are 2,2'-bis(diphenylphosphino)-1,1'-binaphthyl (BINAP)-stabilized AuNPs with an mean diameter of 1.7 nm that could be synthesized *via* a direct route.[48] Ligand characterization was performed by XPS, also showing that the gold atoms are present as Au⁰.

Furthermore, Au₁₁ clusters, stabilized by four BINAP molecules per particle, were reported.[49]

The formation mechanism of diphosphine-stabilized undecagold was investigated in detail by electrospray ionization–mass spectrometry (ESI-MS).[50] It was found that ligand lability is an important factor in the equilibria of relevant gold complex intermediates and that the direct formation of diphosphine-stabilized clusters from diphosphine-gold complexes may be hindered due to high stability of such complexes. A problem in AuNP stabilization with polyfunctional ligands may occur by possible network formation of numerous AuNPs and a resulting aggregation.

Ligands undergo dynamic binding and unbinding processes.[40] The phenomenon of ligand mobility was described in detail for thiols.[51] Kinetics of the exchange rate of ligands depend on the ligand concentration and the character of the competing ligand. Furthermore, some atoms in a cluster are more prone to ligand exchange than others.

Functionalization of AuNPs can be realized either by a ligand exchange or by further chemical modification of the existing ligand shell. The mechanistic aspects of ligand exchange reactions are quite complex and depend on several factors such as the leaving ligand, the incoming ligand, the AuNP size and of course the reaction conditions under which the ligand exchange is performed.[52] In general it is possible to exchange weak binding ligands against stronger ones. This can be done either in one phase or in a two phase system. In a one phase system, AuNPs and incoming ligands can easily interact. A disadvantage is the more elaborate purification. The main drawback of a two phase ligand exchange is the possibly impaired NP stability at the phase boundary, as the AuNPs lose their primary ligands and are partly unprotected during phase crossing.

The aspect of chemical modification of the ligand shell is further discussed in chapter 2.4.

2.1.5 Separation from Possible Impurities

Three key issues are important concerning the purity of AuNPs: Polydispersity of a sample, excess ligand, and metal ion or complex impurities. These factors depend on the synthesis

conditions, and ideally those are adjusted in such a way that sophisticated purification steps are not necessary. Nevertheless, even for well optimized synthesis routes the degree of purity from the raw product might not be sufficient for the envisioned further experiments or applications. Several methods can then be applied to purify the material.

The most frequently used methods for size selectivity include filtration, selective centrifugation, selective precipitation, and column chromatography.

Filtration is useful if considerably larger aggregates have to be removed, but not for samples with a broad size distribution. Filters with different membrane pores down to 20 nm are commercially available, fabricated from different materials such as alumina and various polymers. It is important to choose a suitable material to exclude any interaction of the particles with the membrane material.

Quantitative centrifugation, relying on the sedimentation principle, can also be used to separate particles with a bimodal distribution of different masses.[53] Both the centrifugate or the supernatant may contain the desired product. Sample volumes range from μL to hundreds of mL which makes centrifugation especially interesting for large batches.

Size selective precipitation is based on different solubility of differently sized NPs due to varying numbers of ligands on the particle surface and therefore differing stabilization. NPs are dispersed in a solvent, and a nonsolvent or a salt is added stepwise, enabling the successive precipitation and removal of NP fractions.[54]

Column chromatography or size exclusion chromatography relies on the same principle, as the retention time of NPs depends on the particle size and therefore solubility and polarity.[55] Different materials for the stationary phase are useful for purification of AuNPs, such as cellulose or sephadex (a cross-linked dextran gel). However, not all AuNPs are suitable for column chromatography, as especially larger particles or weakly stabilized ones tend to aggregate on the adsorbent.

Purification methods to eliminate excess of ligand, synthesis by-products, and ionic impurities include centrifugation, washing or precipitation, and column chromatography, but also dialysis. Here, different membranes are commercially available with different molecular weight cut off (MWCO) radii and made of different materials. Although dialysis may be a quite time consuming method when performed over several days, it is easy to perform.

Depending on particle size and ligand stabilization, AuNPs sometimes show problems of stability when kept in solution over longer periods of time. The particle size might change due to ripening effects, and partial decomposition and therefore slow enrichment of impurities is possible. Because of their large surface area and therefore activated state, NPs are thermodynamically metastable. Energy input by elevated temperature or light might enhance further reactions. Also, the medium plays a role, as for example high salt concentrations may impair NP stability.

These facts need to be considered for the preparation, storage and handling of AuNPs. Regularly repeated analysis of the NP quality is essential to ensure that the investigated material has the expected structure.

2.2 Characterization

Two aspects have to be considered in NP analysis: size and polydispersity determination of a sample, and characterization of the ligand shell. Different methods to address these two issues will be briefly explained, together with recent examples of nanomaterial applications. Typically, only a few selected of the presented analysis methods are used and presented by different groups reporting about AuNP synthesis and characterization. One must be aware of the detection limits and the advantages and disadvantages of different techniques when applied to AuNPs. The comparability between different methods is sometimes not directly given and must carefully taken into account. One example of extensive AuNP characterization with various different techniques was given by Leff et al. by the investigation of differently sized alkylamine-stabilized AuNPs.[37]

2.2.1 UV/Vis Spectroscopy

The optical properties of a AuNP sample can easily be investigated by UV/Vis spectroscopy. AuNPs above a certain size (~ 3 nm) exhibit a plasmon resonance peak (2.1.2.2). As this depends on size and NP surrounding, UV/Vis spectroscopy is used for qualitative NP analysis for dispersions of spherical AuNPs. When parameters such as solvent and ligand shell are

equal for two samples, the wavelength of the absorption maximum depends on the particle size and the width of the peak is a measure for the polydispersity of the sample.

Furthermore, assemblies of AuNPs can be investigated. If AuNPs are in close proximity, their valence electrons interact. The excited plasmon of one AuNP induces an alteration of the polarizability of the neighboring AuNPs. The resonance frequency is affected, which leads to a redshift of the plasmon resonance peak maximum.

This is for example used in enzyme sensors. In a recent example, peptide- as well as antibody-functionalized AuNPs were synthesized and mixed.[56] In presence of a kinase, the peptide was phosphorylated and thus compatible for antibody interaction, leading to AuNP aggregation. This colorimetric assay enables the quantification of enzyme and also the determination of kinase inhibitors, which is important in drug development for several diseases.

2.2.2 Electron Microscopy

Electron microscopy (EM) is used in this work to determine mean AuNP sizes. An electron microscope consists of an electron gun, an anode to accelerate the electrons, several electrostatic and electromagnetic lenses to focus the electron beam, a sample holder and a detection system. The detection of EM is performed under high vacuum conditions. It is, depending on the measurement mode, based on elastic or inelastic scattering or diffraction of the electrons by the sample.[57]

The use of an electron beam for the imaging of objects strongly increases the resolution as compared to light microscopy. The resolution of a system is determined by the wavelength of the probe beam, and energy-rich electrons correspond to shorter wavelengths than possible in the visible spectrum (photons). The resolution of a transmission electron microscope (TEM) is approximately 0.1 nm.[58] By using aberration correctors, resolution could be improved to 50 pm in annular dark-field scanning TEM imaging.[59]

However, several obstacles have to be overcome when using TEM for NP size determination. As it is not an integral method, relatively few particles are examined compared to other methods. Analysis of a statistically significant number of particles is therefore important.

For very small NPs, the contrast between particles and substrate (usually an amorphous carbon film) may be low.[60] Due to the high electron density of gold this problem is mostly negligible for AuNPs. The resolution can be improved by measuring in dark-field imaging mode and even further in high-angle annular dark-field (HAADF) mode, using a detector operating in a preselected angular range while excluding the direct electron beam.

The appropriate choice of magnification and accelerating voltage is also crucial. Magnification is especially important for statistical NP size analysis. With higher magnification, the particle size can be determined more correctly. On the other hand, less particles per image are available for evaluation. Higher voltage enhances contrast, but may induce severe sample damage. A compromise has to be found for both. Typical voltages used are of intermediate energy (80–400 keV). To reduce sample damage by the electron beam, scanning transmission EM (STEM) can be performed. A scanning beam is advantageous compared to continuously exposing the entire sample to the electron beam.

Furthermore, the image analysis is an important parameter. Manual evaluation may be defective, but for samples with low contrast, it is preferred compared to software-assisted or fully automated analysis. Smoothing and sharpening processes of the images may come along with loss of information and addition of artifacts.

A state-of-the art example for AuNP EM characterization was presented by Li et al., who used aberration-corrected HAADF-STEM for the three-dimensional analysis of a Au₃₀₉ cluster. They could achieve atomic resolution when combined with cluster simulations.[61]

2.2.3 X-ray Diffractometry

X-ray diffractometry (XRD) is based on elastic scattering of X-rays from the electrons of atoms of a sample. Powder diffraction is used to analyze the crystallographic structure and crystallite size of a material. For very small crystallite sizes, signals in XRD are broadened, a phenomenon described by the Scherrer equation.

XRD is used as a characterization tool for structure analysis of AuNPs. Small angle X-ray diffraction (SAXRD) was used to determine the structure of Au₅₅[(C₆H₅)₃P]₁₂Cl₆ in crystallites, showing a simple close packed arrangement of clusters correlating with an effective cluster distance of 2.3 nm.[62] Until now it was not possible to generate large single crystals

of the Au₅₅ cluster, therefore no single-crystal X-ray structure analysis to solve the complete structure could be performed.[17]

Crystallization of single crystals is however possible for other AuNP species. In 2007, Jadzinsky et al. reported of the crystallization and X-ray structure determination of a *p*-mercaptobenzoic acid (*p*-MBA)-protected AuNP, consisting of 102 gold atoms and 44 *p*-MBA molecules.[63]

2.2.4 DLS and ζ Potential Measurement

In dynamic light scattering (DLS) measurements, laser light is used to determine the size distribution profile of a nanoparticle dispersion.[64] Photons are scattered by particles if the particles are small compared to the wavelength used. For monochromatic coherent laser light, time-dependent fluctuations of the scattering intensity occur, which are induced by the Brownian motion particles undergo in dispersion. From the intensity trace, an autocorrelation function can be generated which typically shows exponential decay. This decay is related to the diffusion coefficient of the NPs. With this it is possible to calculate the hydrodynamic radius of a sphere through the Stokes-Einstein equation.

The ζ potential of a colloidal dispersion describes the potential difference between the dispersion medium and the stationary layer of fluid attached to the dispersed particle.[65] It is a measure to approximate the stability of a NP dispersion. If the absolute value is higher than 30 mV, a dispersion is regarded as stable. Measurement of the ζ potential of a NP dispersion is conducted by applying an electrical field during a DLS measurement and therefore determining its electrophoretic mobility, which correlates with the ζ potential.

Advantageous of DLS and ζ potential measurements is the very fast and easy performance. Opposed to EM, it is an integral method. A great number of particles is measured in one measurement, providing statistically relevant data.

There is however a major drawback related to this. As the intensity of scattered light varies with the sixth power of particle diameter, impurities such as comparatively large dust particles are highly disturbing.

Manufacturers of DLS instruments give values around 1 nm or below as lower size detection limits. However, this value depends strongly on factors as medium viscosity, temperature

and monodispersity of the sample. A critical discussion of potential problems arising in size determination of AuNPs by DLS was given by Khlebtsov et al..[66]

As one example, AuNPs with a mean gold core diameter of 2.7 nm, stabilized by a mixed ligand shell of GSH and cysteamine, were able to be measured in DLS, resulting in a hydrodynamic diameter of 3.1 nm.[67]

In another study, Rotello and co-workers performed ζ potential measurements of 2 nm sized thiol-stabilized AuNPs with mixed ligands shells of tetra(ethylene glycol) (TEG) and 1-pentanethiol and found differences in the values depending on the ratio of ligands bound to the particles.[68] They found a qualitative correlation of ligand shell ratio and ζ potentials.

Furthermore, DLS was used to investigate interactions of AuNPs and biomolecules, namely the interaction of AuNP-bound protein A with the human IgG protein.[69] Here, the binding stoichiometry could be quantified by DLS.

2.2.5 Elemental Analysis

Elemental analysis (EA) is a standard technique for the determination of elemental composition. Most typically, carbon, hydrogen and nitrogen (CHN) amounts are quantified in a sample by combustion and detection of the resulting combustion products.

For AuNPs, EA is useful to characterize the ligand shell composition. If the structure of a cluster and thus the theoretical elemental composition is known, EA can be used to verify the purity of the sample. For $\text{Au}_{55}[(\text{C}_6\text{H}_5)_3\text{P}]_{12}\text{Cl}_6$ the EA result was one of the means to determine its chemical composition.[33]

One problem that intrinsically occurs for EA of AuNPs is the high mass of the gold core and thus the mass ratio between core and shell. This makes it difficult to distinguish for example between samples before and after a ligand exchange, if the chemical formula of the outgoing and incoming ligands are similar. The percental changes of the AuNP species are then small compared to the EA of the pure ligands.

2.2.6 Nuclear Magnetic Resonance Spectroscopy

Nuclear magnetic resonance (NMR) spectroscopy is widely used in chemical analysis to determine molecular structures. It is based on the interaction of nuclear spins of a sample with a magnetic field. NMR active nuclei absorb electromagnetic radiation at a characteristic frequency. For different local chemical environments (on an atomic scale), e.g. depending on the functional group an atom belongs to, the chemical shielding is influenced and the resonance frequency is slightly shifted. This chemical shift is thus characteristic and can be used for example for structural determination of a molecule.

When ligands of a NP species are investigated by NMR spectroscopy, the proximity of the ligand molecules to the metallic core has an effect towards the resulting spectra, e.g. line broadening may occur. This originates from the variability of different chemical shift environments at the surface of the NPs due to ligand mobility of the NP surface.

NMR spectroscopy can be performed in solution, giving averaged signals as the time scale of a NMR experiment is slow compared to molecular movements. It can also be conducted in solid state, which is typically used in polymer analysis and structure determination of huge molecules such as membrane proteins.[70]

For AuNPs, NMR spectroscopy may yield important information about ligand dynamics. This was shown by Schmid et al. for $\text{Au}_{55}[(\text{C}_6\text{H}_5)_3\text{P}]_{12}\text{Cl}_6$ in interaction with excess TPP ligand,[71] and also for similar TPP-stabilized clusters with a mean diameter of 1.8 nm by Sharma et al.[72] They found that if excess TPP (in deuterated form, $d_{15}\text{-PPh}_3$) was added, ligand exchange reactions appear in which the gold(I) complex TPP-Au(I)-Cl is also involved.

2.2.7 Infrared Spectroscopy

In infrared (IR) spectroscopy, vibrational modes of atoms or atom groups in molecules are excited and the respective absorption is detected. This covers the range from $\sim 400 - 4000 \text{ cm}^{-1}$ of the electromagnetic spectrum, typically given in wavenumbers.

As for NMR spectroscopy, IR spectroscopy in context with AuNPs is mainly used to analyze the ligand shell. Characteristic bands from functional groups can be identified to ensure

particle functionalization with the respective molecules. Sometimes, further information can be gained, e.g. for thiols bound to AuNPs. Here, the S–H vibrational mode disappears in AuNP spectra as thiols bind *via* the sulfur atom to the AuNP surface, as for example shown by Brust et al.[36] Again, the problem of signal broadening arises and can hinder the identification of weak bands in an IR spectrum.

2.2.8 Fluorescence Spectroscopy

Fluorescence spectroscopy uses electromagnetic radiation to excite fluorescent molecules. Typically, emission spectra are recorded, but absorption can be detected as well.

As already described before, small AuNPs can be fluorescent (see 2.1.2.2). Several examples for this phenomenon can be found in literature. Polymer-stabilized AuNPs with sizes between 1.1 to 1.7 nm were found to be fluorescent, with 1.1 nm sized AuNPs having the highest quantum yield of 3 %.[73]

Also, fluorophores attached to AuNPs are investigated. When fluorophores are in close proximity to AuNPs, their fluorescence is typically quenched by a Förster resonance energy transfer (FRET).[74] Therefore, fluorescence spectroscopy can be a valuable tool to determine ligand release from AuNPs. This was for example shown by Seferos et al., where fluorescein labeled DNA sequences were hybridized to AuNPs functionalized with complementary strands.[75] DNA melting processes could then be followed by fluorescence spectroscopy due to increasing fluorescence induced by released fluorophore-labeled DNA strands.

2.2.9 X-ray Photoelectron Spectroscopy

In X-ray photoelectron spectroscopy (XPS), X-ray radiation is used as a surface probe to trigger electron emission from the sample surface. As the energies of those are element and oxidation state dependent, information about the chemical composition of the sample surface can be derived.

A limitation of the technique is that ultrahigh vacuum conditions are required. Also, sample degradation can occur during the measurement in the case of irradiating sensitive samples.

As a surface analysis method, XPS can be used to characterize the ligand shell of NPs. Also, the oxidation state of the metal core can be detected as the radiation depth is up to 10 nm of the sample.

Techane et al. used XPS to monitor ligand exchange of 24 nm sized AuNPs that were initially functionalized with cysteamine ($\text{HS}-(\text{CH}_2)_2-\text{NH}_2$) which was then exchanged against a long chain amine-terminated alkanethiol ($\text{HS}-(\text{CH}_2)_{11}-\text{NH}_2$).[76] They found that ligand exchange was complete after 4 days, while the ligand density further increased for the next 10 days.

2.2.10 Electron Paramagnetic Resonance Spectroscopy

Electron paramagnetic resonance (EPR) spectroscopy is a method to detect unpaired electrons in a sample. The physical principles are the same as in NMR spectroscopy, but the resonance frequencies of electrons are detected instead of those of nuclei. Absorption frequency and signal fine structure are compound dependent, and the signal intensity is proportional to the species concentration.

As most stable compounds do not have unpaired electrons, EPR spectroscopy is restricted to the analysis of radical species, paramagnetic transition metal complexes or excited molecules in the triplet state. This restriction is on the other hand an advantage as it makes EPR spectroscopy highly specific, even in complex systems such as *in vivo* analyses.[77]

Stable radicals can be used as a probe to investigate interactions with EPR inactive compounds such as AuNPs. This was for example shown by Zhang et al., who used 4-Amino-2,2,6,6-tetramethylpiperidine-1-oxyl (Amino-TEMPO) to determine the interaction with citrate-stabilized AuNPs. They found that Amino-TEMPO is adsorbed on the AuNP surface, leading to a signal decrease. In the presence of oxygen, Amino-TEMPO was oxidized to its oxo derivative, potentially catalyzed by the AuNPs.[78]

2.3 Biological Effects of Gold Nanoparticles

As the number of envisioned applications of AuNPs in biomedical applications rapidly increases, the effects towards biological systems need to be analyzed. This field can be gener-

ally divided into *in vitro* and *in vivo* investigations. Although the latter is closer to realistic application scenarios, the former has also its value, as important basic knowledge can be gained and some general principles of the interactions of AuNPs with living organisms may already be found and understood in the easier accessible, cheaper and ethically better justifiable cell experiments. Also, the analysis of *in vivo* experiments comprises a higher degree of complexity due to parameters such as uptake pathway, organ distribution, retention time and the complex interplay of numerous different cell types. *In vitro* assays may enable easier access of structure-property relationships as a lower number of parameters must be taken into account.

This work is restricted to *in vitro* experiments. Two recent overviews of *in vivo* investigations were given by Alkilany et al. and Li et al..[79, 80]

2.3.1 Methods

Different methods exist to determine cytotoxicity.[6] Besides light microscopy to analyze changes in cellular structure, staining assays are widely used. Some are based on the fact that dying cells become leaky, such as Neutral Red, which usually accumulates in lysosomes of healthy cells, so that reduced uptake is a sign for impaired cell viability, and Trypan Blue that is only permeable to cells with compromised membranes.

Mitochondrial activity can be analyzed by the widely used MTT assay. Here, the dye 3-(4,5-dimethylthiazol-2-yl)-2,5-diphenyl tetrazolium bromide (MTT) is colorimetrically quantified. In living cells, it is metabolized to its blue formazan derivative, thus a correlation of cell viability can be drawn. Other dye assays working on the same principle are MTS, WST and XTT. As a measure, typically the half maximal inhibitory concentration (IC_{50}) is given as the concentration of the toxic compound that impaired cell viability by 50 %.

Cytotoxic compounds may induce inflammation reactions within living organisms. Thus, concentrations of inflammation biomarkers such as IL-1 β , IL-6, and TNF- α together with IL-8 can be quantified.

To differentiate between necrosis (sudden cell death as cellular response of acute cellular injury) and apoptosis (programmed cell death leading to cell fragments that can be digested), double staining with two dyes and subsequent flow cytometry is often used. Annexin V is a

staining reagent for phosphatidylserine, a membrane lipid which concentration is increased on the extracellular side during apoptosis. Propidium iodide is a nuclear stain for impaired membrane integrity, hence for necrosis. By differentiation between single annexin V stained apoptotic cells and double stained necrotic cells, the cell death mechanism can be elucidated.

2.3.2 Uptake Mechanisms

Endocytosis is the generic term for several uptake mechanisms. Cells capture extracellular molecules in vesicles consisting of plasma membrane. Depending on the size of the resulting vesicles, endocytosis is differentiated into phagocytosis (0.1 - 10 μm) and pinocytosis (up to 100 nm for micropinocytosis and up to 1000 nm for macropinocytosis). There are several sub-mechanisms described, depending on whether cell membrane receptors are involved or not.[81]

Concerning NPs, the kind of cellular uptake is dependent on nanomaterial intrinsic factors such as size, shape, surface chemistry determined by charge and ligand type (hydrophilic or hydrophobic), and potential biologically active species like receptor affine functionalities.[82] This number of determining parameters complicates a general prediction. Some recent examples from literature will describe the different and sometimes contradictory results.

A study about the uptake of 14, 50, and 74 nm sized AuNPs, stabilized with citric acid, revealed size-dependent kinetics.[83] Here, 50 nm sized AuNPs were most efficient in uptake. The investigation of differently sized PEGylated AuNPs was described by Oh et al. AuNPs from 2.4 to 89 nm were functionalized with cell penetrating peptides (CPPs), and uptake was investigated in COS-1 cells.[84] They found that cellular uptake is directly dependent on the surface display of the CPP whereas the final intracellular destination is further determined by AuNP diameter. 2.4 nm sized AuNPs were found in the nucleus. 5.5 and 8.2 nm sized AuNPs were partially taken up by cells into the cytoplasm, while larger AuNPs with mean diameters of 16 nm and larger were not taken up at all. This last finding significantly differs from another report in which AuNPs of 18 nm size were endocytosed and ended in endocytic vesicles.[11]

The endocytotic uptake of single AuNPs was investigated by atomic force spectroscopy. 4, 12, and 17 nm sized L-cysteine-stabilized AuNPs were used. Uptake forces increase with

AuNP size, which can possibly be attributed to the increased interaction area between AuNP and cell membrane. Endocytosis could be inhibited by treating the cell with the cytoskeleton inhibitor cytochalasin B.[85]

Furthermore it was found by Verma et al. that even the surface structure of the ligand shell can influence the uptake mechanism.[86] AuNPs of the same size of 4.5 nm and with a mixed ligand shell of the same composition, but with either unordered or stripe-like ordered ligands, were either trapped in endosomes or could pass the cell membrane without bilayer disruption.

In biological tissue as well as in cell culture medium, particles will be wrapped in a shell of the proteins present. For 10 - 20 nm sized FePt and CdSe/ZnS NPs stabilized by a polymer coating, this so-called protein corona could be quantified to have a thickness of 3.3 nm.[87] The occurrence of a protein corona around AuNPs could be shown for citrate-stabilized AuNPs of 5 - 100 nm in interaction with typical blood proteins such as albumin and insulin.[88] The binding constant and also the thickness of the final protein layer depend on the particle size, both increasing with increasing AuNP size.

Mirkin and co-workers describe a dependence of the oligonucleotide density of 13 nm sized AuNPs and the number of proteins absorbed, thus affecting the cellular uptake in a mouse cell line (C-166) and two human cell models (HeLa and A594).[89]

2.3.3 Cytotoxicity

As a result of AuNP uptake, cytotoxicity may occur. Within the last years, several studies were published concerning the toxicity of AuNPs. Various AuNPs were analyzed by different methods, which complicates a direct comparison or the statement of a general hypothesis. The lack of systematic investigations and reports of sometimes contradictory results by different groups were the starting point for the DFG project in which framework this work was conducted.

There are some recent reviews concerning the topic of nanoparticle cytotoxicity.[6, 90] The most relevant publications with regard to the present work will be discussed here.

Surprisingly high cytotoxicity was found for $\text{Au}_{55}[(\text{C}_6\text{H}_5)_2\text{P}(\text{C}_6\text{H}_4\text{SO}_3\text{Na})]_{12}\text{Cl}_6$ clusters (abbreviated as Au1.4MS in the present work) in eleven different cancer and healthy human

cell lines after an incubation time of 24 h, determined by MTT assay.[8] Further, the intracellular distribution was investigated by neutron activation analysis (NAA). 57.5 % of the radioactive gold isotope was located in the cytoplasmatic fraction, 42.5 % was bound to the cell nucleus. After removal of the nuclear proteins, 21.1 % were found in the DNA fraction. However, this was possibly an artifact of the sample preparation because the nuclei always fractionate with the pellet and thus together with the AuNPs.

Connor et al. revealed the uptake of 18 nm sized citrate- or biotin-capped AuNPs in K562 leukemia cells.[11] An MTT assay after three days of incubation did not show toxicity induced by the AuNPs up to gold atom concentrations of 250 μM . The same was determined for cysteine- and citrate-capped 4 nm sized and glucose-stabilized 12 nm sized AuNPs (up to 25 μM).

Another study reported of 13 nm sized citrate-stabilized AuNPs in human dermal fibroblast cells.[10] After incubation times of 2, 4 and 6 days, proliferation of the cells was impaired. Moreover, it was found that the formation of actin filaments was disturbed.

2 nm sized thiol-stabilized AuNPs with either cationic ammonium or anionic carboxylate functional end groups were analyzed for their effects towards COS-1 cells, red blood cells and *E. coli* bacteria cells.[91] Cells were incubated with up to 3 μM AuNPs for a maximum of 24 h and analyzed by MTT assay. *E. coli* cells were found to be slightly more resistant to AuNP toxicity that was induced by the cationic AuNPs. The anionic species had no toxic effect, which was explained by less favored interaction with the negatively charged lipid bilayer of which a cell membrane consists.

In 2009, 8 nm sized poly(vinylpyrrolidone)-stabilized AuNPs were investigated in madine darby canine kidney cells (MDCK) and human hepatocellular carcinoma cells (HepG2) after 24 h of exposure.[92] No cytotoxicity was found with Neutral Red uptake and colony forming efficiency tests.

From these findings, no clear trend could be found yet concerning the size- or ligand-dependent cytotoxicity of AuNPs, obviously resulting from the different protocols, descriptions of dosage and reference compounds used so far.

2.3.4 Oxidative Stress & Reactive Oxygen Species

Oxidative stress describes a state in metabolism in which a critical concentration of reactive oxygen species (ROS) is formed. These are the superoxide O_2^- , hydrogen peroxide H_2O_2 and the hydroxy radical $\cdot OH$. The concentrations of cellular antioxidant defenses such as glutathione (GSH) are depleted. In consequence, lipid membranes, proteins and DNA are affected and become oxidized which may critically disturb their vital functionalities.

A general model of NP induced oxidative stress, the determining factors and the consequences in biological organisms was presented by Nel et al.. The nanomaterial factors include material composition, electronic structure, surface bound species, surface coatings and solubility. It is therefore not possible to predict if a certain nanomaterial will induce oxidative stress in cells but has to be individually investigated.[13] Some studies indicate that AuNPs may induce oxidative stress in cells.

A MRC-5 human fetal lung fibroblast cell line was treated with 20 nm citrate-stabilized AuNPs which were further passivated with fetal bovine serum (FBS).[93] The highest AuNP concentration used was 1 nM (particle concentration) and was incubated up to 72 h. A decrease in total cell number was found. Furthermore, the generation of 8-Oxo-2'-deoxyguanosine (8-OH-dG) could be shown. This is related to oxidative stress and genotoxicity (see below in section 2.3.5). The AuNPs also affected genes associated with genomic stability and DNA repair.

13 nm sized citrate-stabilized AuNPs were analyzed for their potential to produce NO in blood serum.[94] Concentrations up to 80 μM clearly induced NO release. It is speculated that *S*-nitroso adducts with a thiol group, such as *S*-nitrosoalbumin, *S*-nitrosocysteine, and *S*-nitrosoglutathione are the source for NO release. This conclusion was drawn from the occurrence of a thiolate peak in XPS spectra of the AuNPs after contact with blood serum.

Cationic AuNPs with thiols of different alkyl chain lengths were analyzed towards HeLa cells determined by alamar blue assay.[95] The production of ROS was shown by 2'-7'-dichlorodihydrofluorescein diacetate (H_2DCFDA) staining. Increasing the hydrophobicity of the particles increased their cytotoxicity and also ROS production.

2.3.5 Genotoxicity

Oxidative stress can damage DNA and induce single-strand breaks, double-strand breaks, oxidatively induced base damage, and other DNA lesions. This can further lead to mutagenesis, carcinogenesis, or other age related diseases.[96]

There are different methods to investigate NP induced genotoxicity. One common method is the comet assay, which is based on gel electrophoresis of a single cell after lysis. It is a relatively simple and fast assay. One disadvantage is the lack of information about the targets of oxidative damage.

For a more detailed investigation, single DNA base oxidation products can be quantified. Typically, this is done by HPLC or ELISA detection for 8-OH-dG, an oxidation product of deoxyguanosine with mutagenic and promutagenic activity.[97]

However, there are several other DNA oxidation products (lesions) with adverse effects that are more difficult to detect as they are present in lower concentrations. A detection method for identification and quantification of numerous lesions is GC/MS. If this is performed together with a so-called isotope-dilution procedure for which known concentrations of the respective, isotopically labeled lesions are added, it is possible to quantify the concentrations of several lesions in a single measurement of one sample.[98] Despite the more elaborate sample preparation compared to other assays, the latter method was chosen in this work to investigate AuNP induced genotoxicity, thus enabling the detection of multiple DNA lesions simultaneously.

An analog technique to quantify DNA damage that was also used here is liquid chromatography/tandem mass spectrometry (LC/MS/MS). Similar sensitivities as compared to results from GC coupled systems could be shown.[99] An advantage compared to GC/MS is that the analyte does not have to be derivatized prior to the measurement.[100]

The tandem mass spectrometry measurement unit enables the selection of a certain ion from a first overview mass spectrometry unit, its fragmentation and subsequent analysis of secondary fragments. This allows simultaneous detection of lesions and recording of fragmentation patterns thereof.

2.3.6 Ion Channels & Patch Clamp Technique

One important step to bridge the huge gap between *in vitro* toxicity assays and *in vivo* studies is the investigation of negative effects towards ion channels of cells by the patch clamp technique.[101]

Nowadays, many new chemical compounds are abandoned early in the drug development process because they interfere with the K_V11.1 potassium ion channel (encoded by the hERG gene and therefore abbreviated as hERG).[102] The hERG ion channel is a voltage gated potassium channel that, together with other ion channels, regulates the heartbeat as it mediates the rapid delayed rectifier K⁺ current in heart (IKr). IKr is activated by membrane depolarization and is a major determinant of the duration of action potentials in the ventricle. Mutations in hERG leading to a complete or partial loss of channel function are a major cause of inherited long QT syndrome (LQTS). More often, dysfunctions of hERG that lead to LQTS are caused by a blockade of medications as an undesirable side effect. This has already led to the removal of several drugs from the market and is now an indispensable pretest in the development of new drugs. Therefore, new drug candidates have to be tested for a potential inhibitory effect on the hERG current (Guidance ICH S7A, S7B by the FDA). This susceptibility relates to the special structure of hERG.[103]

Distinct from other voltage gated K⁺ channels the S6 loop of the hERG protein lacks a proline-X-proline motif that is proposed to insert a 'kink' in this inner helix. Therefore, the cavity of the hERG channel is supposed to be wider compared to the related K⁺ channels and thus providing more space for chemical compounds, e.g. small NPs, interacting with putative binding sites.

With the patch clamp technique, the electrophysiology of cells, i.e. the membrane potential and channel currents of ion-channel expressing cells can be examined.[104] Undesirable interactions of potential drugs that compromise or inhibit the channel functionality can be analyzed. For this purpose, the patch electrode (a glass micropipette filled with an electrolyte solution and a chlorinated silver wire) is brought in close contact to the cell which is adherent in the medium filled cell chamber. Depending on the question that is addressed, different pipette-cell configurations can be realized. In a typical experiment, the

glass capillary is placed in contact with the cell membrane. By applying a slight suction the cell-to-capillary contact is sealed ("gigaseal"). By enhancing the suction the membrane is ruptured and the electrode is in contact with the cytosol ("whole cell configuration"). *Via* this patch electrode and with a counter electrode in the cell chamber it is now possible to apply a certain potential to the cell membrane as well as to measure the ion current through the ion channels of the entire cell. The test compound can then be added to the cell culture medium in the cell chamber, and influences on the channel activity can be detected. Patch clamp is now a standard technique for new therapeutics.

In a first example for an application of patch clamp measurements on NP incubated cells, Parak and co-workers investigated the effect of differently coated CdSe NPs with a core diameter of 2.4 nm towards hERG expressing CHO cells.[105] They found that particles of this size do not cause any effects towards characteristic electrophysiological properties of the cells, but a quantified cytotoxicity of CdSe NPs that could be related to the release of Cd^{2+} ions.

2.4 Modification of AuNPs for Biomedical Applications

Cytostatic drugs used nowadays in chemotherapy have several disadvantages that have to be solved for a better treatment of patients. One huge disadvantage is the general toxicity of most cytostatic drugs, thereby leading to severe side effects during cancer therapy such as depression of the immune system, fatigue, nausea and others. Therefore, anticancer drugs need urgently to be improved and to be made more specific.

NPs can easily be functionalized *via* their ligand shell. Thus, targeting molecules can be attached to the NP surface, leading to a specific interaction with cells having suitable receptors. Appropriate target molecules include peptides, proteins, enzymes and antibodies, depending on the aspired application.[40]

NPs with active targeting functionalities are classified as third generation NPs and are capable of specifically recognizing their target. Typically, they interact with receptors present on the cell surface via peptides, proteins, aptamers and antibodies. Uptake can then occur through receptor-mediated endocytosis.[106]

This was for example shown for a variety of AuNPs (10, 20, 30, and 60 nm diameter, respectively), functionalized with mixed ligand shells of PEG and two different receptor-mediated endocytosis-triggering peptides in HeLa cells. Efficient uptake could be confirmed by induced coupled plasma-optical emission spectroscopy (ICP-OES) of the lysed cells.[107] 2.8 nm sized AuNPs functionalized with tiopronin and then further with a Tat protein-derived peptide sequence were tested in a human fibroblast cell line by TEM. Specific nuclear targeting could successfully be performed.[108]

A TEM based study with 16 nm sized AuNPs investigated the uptake in HeLa cells depending on functionalization.[109] If the AuNPs were coated with CPPs, the uptake did no longer happen *via* endocytosis, or possibly the AuNPs were able for endosomal escape, as they were not found in endosomes within cells. When they were functionalized with a mixture of CPPs and nuclear localizing signal (NLS) peptides, it was possible to induce nuclear targeting with these AuNPs.

2.4.1 Targeting with Bombesin

Bombesin is an oligopeptide consisting of 14 amino acids which was first found in the skin of a toad, *Bombina bombina*. [110] It shows antitumor activity as it binds to gastrin releasing peptide receptors (GRPR). GRPR are overexpressed in a number of different cancer cells, such as prostate, gastrinoma and breast cancer cells.[111] It is thus an excellent marker for early molecular events in carcinogenesis.[112]

Bombesin was already used for AuNP targeting. When 16 nm sized AuNPs were functionalized with a thioctic acid-bombesin derivative, enhanced specificity towards GRPR expressing cells could be shown *in vitro*, as well as *in vivo* in a prostate tumor bearing mice model. Biodistribution was followed by using radiolabeled ^{198}Au . [113]

Furthermore, Kogan and co-workers synthesized multifunctional 20 nm sized AuNPs, functionalized with a bombesin analogue and an analogue of the RAF peptide as a drug peptide.[114] They also found an enhanced activity and selectivity towards GRPR expressing cells, the latter induced by the targeting entity bombesin.

One advantage of bombesin and its analogues compared to other targeting entities such as antibodies is its relatively small size. This is especially important if small AuNPs are

functionalized, as it might not be possible to attach a huge biomacromolecule to small gold clusters for sterical reasons.

2.4.2 Labeling with Fluorophores/Aminofluorescein

Besides a functionalization to induce target specificity, it is also possible to attach marker molecules such as fluorophores to AuNPs to enable visualization within organic matter. If a fluorophore is attached to a AuNP, quenching effects can occur, depending on the AuNP size and the linker length.[74] This can be used to visualize ligand desorption from the particles which results in increasing fluorescence.

2nm sized AuNPs with thiol ligands were partially functionalized with a fluorescein derivative that was bound *via* a TEG linker containing additional 9 CH₂ groups. Here, effective quenching between fluorophore and AuNPs was observed, and the particles were used to quantify ligand release by fluorescence spectroscopy.[68]

3 Results and Discussion

3.1 Syntheses of AuNPs

Different routes were followed to synthesize a variety of AuNP species, varying in size, ligand shell and functionalization. The syntheses performed in this work were all based on wet chemical synthesis, i.e. the reduction of a gold salt or complex in solution. Depending on the synthesis conditions, different AuNPs could be produced and further modified. For this purpose, two main strategies were pursued: ligand exchange reactions which could be performed in one or two phase systems, or further chemical modification of the existing ligand shell.

Many AuNPs described in this work are based on the Au₅₅ cluster first synthesized by Schmid et al.[33] and its water soluble derivative Au_{1.4}MS.[34] Furthermore, citrate-stabilized AuNPs with mean diameters between 10 - 15 nm, synthesized by the Turkevitch method [32], were often used as precursor AuNPs for further functionalization. Some other synthesis strategies were also performed and are described at the respective parts.

All AuNPs were analyzed regarding two aspects: their size and monodispersity, and the chemical composition of their ligand shell. Different analytical tools were used for these purposes: UV/Vis spectroscopy, electron microscopy and dynamic light scattering for size determination; elemental analysis, IR and NMR spectroscopy for the chemical constitution. Mean diameters correspond to values determined by statistical analysis of electron microscopy micrographs if not stated differently. The results for the different AuNPs are described at the respective parts.

3.2 Size-Dependent Cytotoxicity

A variety of differently sized AuNPs between 0.8 and 15 nm, all stabilized with a TPPMS ligand shell, was synthesized, characterized and the cytotoxicity of each species was evaluated. The cell experiments were conducted by Dr. Yu Pan-Bartneck at the University Hospital Aachen (UKA), and parts of the results of these tests are described in her PhD thesis.[12]

Au0.8MS, Au1.4MS and Au15MS were synthesized according to known protocols [19, 34, 115] (see also chapter 5 for details). The UV/Vis spectra of the three materials are shown in fig. 3.1. The spectrum of Au0.8MS shows discrete peaks in the range below 500 nm and is consistent with a spectrum of a Au_8 cluster.[19] Au1.4MS shows a smooth spectrum with decreasing absorbance to longer wavelengths, but without discrete absorptions as small clusters or a plasmon resonance peak as colloids. The spectrum of Au15MS shows a typical surface plasmon band with an absorption maximum at a wavelength of 524 nm.

STEM micrographs for Au1.4MS and Au15MS are shown in fig. 3.2 and show AuNPs with a narrow size distribution (1.4 ± 0.2 nm and 15 ± 1 nm, respectively).

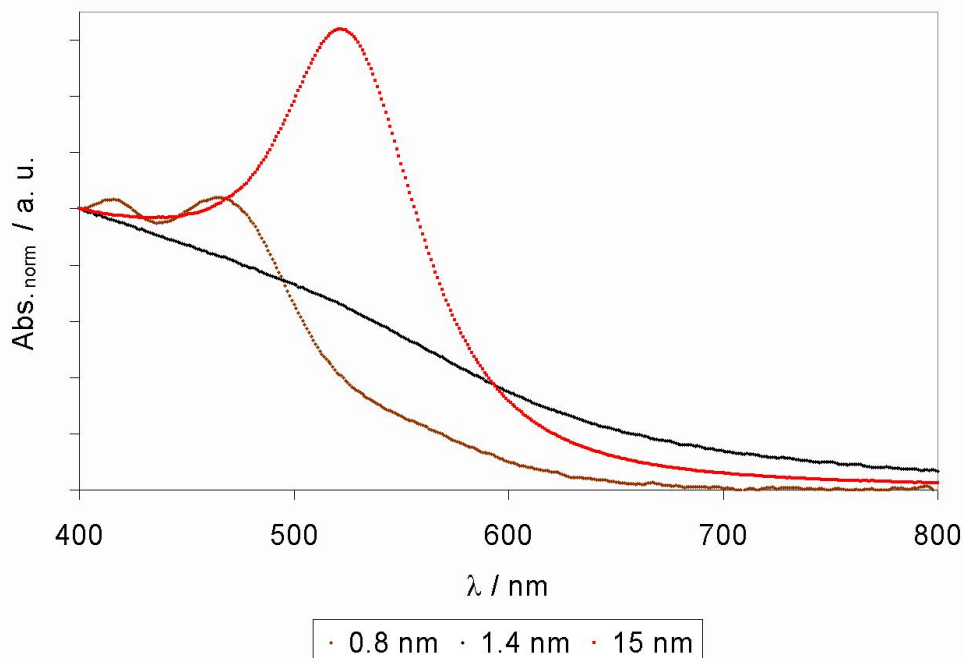


Figure 3.1: UV/Vis spectra of Au0.8MS, Au1.4MS and Au15MS.

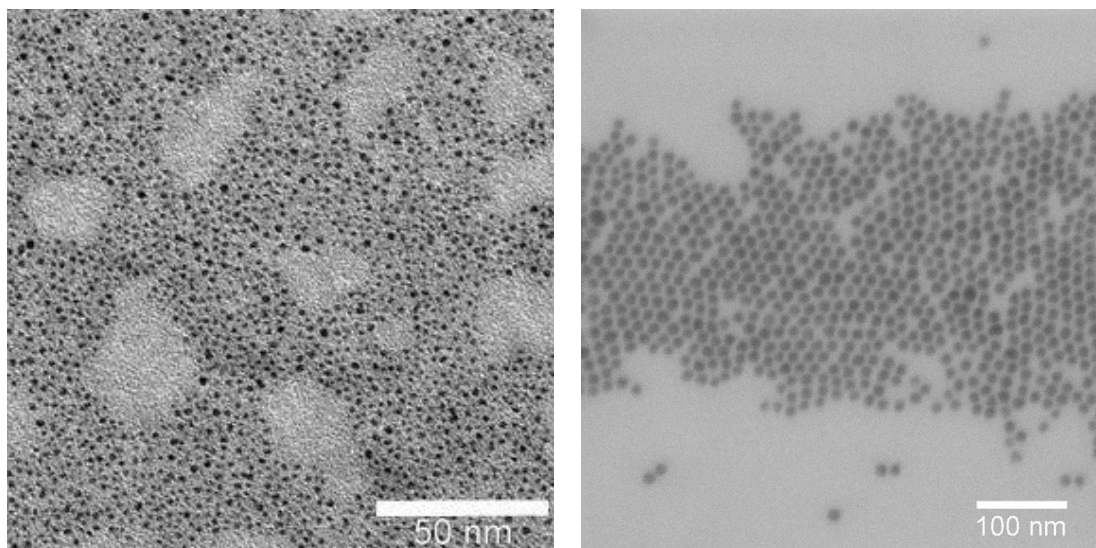


Figure 3.2: STEM micrographs of 1.4 nm (left) and 15 nm (right) sized, TPPMS-stabilized AuNPs.

In a newly developed route, AuNPs with a mean diameter of 5.6 nm (Au5.6MS) were synthesized in a two step procedure. First, dodecylamine-stabilized AuNPs were synthesized and dispersed in dichloromethane.[37] In a two phase ligand exchange reaction, these particles were functionalized with TPPMS and transferred to the aqueous phase. The UV/Vis spectrum, showing a distinct plasmon resonance peak at 518 nm, and a representative STEM micrograph are shown in fig. 3.3, respectively.

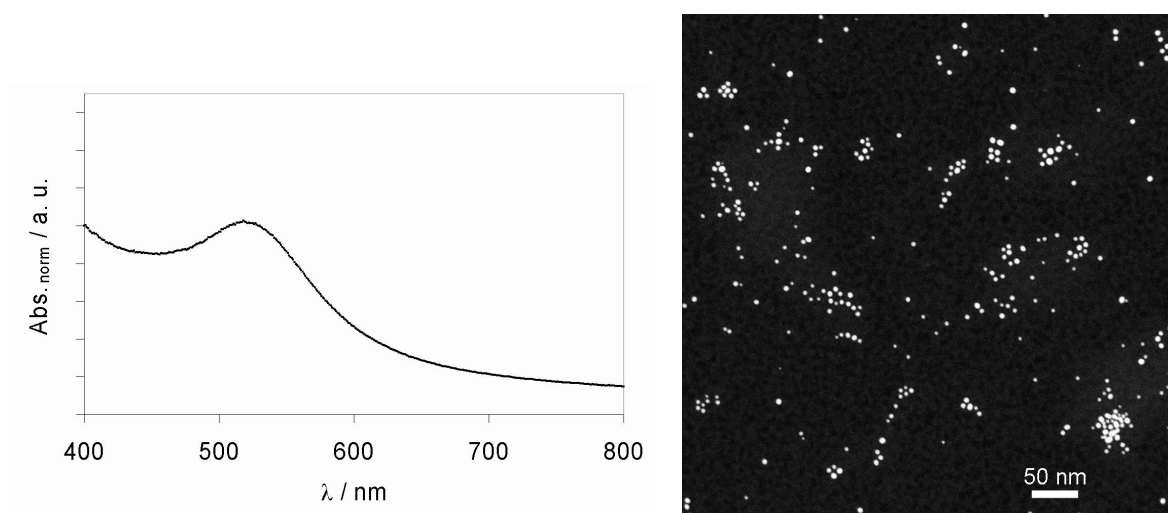


Figure 3.3: UV/Vis spectrum (left) and STEM micrograph (right) of Au5.6MS.

Furthermore, the cytotoxicities of two AuNP species with sizes of 1.2 and 1.8 nm (Au1.2MS and Au1.8MS, respectively), kindly provided by *STREM Chemicals Inc*, were examined as well.

First, the stabilities of all AuNP species in cell culture medium were confirmed. The AuNP cytotoxicities were then evaluated in an MTT assay with an incubation time of 48 h. Tauredon[®], a gold(I) thiomalate complex which is in clinical use as an anti-rheumatic drug, was tested as a reference. This complex does not exist in its molecular form in solution, but forms polymeric structures. Number and nature of the species thereby depend on parameters such as concentration, pH and nature of the cation (here Na⁺).[116]

The first AuNPs tested (Au0.8MS, Au1.2MS, Au1.4MS, Au1.8MS, and Au15MS) were tested in four different cell lines: HeLa cervix carcinoma epithelial cells (HeLa), SK-Mel-28 melanoma cells (SK-Mel-28), L929 mouse fibroblast cells (L929), and mouse monocytic/macrophage cells (J774A1). The sensitivity difference between different growth phases of cells, i. e. the logarithmic growth phase after 72 h of cell seeding into microtiter plates and the stationary phase after seven days of cell culturing, was also investigated. Later, HeLa cells in the logarithmic growth phase were used as the standard experiment conditions for all AuNPs.

A size-dependent cytotoxicity was found for all cell lines and incubation conditions (see fig.3.4 for the results from the logarithmic growth phase). The different cell lines resulted in slightly different absolute IC₅₀ values, but the trends were the same in all cell lines. Cells in the logarithmic growth phase were generally more sensitive to all toxic species by a factor of 1.5 - 3.3 compared to cells in the stationary phase.

Au1.4MS was the most toxic species with an IC₅₀ of 46 µM in HeLa cells in the logarithmic phase. Smaller (Au0.8MS, Au1.2MS) and larger AuNPs were less toxic (Au1.8MS) or even non-toxic (Au15MS) in the highest concentration that was applied. Au5.6MS was tested up to a concentration of 150 µM and was not toxic in this concentration. In a subsequent experiment it was found that the IC₅₀ of Au4.6MS, a different batch but synthesized *via* the same route as Au5.6MS, is 370 µM.[118] The IC₅₀ value for Au5.6MS is presumably in the same order of magnitude or even higher than this value.

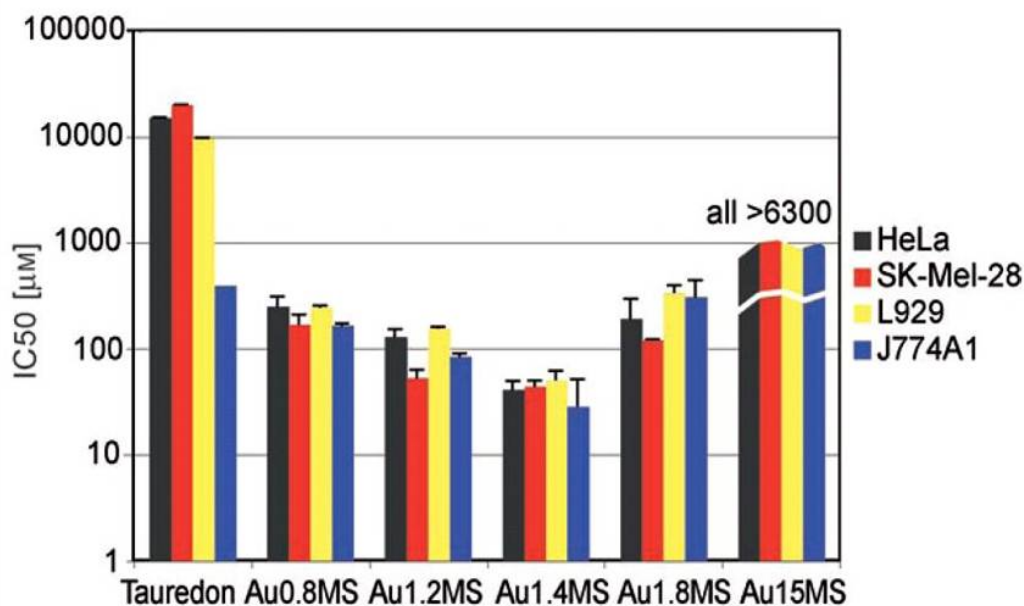


Figure 3.4: IC_{50} values of different AuNPs and Tauredon as reference for four different cell lines, determined in the logarithmic growth phase.[117]

The mononuclear reference substance, Tauredon[®], had an IC_{50} value of 19 mM in logarithmically growing HeLa cells. This is a first indicator that the cytotoxicity of AuNPs is not induced by ionic gold species; this issue is further discussed in chapter 3.7.

The pure ligand TPPMS was also tested and resulted in an IC_{50} value of 600 μ M. For the most toxic species, Au1.4MS, the molecular ratio of Au:TPPMS is 55:12. At the IC_{50} concentration of 46 μ M (gold atom concentration), the TPPMS concentration thus amounts to 10 μ M, being significantly below the IC_{50} concentration of TPPMS itself. It could be imaginable that the AuNPs act as a carrier for TPPMS. This would lead to spatially accumulated TPPMS molecules and a locally increased ligand concentration, potentially being more harmful than the free TPPMS. However, this hypothesis would not explain the size dependence with a maximum for a medium size of 1.4 nm as it was found. Furthermore, this could later be disproven when a mixture of Au1.4MS with additional TPPMS was tested (see chapter 3.4.3) and showed a significantly lower cytotoxicity than Au1.4MS alone. The moderate cytotoxicity of TPPMS is therefore considered to be not related to the high toxicity of Au1.4MS.

For the size dependence of AuNP cytotoxicity a variety of potential mechanisms can be named.

Nano-objects are in the same size range as cell components and proteins. A size-specific interaction of AuNPs with certain important cell functionalities is conceivable. Such an interaction might block the target entity and induce a fatal disturbance in the cellular signaling, motility and metabolism. It is possible that AuNPs of certain sizes fit better in the blocked structures than others and that there is a maximum of interaction and a resultant toxicity maximum for Au1.4MS. One possible target of such a size- or structure-related interaction is DNA, as explained by the model presented by Liu et al..[9] Here, an interaction of Au1.4MS with the phosphate groups in the major groove of the DNA double helix backbone is hypothesized. Such an interaction could block DNA transcription and therefore cause cell death. For a further discussion, see chapter 3.4.2.

Also, proteins might be impaired by AuNPs. It was shown for other nanomaterials (copolymer particles, cerium oxide particles, quantum dots, and carbon nanotubes) that they induce protein fibrillation which is related to various diseases.[119] A similar effect might be the reason for the cytotoxicity of AuNPs.

Another potential location of activity is the cell membrane. Nanoparticles may induce disruption of the membrane, or block certain essential functional entities. The effect of AuNPs towards HEK 293 cells, transfected with the hERG gene leading to a high expression of potassium channels, is further discussed in chapter 3.8. But also in other cell types without an enhanced number of ion channels in the membrane, lethal effects of AuNPs are imaginable.

It is also known that AuNPs with very small diameters are catalytically active for a range of reactions such as oxidation and hydrogenation reactions. The size dependence here is explained by the number of active sites, relative to the number of total gold atoms, i.e. the smaller the particle, the more energetically favored surface atoms are present. The toxicity of nanoparticles has been related to oxidative stress and reactive oxygen species (ROS) before.[13] It is imaginable that the cytotoxicity of AuNPs is directly related to the generation of ROS and that Au1.4MS is, due to its structure, the most potent ROS generating species of the AuNPs tested (see chapters 3.4.3 and 3.5 for further discussion).

In all scenarios the accessibility of the AuNP surface is crucial. If the effect is based on a blockade of cell functions, it seems plausible that the TPPMS shell is stripped at some time point of the cell incubation, and that it is the bare gold core that interacts with the target. On the other hand, the generation of ROS would very probably take place on the gold particle surface as well. In both cases, the interaction between gold core and ligand shell might play a role in the toxicity progress, and varying the binding strength between gold and ligand might affect the toxicity potential of a given AuNP size.

3.3 Ligand-Dependent Cytotoxicity: Phosphine vs. Thiol

Thiols have a generally higher affinity towards gold than phosphines (see chapter 2.1.4). DFT calculations on small clusters (Au_{38} and Au_{39}) resulted in a binding energy of 0.93 eV for the $\text{Au}-\text{PH}_3$ bond compared to 2.45 eV for $\text{Au}-\text{SCH}_3$.^[44]

Therefore, small thiol-stabilized AuNPs with a glutathione (GSH) ligand shell (Au1.1GSH) were synthesized in a direct synthesis approach.^[39] The UV/Vis spectrum and a STEM micrograph are depicted in fig. 3.5, respectively. The UV/Vis spectrum shows a simple decay which is typical for very small AuNPs. This is confirmed by the STEM analysis, resulting in a mean particle diameter of 1.1 ± 0.2 nm. Note that for other batches synthesized, AuNPs with a mean diameter of 1.5 nm were produced, therefore abbreviated as Au1.5GSH at the respective parts.

The cytotoxicity was tested under the standardized conditions. These particles were clearly less toxic than AuNPs of a comparable size but with the weaker binding TPPMS ligand. They showed an IC_{50} value of 3131 μM in HeLa cells in the logarithmic growth phase and are therefore 68-fold less toxic than Au1.4MS.

Furthermore, a mixture of Au1.4MS and 10 eq GSH was incubated and tested. The IC_{50} value determined was 181 μM . As thiols have a generally higher affinity to gold than phosphines, a ligand exchange resulting in Au1.4GSH was assumed. A first hint for a chemical reaction was the distinct solubility behavior, as the reaction product was less soluble in

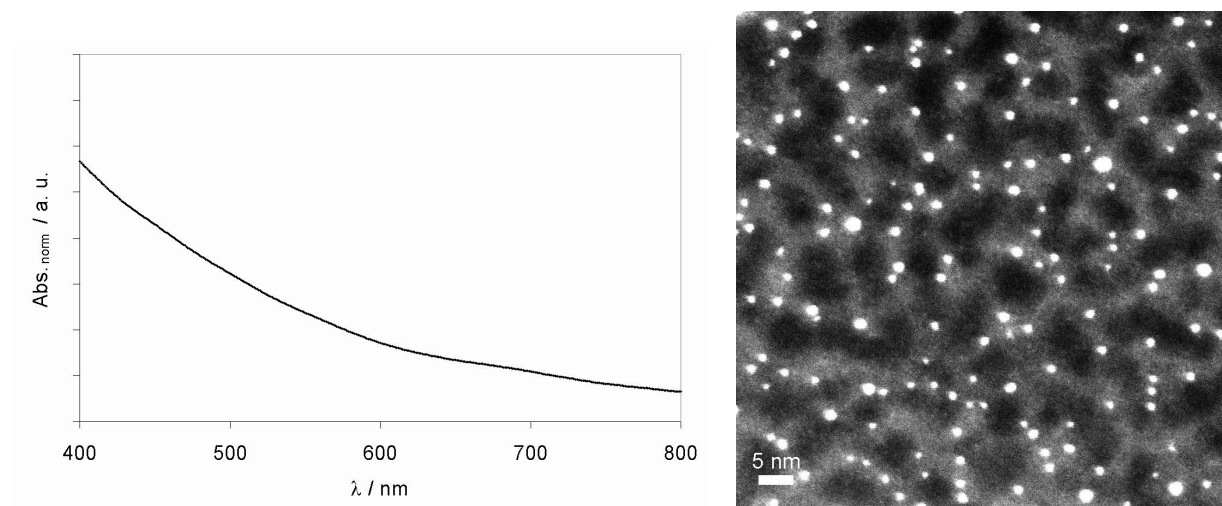


Figure 3.5: UV/Vis spectrum (left) and STEM micrograph (right) of Au1.1GSH.

bidistilled water, but was amphoteric and well soluble in acidic and basic solution. ζ potential measurements resulted in -48 mV in basic and +25 mV in acidic solution and confirmed the amphoteric nature of the AuNPs. Compared to that, Au1.4MS has a ζ potential of -42 mV in H₂O at pH 7 due to its acidic sulfonate group.

The method of ζ potential determination is exactly valid only for larger particles than the species investigated here. Thus, the quantitative values measured here are questionable. However, order of magnitude and especially the positive and negative prefixes point towards a ligand exchange reaction.

A ³¹P-NMR spectrum of washed and resuspended Au1.4GSH showed no signal, indicating a complete ligand exchange and no residual TPPMS. The IR spectrum showed the characteristic features of GSH, whereas the S-H stretching vibration at 2526 cm⁻¹ was missing (see fig.3.6). This indicates a binding mode of GSH towards the AuNP surface *via* the thiolate function.[120]

STEM analysis revealed a slightly broadened size distribution of the AuNPs, but still a mean diameter of 1.4 nm (see fig.3.7). The analytical investigations proved the ligand exchange of TPPMS against GSH.

Another analyzed material was the commercially available AurovistTM which consists of AuNPs with a mean diameter of 1.9 nm. The exact chemical formula of the ligand shell

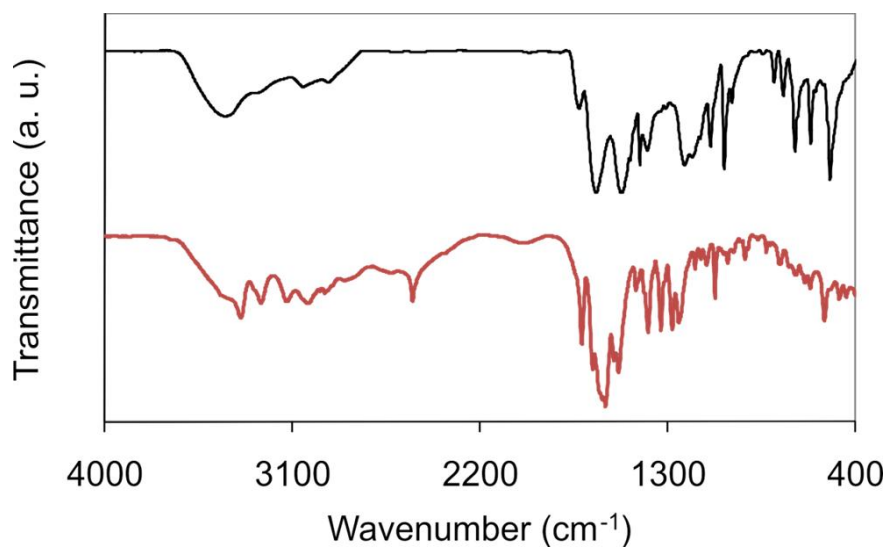


Figure 3.6: IR spectra of Au1.4GSH (black) and GSH (red).

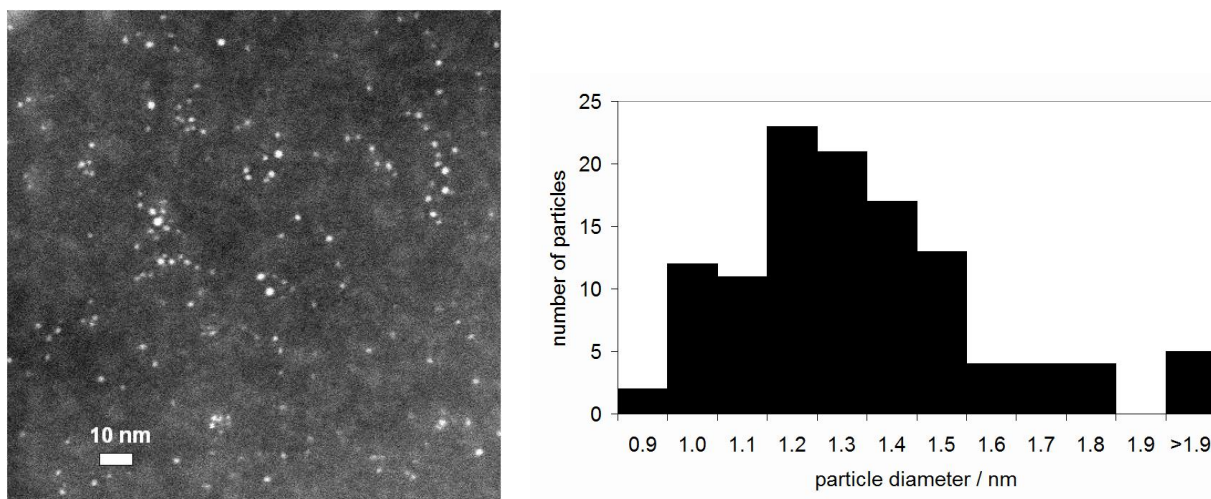


Figure 3.7: STEM micrograph (left) and histogram (right) of Au1.4GSH.

is not known for this material, but it consists of carboxylic acid containing thiols.[121] The IC_{50} value was determined to $9532\text{ }\mu\text{M}$.

Small thiol-stabilized AuNPs are obviously less toxic than phosphine-stabilized ones of a comparable size. As briefly explained above, this phenomenon is in accordance with both models of toxicity. The gold core is either too tightly wrapped into the thiol shell so that ligand stripping is inhibited, and the gold surface is not accessible to bind to a target cell functionality. Or the bound thiols shield the gold surface against O_2 adsorption so that no ROS can be generated and cause cell death. This can be compared to "poisoning" of the gold surface by thiols, as it is known for catalytic processes using metal surfaces or NPs in interaction with impurities of sulfur containing molecules in the feed.[122]

Further experiments that corroborate this finding are discussed in chapter 3.4.3. Another approach for a deeper understanding of the correlation between ligand–gold binding strength and toxicity was the synthesis of diphosphine-stabilized AuNPs (see chapter 3.10). Here, the chelating effect of a ligand molecule with two phosphine groups should enhance the stability of the bond between ligand and particle surface.

3.4 Cellular Response Reactions

3.4.1 Necrosis vs. Apoptosis

The mechanism of cell death was further investigated. HeLa cells in the logarithmic growth phase, incubated with AuNPs, were double stained with propidium iodide and annexin V and analyzed by flow cytometry. By this method, the two main cell death pathways necrosis and apoptosis can be differentiated. Au1.2MS and Au1.4MS were both used in their respective double IC_{50} concentrations (Au1.2MS: $285\text{ }\mu\text{M}$; Au1.4MS: $90\text{ }\mu\text{M}$). Cells were incubated for increasing incubation times (6, 12, 18, 24, 30, 39, 48 h). Untreated cells were analyzed as negative control. As a positive control to induce apoptosis, staurosporine was used. The percental values from flow cytometry are plotted in fig. 3.8.

Interestingly, the two AuNP species tested showed opposite results. Au1.2MS caused apoptosis to a larger extent (fig. 3.8 C). After 48 h, 90 % of the cells were dead, whereof 60 % went

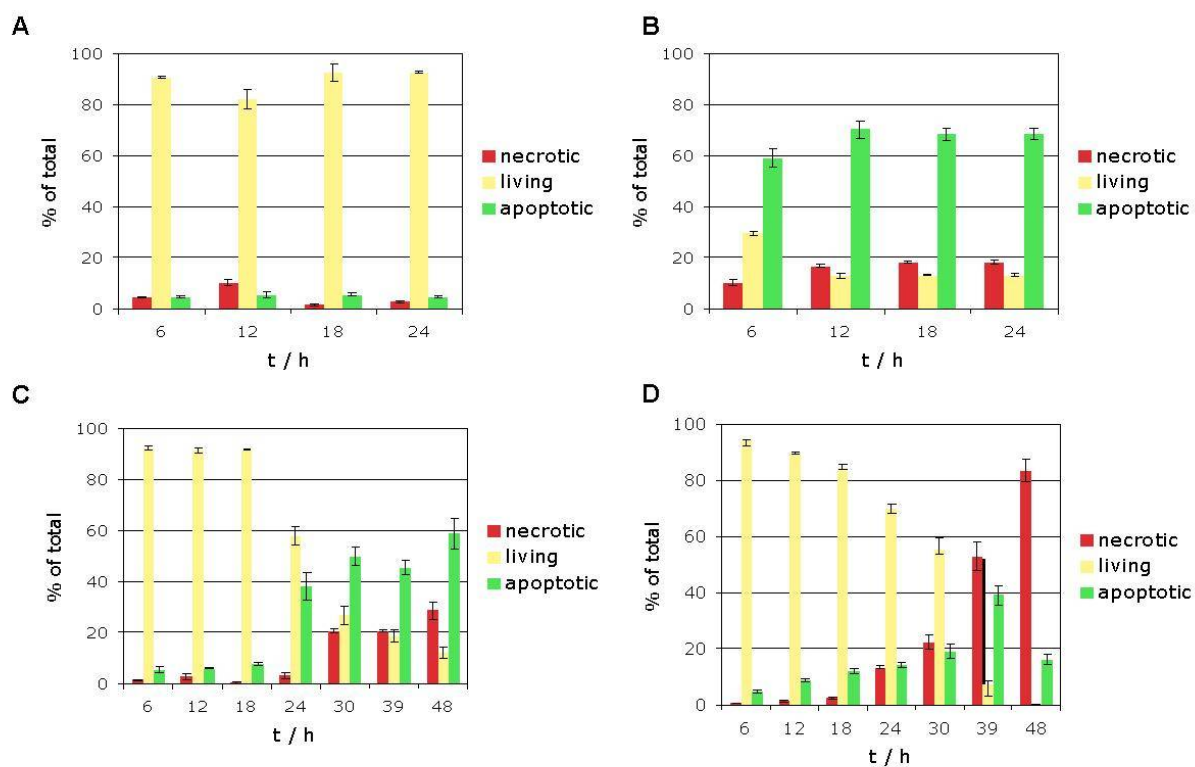


Figure 3.8: Results of flow cytometry after double staining with propidium iodide and annexin V (HeLa cells). A: untreated reference, B: staurosporine as positive apoptosis control, C: 285 μ M Au1.2MS, D: 90 μ M Au1.4MS.[117]

into apoptosis. On the other hand, Au1.4MS induced mainly necrosis (fig.3.8 D). After 48 h, 100 % of the cells were dead with 80 % necrotic cells. This difference in cell death mechanism was not obvious from the MTT assay, which is a classical end point analysis, but was only revealed by the kinetic study design.

The two materials comprise the same chemical components as they both consist of atomic gold cores and TPPMS ligand shells. Their main difference is a variation of 0.2 nm in the mean diameter of particle size, accompanied by a slightly varying number of TPPMS molecules per particle, caused by distinct synthesis routes. The number of TPPMS molecules per Au1.2MS particle was approximated to 30. The gold core consists of approximately 39 gold atoms (estimated by calculating the volume of a 1.2 nm sized sphere, with the atomic radius of gold of 144 pm and an atomic packing factor of 0.74 for the ccp structure). Au1.4MS has a gold atom to ligand ratio of 55:12, thus a lower relative concentration of TPPMS. Anyhow, for both materials the TPPMS concentration is below its critical concentration for the IC₅₀ concentrations of the AuNPs.

The fact that Au1.2MS and Au1.4MS induce different kinds of cell death can be interpreted in two ways. Depending on the exact toxicity mechanism behind, it is possible that the two AuNP species trigger different cell response cascades. This would for example be the case if a size-specific blocking of a biologically essential functionality by the AuNPs is taking place, and the two different AuNP species hit different points of action. On the other hand, Au1.4MS was found to be more toxic than Au1.2MS. It is therefore possible that simply the severity of toxicity causes a sudden necrotic cell response, whereas the slightly less toxic Au1.2MS enables the cell to activate the apoptosis pathway.

3.4.2 Gene Regulation

With a genome-wide mRNA expression analysis (Affymetrix Genechips®), the influence of AuNPs on cellular gene expression was investigated. HeLa cells were incubated with 100 µM Au1.4MS and 1000 µM Au15MS for 1, 6 and 12 h. mRNA was extracted from the cells and reverse transcribed into cDNA. The purified cDNA was used to synthesize biotinylated complementary RNA samples which were hybridized to the DNA array. By comparing

the read-out values to results from untreated cells and by performing a hierarchical cluster analysis, differences in gene regulation could be identified.

Cells incubated with Au1.4MS showed a distinct gene profile compared to the reference. After an incubation time of 1 h, some genes were already significantly up-regulated (fig. 3.9). After 6 h and more pronounced after 12 h, Au1.4MS had induced an oxidative stress response. 35 genes showed an enhanced expression. These were mainly heat shock and stress related genes. On the other hand, several cell cycle related genes were down-regulated. In contrast, the non-toxic Au15MS did not induce a strong reaction towards the gene regulation for any incubation time.

The results show that the cytotoxicity of Au1.4MS is not primarily based on a DNA interaction, leading to a direct transcriptional inhibition, as some genes are up-regulated within the time frame of the experiment. However, an interaction with DNA at a later date cannot be excluded from these results. Also, the findings are in agreement with the fact that Au1.4MS induces mainly necrosis.

3.4.3 Oxidative Stress

As mentioned above, the generation of ROS is an often discussed topic concerning the toxicity of nanoparticles. To investigate if this holds true for AuNPs as well, another flow cytometry experiment was performed. Here, 5-(and-6)-chloromethyl-2',7'-dichlorodihydrofluorescein diacetate, acetyl ester (CM-H₂DCFDA) was used as a staining reagent. This fluorescein derivative has two acetate groups and shows no fluorescence in its reduced form. In the presence of ROS, CM-H₂DCFDA is oxidized, the acetate groups are cleaved and the fluorescence of the reaction product is detectable (fig. 3.10).

HeLa cells were incubated for 48 h with 1000 μ M of Au1.1GSH and Au15MS, respectively. Au1.4MS was applied in a lower concentration of 100 μ M with increasing incubation times (6, 12, 18, 24, and 48 h, respectively). Untreated cells were analyzed as negative control, and 30 min incubation with 0.3 % H₂O₂ served as positive control for oxidative stress.

The fluorescence curves (see fig. 3.11) clearly show that Au1.4MS causes oxidative stress in HeLa cells in a time-dependent manner. The non-toxic AuNPs Au1.1GSH and Au15MS on the other hand do not induce ROS formation although applied in 10-fold higher con-

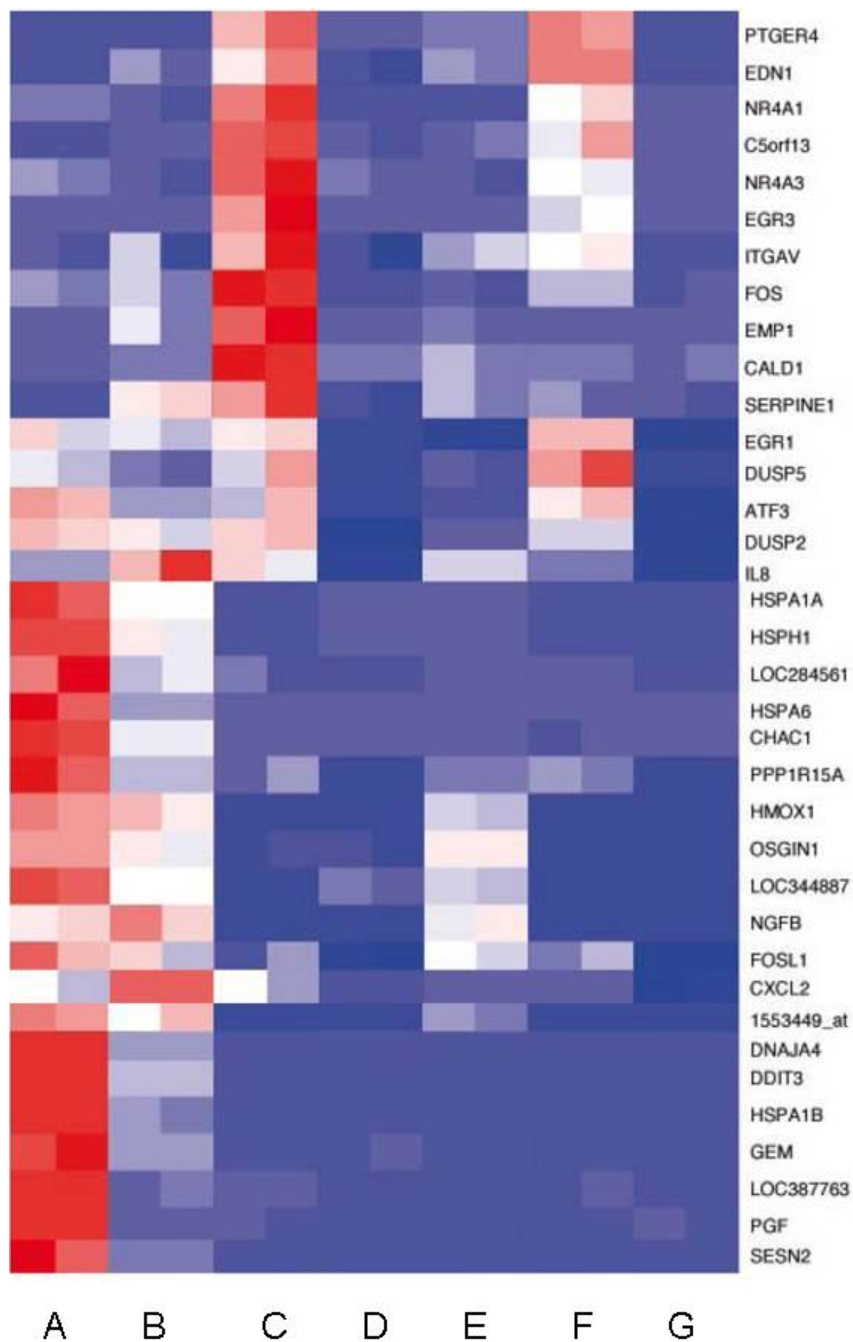


Figure 3.9: Gene chip results. Vertically ordered rows: genes with distinct expression profiles. The boxes show (in duplicate) from right to left: expression profile of control (G); after incubation with Au15MS after 1 (F), 6 (E) and 12 h (D), and Au1.4MS after 1 (C), 6 (B) and 12 h (A), respectively, compared with the median expression level of the gene's transcript for all samples shown. Blue: below median; white: equal to median; red: above median.[123]

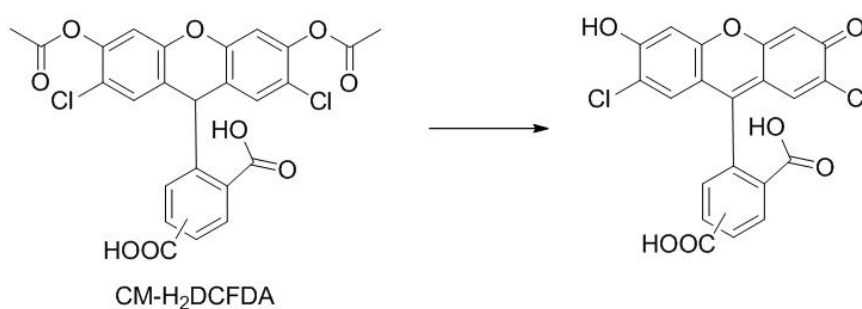


Figure 3.10: Reaction of CM-H₂DCFDA to its fluorescent derivative. This reaction is used to indicate the presence of ROS.

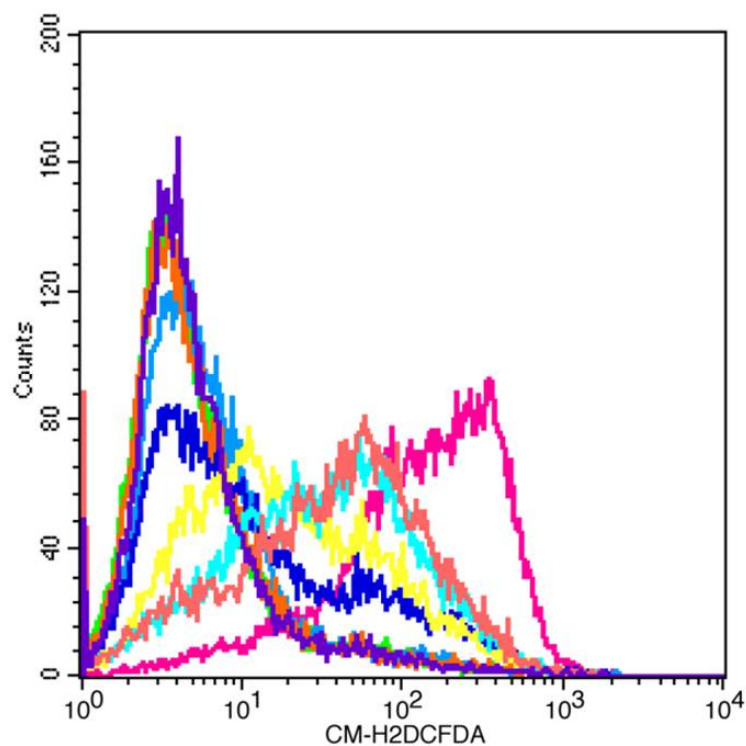


Figure 3.11: Flow cytometry results, plotted as one-parameter histograms, of cells incubated with Au1.4MS, Au15MS and Au1.1GSH and stained with CM-H₂DCFDA.

Green: untreated HeLa cells (no oxidative stress). Pink: HeLa cells treated with 0.3 % H₂O₂ for 30 min (strong oxidative stress). Violet: HeLa cells treated for 48 h with 1000 μ M Au15MS. Orange: 1000 μ M Au1.1GSH. All others: HeLa cells treated with 100 μ M Au1.4MS for 6 (medium blue), 12 (dark blue), 18 (yellow), 24 (light blue), and 48 h (light orange), respectively.[123]

centrations. This result is a hint that the cytotoxicity of Au1.4MS is related to oxidative stress.

Unfortunately, this result is ambiguous as it is also possible that the detected oxidative stress is an indirect secondary effect of the necrosis that Au1.4MS definitively induces. The different sources for nanoparticle related oxidative stress were also discussed by Krug et al.: the direct generation of ROS at the nanomaterial surface or a catalytic effect of transition metals, damage of mitochondria and thereby a disturbance in the respiratory chain, or an increased ROS level induced by the activation of macrophages or neutrophils.[5]

The effect of anti-oxidants towards the cytotoxicity of Au1.4MS was investigated. *N*-acetylcysteine (NAC), GSH, TPPMS and ascorbic acid were used (NAC in 3 mM; GSH, TPPMS, and ascorbic acid in 1 mM concentrations). The chemical structures and IUPAC names are shown in fig. 3.12.

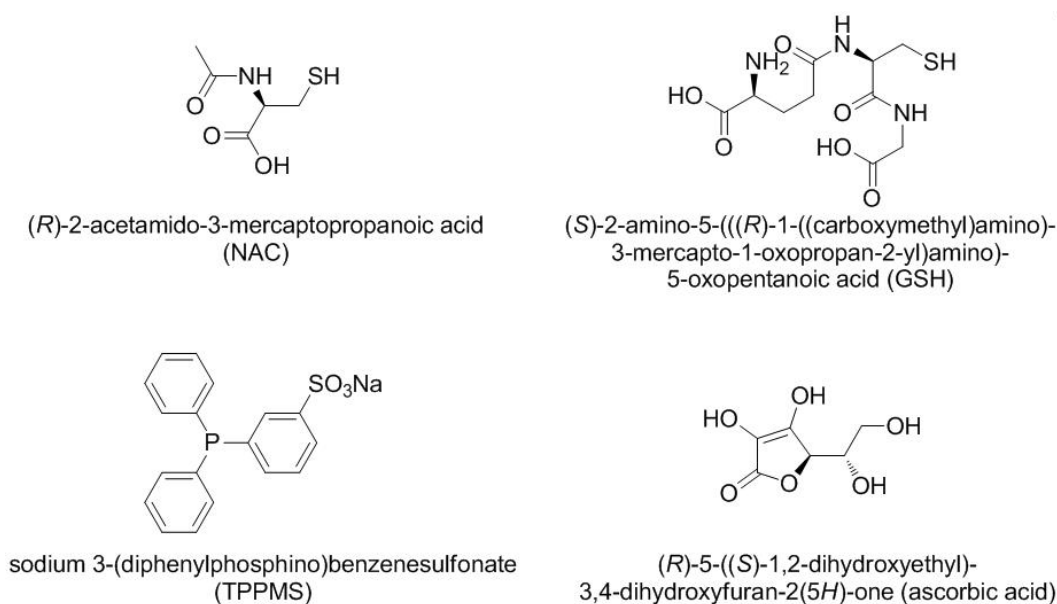


Figure 3.12: The four anti-oxidants tested for their inhibition potential of Au1.4MS toxicity.

Different incubation schemes were followed: either the HeLa cells were pre-incubated with anti-oxidants and subsequently with 100 μ M Au1.4MS (with (C) or without interjacent washing (E)), or Au1.4MS was pre-treated with anti-oxidants and added immediately (F) or after 3 h (D) to cells. The effects of the pure anti-oxidants was also tested (G).

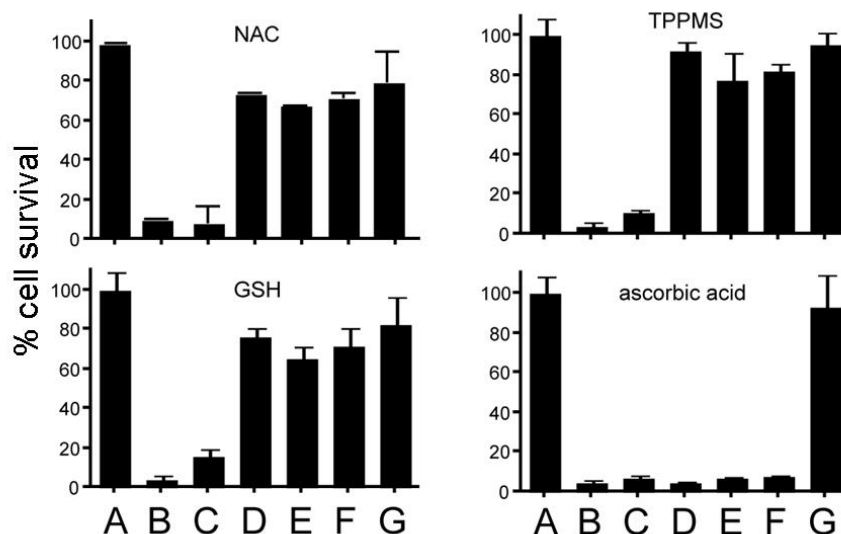


Figure 3.13: Effect of diverse anti-oxidants towards cytotoxicity of Au1.4MS.

A: untreated reference. B: positive reference (100 μ M Au1.4MS). C: cells pre-incubated with anti-oxidants, washed, incubated with Au1.4MS. D: Au1.4MS pre-incubated with anti-oxidants (3 h), mixture added to cells. E: cells pre-incubated with anti-oxidants, no washing step, incubated with Au1.4MS. F: Au1.4MS pre-mixed with anti-oxidants, mixture added to cells immediately. G: pure anti-oxidants.[123]

As can be seen in fig.3.13, NAC and GSH can protect the cells from the toxic impact of Au1.4MS if the AuNPs are pre-incubated with the anti-oxidants (D, F) or if those are present in the cell culture medium when the AuNPs are added (E). TPPMS has the same tendency, but with lower efficacy. A pre-incubation with subsequent washing of the cells does not influence the toxicity of Au1.4MS (C). This points to an interaction of the anti-oxidants with Au1.4MS, not with the cells. This interaction could be a direct ligand exchange as shown before (3.3), or an indirect interaction by capturing and neutralizing the ROS that are potentially generated and related to the AuNP toxicity.

Ascorbic acid on the other hand does not have a protecting effect. NAC and GSH as thiols and TPPMS as a phosphine have functional groups with high binding affinities to the AuNP surface. This is not the case for ascorbic acid, as its OH groups have only weak affinity towards gold. It is therefore likely that a direct interaction of NAC, GSH and TPPMS with the AuNP surface is responsible for the reduced toxicity. A ligand exchange with GSH was already shown (see 3.3). NAC will probably react in the same way with AuNPs. TPPMS

will either build a closer packed ligand shell around the particles, or an excess of TPPMS influences the desorption equilibrium in solution and leads thereby to a less accessible AuNP surface. Ascorbic acid cannot attach strongly onto the AuNP surface and has therefore no effect in this experiment.

3.5 EPR Spectroscopy with AuNPs

One hypothesis concerning the toxicity mechanism of nanomaterials states that the generation of ROS plays a key role. This is related to the ability of AuNPs to catalyze oxidation reactions (chapter 2.1.2.3). Likewise the findings about the cytotoxicity of AuNPs, their catalytic activity is often related to size and functionalization. The former, the AuNP size, determines the number of active surface atoms per particle, especially activated edge and vertex atoms. The ligand shell chemistry affects the accessibility and the chemical and therefore catalytic activity of these surface atoms. Corresponding to toxicity, small AuNPs with weakly bound ligands are potentially more active to generate toxic oxygen radicals than larger particles or particles with inactivating, strongly bound ligands.

The findings of Turner et al. that especially $\text{Au}_{55}[(\text{C}_6\text{H}_5)_3\text{P}]_{12}\text{Cl}_6$ is more potent than other AuNPs in the oxidation reaction of styrene to benzaldehyde enforced the hypothesis that the strong cytotoxicity of Au1.4MS could be based on the generation of ROS.[29] The general correlation between oxidative stress and AuNP toxicity could be shown with the substrate CM- H_2DCFDA (3.4.3), although it is here not possible to differentiate between primary ROS generation and subsequent cell death or firstly induced necrosis and, as a secondary effect, related increase of oxidative stress in dying cells (see fig 3.14).

One way to analyze the potential catalytic activity towards oxidation reactions of AuNPs is the reaction with a stable radical substrate and the analysis by EPR spectroscopy.[78] According to the experiments of Zhang et al., 4-Amino-2,2,6,6-tetramethylpiperidine-1-oxyl (Amino-TEMPO), a stable radical, was used as a substrate for an indirect detection of ROS. It can catalytically be oxidized to the also EPR active 4-Oxo-2,2,6,6-tetramethyl-1-piperidinyloxy (Oxo-TEMPO) (reaction scheme in fig. 3.15).

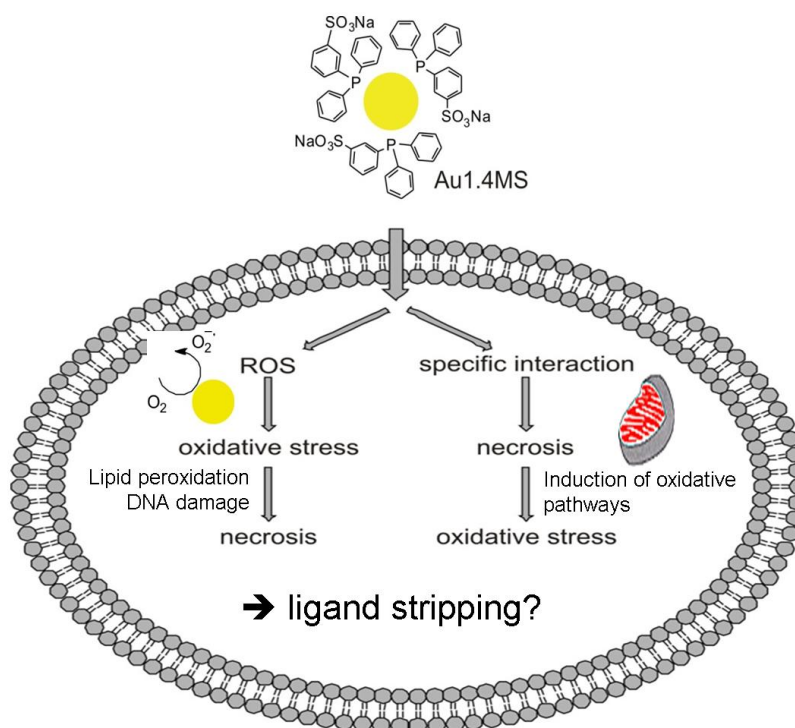


Figure 3.14: Scheme depicting the possible pathways related to oxidative stress induced by AuNPs, as a primary (left) or secondary (right) effect in the cell. Both pathways might include a ligand stripping step.

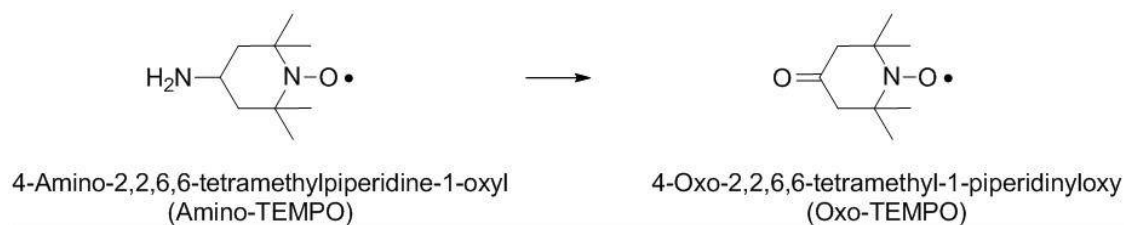


Figure 3.15: Oxidation reaction of Amino-TEMPO to Oxo-TEMPO.

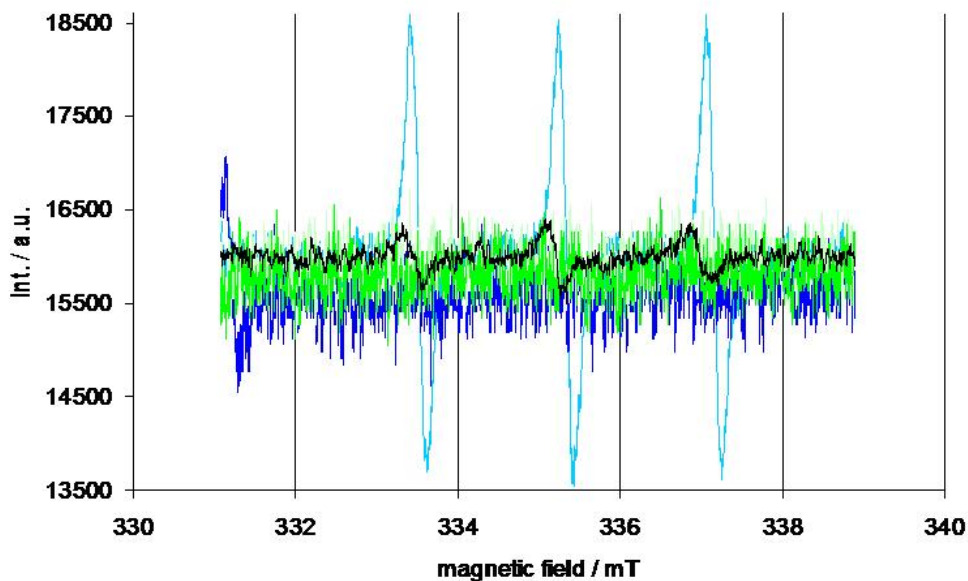


Figure 3.16: EPR spectra of Amino-TEMPO solutions with different concentrations of Au15Citrate. Light blue: Amino-TEMPO reference; blue: 5.8 mM; gray: 2.9 mM; green: 1.16 mM; black: 0.58 mM.

Concentrated solutions of Au15Citrate, Au15MS, Au1.4MS and Au1.5GSH were saturated with O_2 or Ar, respectively. The oxidation reaction of Amino-TEMPO to Oxo-TEMPO should be inhibited in the samples prepared under Ar atmosphere, the saturation with O_2 should on the other hand facilitate the reaction. The prepared AuNP solutions were mixed with equally treated saturated stock solutions of Amino-TEMPO at moderately basic pH, and the amounts of detectable Amino-TEMPO were determined by EPR spectroscopy.

Interestingly, in difference to the findings of Zhang et al., in none of the experiments a generation of Oxo-TEMPO was observed. The effects under oxygen and argon atmosphere were very similar. From the four AuNP species tested, only Au15Citrate was able to quench the EPR signal of Amino-TEMPO (see fig. 3.16).

This points to an adsorption of the Amino-TEMPO molecules onto the AuNP surface. In this manner, the unpaired electron of the radical may interact with the electron pool of the metallic nanoparticle, and therefore the radical character of Amino-TEMPO is lost and it is not detectable in the EPR anymore. As can be seen in fig. 3.16, the quenching potential of Au15Citrate is concentration dependent. In the lowest concentration of approximately 0.58 mM (black curve in fig. 3.16), the characteristic features of the EPR spectrum of Amino-

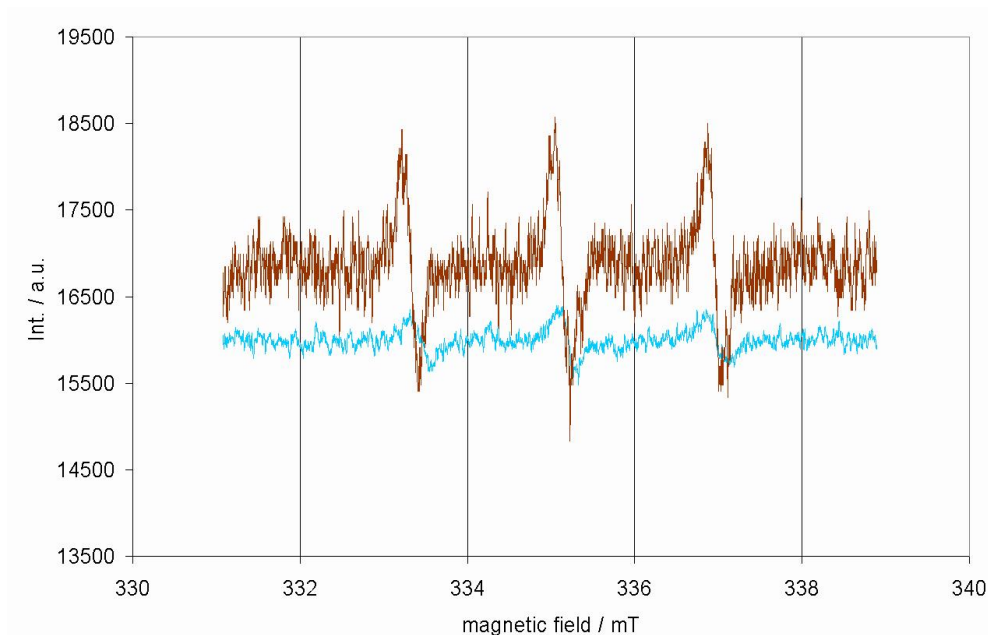


Figure 3.17: Sample of Au15Citrate with Amino-TEMPO, measured directly after mixing (brown) and after 24 h (blue).

TEMPO are still visible, although already with considerably lower signal intensity. In higher AuNP concentrations, the signal is completely quenched. Moreover it was observed that the signal of Amino-TEMPO in a sample further decreased over longer periods of time. A sample that was left at room temperature for 24 h and was measured again showed a further drop in signal intensity to approximately 20 % of the original intensity, indicating a continued slow adsorption (fig. 3.17).

All other AuNPs behaved differently in the experiments (fig. 3.18). The Amino-TEMPO signal was not quenched at all by Au15MS, Au1.4MS and Au1.5GSH, not even at concentrations of 8.2 mM (Au15MS), 4.7 mM (Au1.4MS) and 5.4 mM (Au1.5GSH), respectively. The results under oxygen and under argon atmosphere were identical. This finding indicates that the accessibility of the AuNP surface plays a crucial role for the Amino-TEMPO adsorption. In the case of citrate which is the weakest ligand in this set of AuNPs, Amino-TEMPO can interact with the AuNP surface, probably *via* its amino function as amines are known to act as AuNP ligands as well. Possibly, the Amino-TEMPO replaces the citrate from the AuNP surface and becomes thereby EPR inactive. In case of TPPMS- or GSH-stabilized AuNPs, the ligands bind more strongly to the AuNP surface and a reaction with

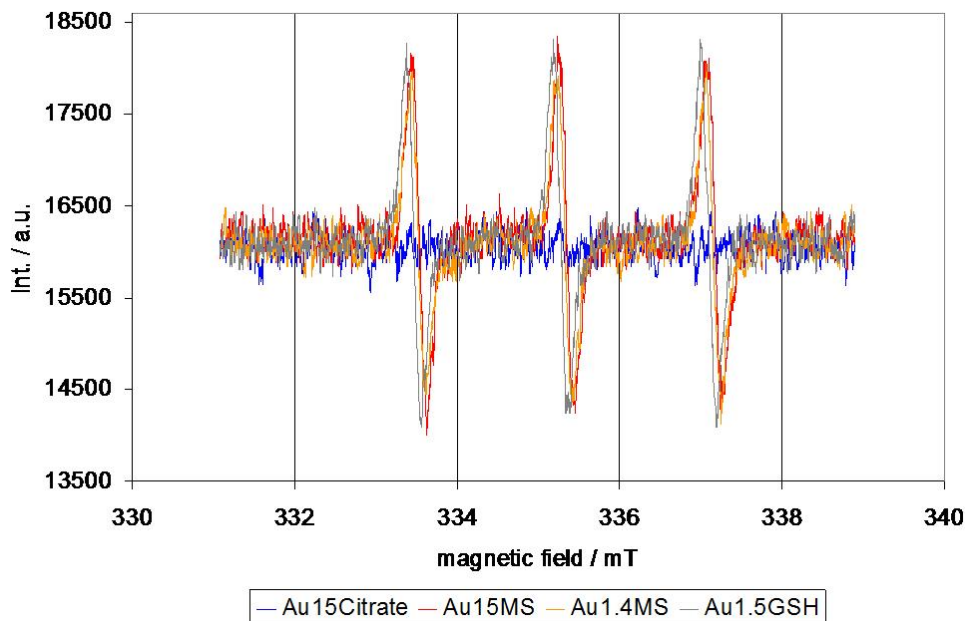


Figure 3.18: EPR spectra of samples of Amino-TEMPO with different AuNP species (blue: Au15Citrate (2.3 mM), red: Au15MS (8.2 mM), orange: Au1.4MS (4.7 mM), gray: Au1.5GSH (5.4 mM)).

Amino-TEMPO is inhibited. A reference experiment with pure citrate was performed to exclude any reaction between citrate and Amino-TEMPO. Here, the Amino-TEMPO was detectable without any quenching.

A set of experiments, under the same conditions as the previously performed ones but with the addition of Oxo-TEMPO instead of Amino-TEMPO, was conducted. The results were comparable to the Amino-TEMPO experiments: Au15Citrate was able to quench the radical, the other AuNPs had no influence on the signal intensity. Obviously, the oxo function of Oxo-TEMPO, or the tertiary amine, or both in a concerted way, may interact with the AuNP surface of weakly stabilized AuNPs. This differs from the results found by Zhang et al., who proposed that Oxo-TEMPO interacts less strongly with AuNPs than Amino-TEMPO and becomes therefore detectable after an oxidation reaction of Amino-TEMPO with AuNPs.

The results from EPR spectroscopy show an interaction of Amino-TEMPO only with Au15Citrate, probably as an adsorption, but not necessarily an oxidation reaction. As it was found that Oxo-TEMPO is quenched by Au15Citrate as well, this question cannot

be answered by EPR spectroscopy. The results from the experiments performed under O₂ and Ar atmosphere are comparable. This points noticeably to an adsorption rather than an oxidation reaction.

Furthermore, it is obvious that the reactivity of different AuNPs with Amino-TEMPO does not correlate with their cytotoxicity. This is in opposition to the hypothesis that primary ROS generation plays a crucial role in the toxicity mechanism of Au1.4MS.

3.6 Genotoxicity Studies

The cytotoxicity of AuNPs is possibly related to the blockade and/or damage of important cellular structures. Besides potential contact points such as the cell membrane, proteins, enzymes or organelles like the mitochondria, another possible target of such an interaction is DNA. Conflicting conclusions can be drawn from the so far discussed results. A cell fractionation experiment with BLM cells, treated with Au1.4MS and subjected to subsequent neutron activation analysis (NAA) showed a gold content of 42.5 % in the nuclear fraction with 21.1 ± 2.9 % bound to DNA.[8] A possible interaction of Au1.4MS with the major groove of the DNA backbone was proposed. On the other hand, the gene chip analysis (see chapter 3.4.2) revealed predominantly up-regulation of a number of genes after AuNP incubation. This controverts a full blockade of DNA transcription, i. e. the immediate inhibition of transcription activity.

Further experiments were necessary to answer the question of AuNP induced genotoxicity. An elegant method to determine DNA damage is the GC/MS analysis of DNA, more precisely the detection and quantification of oxidized DNA bases.[98]

Two sets of samples were prepared by Dr. Yu Pan-Bartneck (UKA). HeLa cells were incubated for 3, 24, and 72 h with three different AuNP species, respectively: Au1.4MS, Au15MS and Au1.1GSH. Afterwards, the DNA was extracted from the cells (see fig. 3.19). Furthermore, the same AuNPs and incubation times were applied on pure DNA which was previously extracted from HeLa cells.

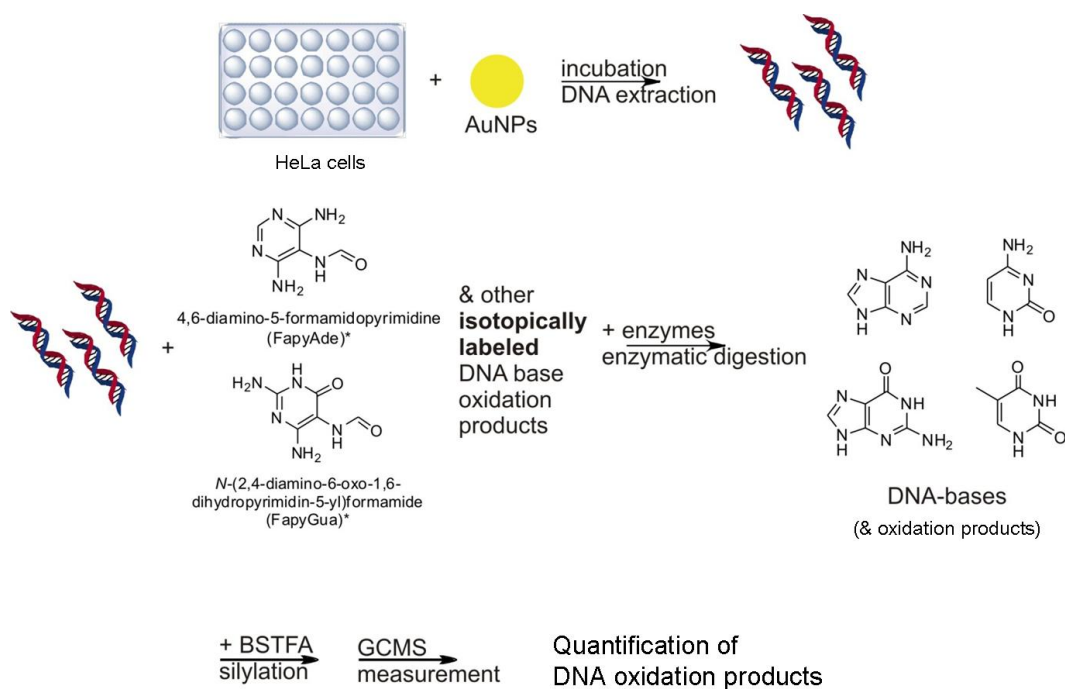


Figure 3.19: Scheme of sample preparation for genotoxicity studies (sample set 1). HeLa cells were incubated with AuNPs, DNA was extracted, isotopically labeled DNA oxidation products were added, and after further treatment the concentrations of DNA oxidation products were determined by GC/MS.

The further treatment of the samples and the GC/MS measurements were conducted at the National Institute of Standards and Technology (NIST; Gaithersburg, MD, USA), together with Dr. Bryant Nelson and Dr. Elijah Petersen.

Defined amounts of isotopically labeled derivatives of seven typical oxidation products (lesions) of DNA bases were added to the samples prior to an enzymatic digestion of the DNA (all lesions that were investigated are shown in fig. 3.20). The samples were analyzed by GC/MS, and the amounts of lesions could be quantified by comparing the integrals of the gas chromatography peaks of the lesion and the respective isotopically labeled species.

In the case of oxidative damage of DNA induced by AuNPs, a significant increase of one or several lesion concentrations compared to the reference samples was expected. Interestingly, in the first set of samples (the incubated cells), the concentrations of the lesions FapyAde and FapyGua were significantly decreased by Au1.4MS and Au1.1GSH (fig. 3.21). This was

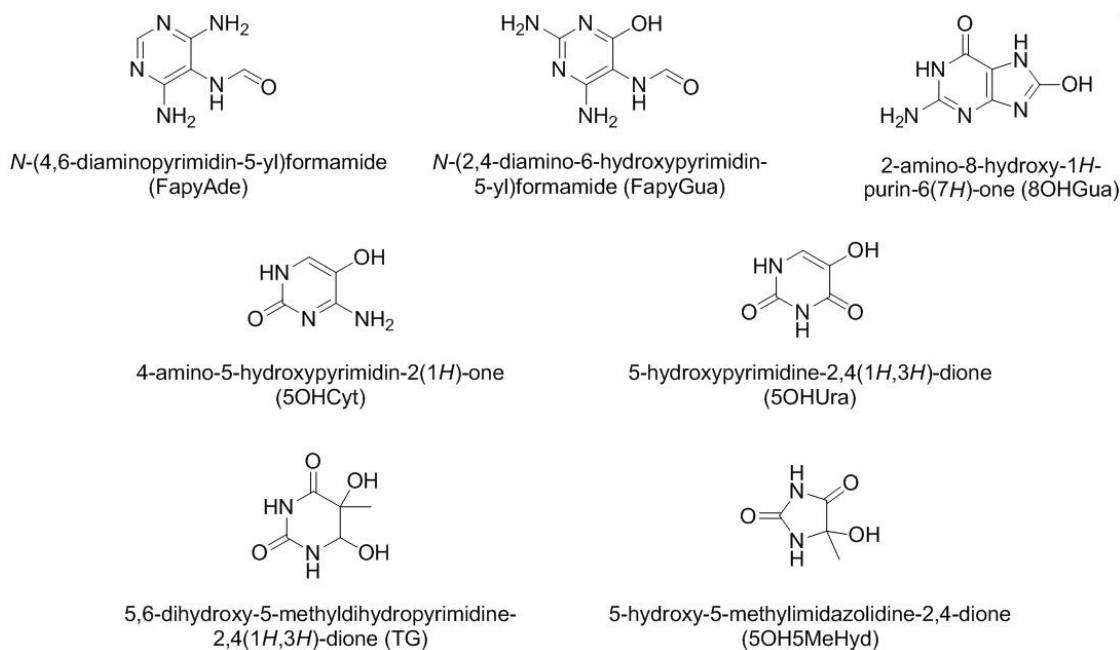


Figure 3.20: The DNA oxidation products (lesions) that were examined by GC/MS in DNA samples from HeLa cells, incubated with AuNPs.

constant over all time points. The concentrations of the other lesions investigated were not altered significantly. Also, Au15MS had no measurable effect at any time point.

These findings were surprising for two reasons: No lesion concentration was increased, as was expected before; instead, two lesions were depleted. Furthermore, Au1.1GSH behaved similarly as Au1.4MS, although the two AuNP species have completely different cytotoxicity profiles. A distinction of FapyAde and FapyGua from the other lesions can be explained by the formation mechanism of these two lesions.

Generally, DNA bases are attacked by a ROS, typically the $\cdot\text{OH}$ radical. The thus formed base radical can further react in different ways. For FapyAde and FapyGua, the second reaction step is a one-electron reduction, either preceded or followed by a ring opening. This one-electron reduction is unique for these two lesions and might be the impaired reaction step.[99]

The second sample set on the other hand, the samples of DNA incubated directly with AuNPs, did not show any significant change, irrespective of the AuNP species or the incubation time (fig. 3.22). No lesion concentration was increased which would have pointed

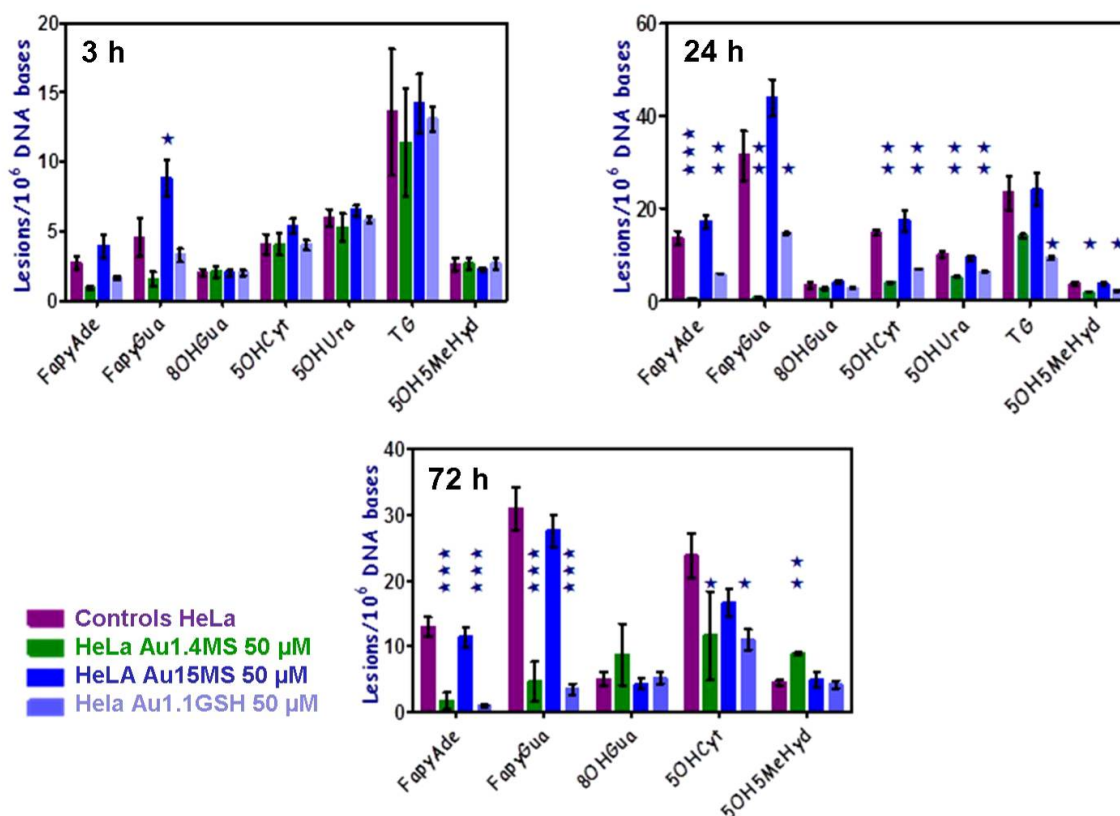


Figure 3.21: Lesion concentrations from the first sample set (HeLa cells). Each lesion point consists of four values: untreated reference (purple), cells treated with Au1.4MS (green), Au15MS (blue), and Au1.1GSH (light blue; all AuNPs applied in 50 μ M, respectively). The three graphs depict three incubation times (3; 24; 72 h). For 72 h, 5OHUra and TG are not depicted because the GC/MS data were not integrable. Results were statistically analyzed by analysis of variance (ANOVA). P values: < 0.001: Extremely significant ***. 0.001 to 0.01: Very significant **. 0.01 to 0.05: Significant *. >0.05: Not significant.

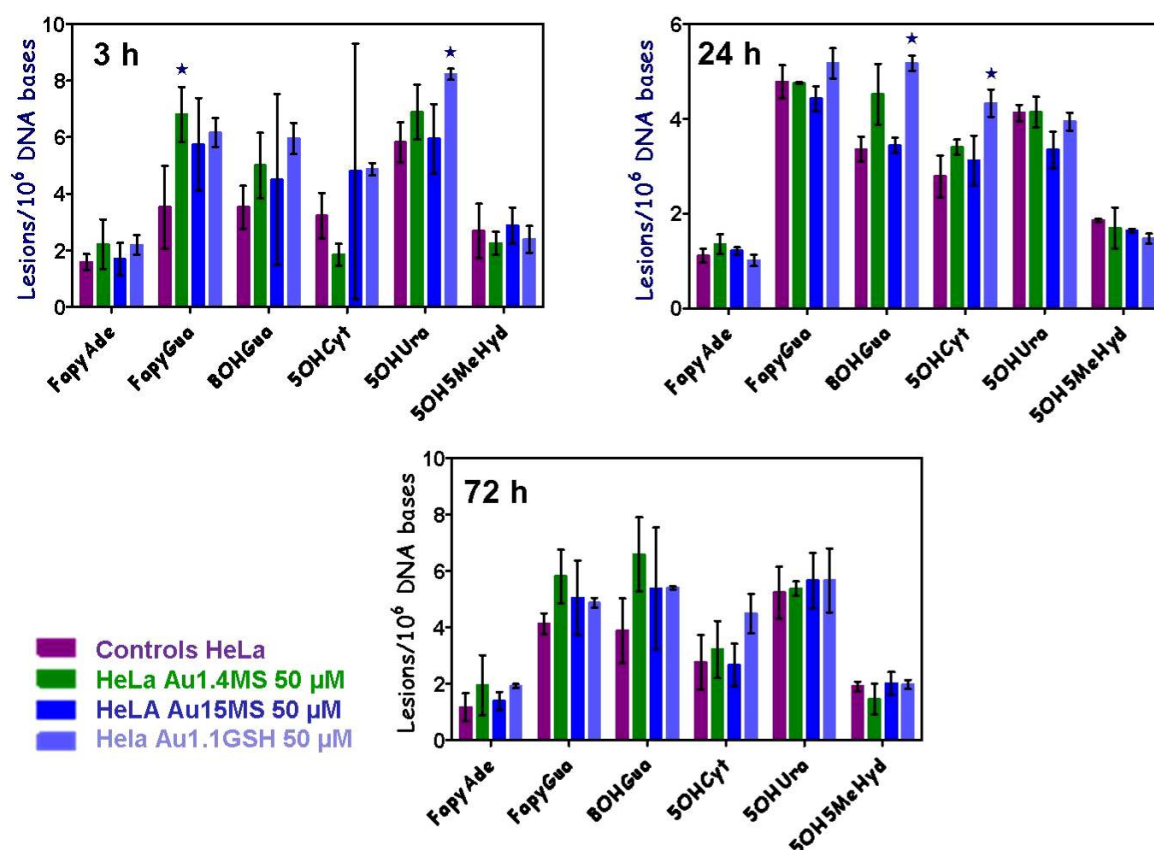


Figure 3.22: Results from second sample set (extracted DNA treated with AuNPs). Each lesion point consists of four values: untreated reference (purple), DNA treated with Au1.4MS (green), Au15MS (blue), and Au1.1GSH (light blue; all AuNPs applied in 50 μ M, respectively). The three graphs depict three incubation times (3; 24; 72 h). Results were statistically analyzed as in fig. 3.21.

to a catalytic oxidation effect by AuNPs; also, no decrease of FapyAde and FapyGua was found as in the case of incubated cells.

All samples should be further investigated by the more sophisticated LC/MS/MS method. Besides a different separating step (liquid chromatography (LC) instead of gas chromatography (GC)), in LC/MS/MS either two mass spectrometry units are connected in series, or ion traps are included. Ions can be separated and specifically further ionized and analyzed. Fragmentation patterns can thus be investigated in detail.

However, no clear results were received. As these measurements were performed several months after the GC/MS investigations and the samples were stored in the freezer ($T =$

–20 °C) in between, but exposed to air, it is very probable that the samples had been altered during storage. The results from these measurements were therefore discarded and not further interpreted.

From the findings of the GC/MS measurements, no direct correlation between the results and the AuNP cytotoxicity can be found, as Au1.4MS and Au1.1GSH give similar results despite their different cytotoxicities. Some hypotheses regarding these surprising results can be discussed:

The catalytic properties of AuNPs were already discussed before. As such reactions on the AuNP surface depend on the chemical equilibrium, under certain conditions it is conceivable that the back reaction takes place. In the case of a relatively high concentration of radicals, the AuNPs could potentially capture these and catalyze a reaction to less reactive species. However, a correlation between toxic effects and catalytic activity of AuNPs could not been shown in other experiments. Also, there is no reason why two out of seven investigated lesions should preferentially be protected from oxidative damage.

Another concept is a protecting interaction of AuNPs with DNA. A preference towards certain lesions could then stem from a stronger interaction of the AuNPs with the respective bases; but this hypothesis does not explain why the AuNPs did not have the same effect on the second sample set of pure DNA.

The third scenario is the enhanced activity of DNA repair enzymes. This can either happen *via* an activation of present enzymes through some kind of interaction of the AuNPs with these enzymes, or as an up-regulation of transcription of certain enzymes induced by the AuNPs. This would explain why the whole cells incubated with AuNPs showed significantly altered lesion concentrations whereas the pure DNA without repair enzymes present and without ongoing transcription did not show the same effects. Furthermore, there are base specific DNA repair enzymes which would account for the decrease of only two of the examined lesions.

One example of a purine specific DNA repair enzyme is encoded by the *nei* endonuclease VIII-like 1 gene and therefore abbreviated as NEIL1.[124] The results from the gene chip analysis (see chapter 3.4.2) showed no up-regulation for NEIL1. However, it is possible that the AuNPs do not induce enhanced transcription but an enzyme activity enhancement.

Further experiments were therefore conducted at NIST. Two sample sets were generated: the enzyme NEIL1 was pre-incubated with Au1.4MS and then added to DNA. Here, γ -ray irradiated calf thymus DNA (ct-DNA) with an artificially increased number of lesions was used. In the second set, AuNPs and ct-DNA were pre-incubated and NEIL1 was added in a second step. An excision assay was performed, i. e. the supernatants of the samples were analyzed by GC/MS for lesion concentrations of FapyAde and FapyGua.

If NEIL1 was activated by the presence of Au1.4MS, the concentrations of FapyAde and FapyGua should be increased in the supernatant. Interestingly, the opposite was the case. In the first sample set, both Fapy lesion concentrations were decreased compared to the reference. This points towards a deactivation of NEIL1 by the AuNPs which does not occur when the order of incubation is inversed and the reaction time between AuNPs and NEIL1 is short.

In general, a deactivation of a repair enzyme by cytotoxic AuNPs is not surprising, as adverse effects on biological materials are expected. Here, NEIL1 was one candidate to explain the surprising results from the first GC/MS experiments on cells incubated with AuNPs. Obviously, this enzyme is not affected in a stimulating way by AuNPs to enhance DNA repair. As there are numerous DNA repair enzymes with different lesion repair patterns, other enzymes should be investigated in the same way as NEIL1 to potentially find a candidate which can be activated by AuNPs. Other potential enzyme candidates include NEIL3, Fpg, Ogg1 and Nth.

3.7 The Au(I) Question

As another reference material for the cytotoxicity experiments, a gold(I) complex, the sodium salt of chloro[diphenyl(3-sulfonatophenyl)phosphine]gold(I) (referred to as TPPMS-Au(I)-Cl afterwards), was tested. It was found that this Au(I) species is highly cytotoxic as well ($IC_{50} = 50 \mu M$ in HeLa cells in the logarithmic phase). This raised the question if the cytotoxicity is predominantly based on the toxicity of Au(I) species and not the AuNPs themselves. A similar mechanism is in discussion concerning the toxicity of silver nanopar-

ticles (AgNPs).[125] AgNPs possibly serve as a source for constant Ag^+ ion release which then cause toxicity.

Furthermore, the equilibrium between AuNPs, phosphine ligands and Au(I) species was investigated by Sharma et al.. They performed extensive NMR studies on 1.8 nm sized TPP-stabilized AuNPs in CH_2Cl_2 . They found that both TPP and a TPP-Au(I)-Cl species can be released from the AuNP surface.[72] In H_2O , a polar solvent, and with TPPMS the situation might though be different.

Hence, it was important for two reasons to investigate if there are Au(I) impurities in the Au1.4MS material: firstly, to find out whether the cytotoxicity of Au1.4MS was based on Au(I) and not on a nanoparticle specific effect, and secondly, to certify the purity of the synthesized Au1.4MS in general.

By comparing the IC_{50} values of Au1.4MS ($\text{IC}_{50} = 46 \mu\text{M}$) and TPPMS-Au(I)-Cl it becomes obvious that Au1.4MS would have to be degraded completely to Au(I) species to induce such a toxic effect. This is definitely not the case, as the cell culture solutions are still colored brown from the Au1.4MS after the incubation time, whereas TPPMS-Au(I)-Cl is colorless. The AuNPs could also be found in TEM micrographs of incubated cells, although a size determination was not possible due to the low contrast of the AuNPs in the biological matrix.[12] The relation between Au1.4MS and TPPMS-Au(I)-Cl was further investigated nevertheless to exclude any side effects.

Au1.4MS is synthesized *via* Au1.4TPP, whose precursor is the water-insoluble chlorotriphenylphosphine gold(I) (TPP-Au(I)-Cl), and a subsequent two-phase ligand exchange reaction. Therefore, no water-soluble Au(I) species should be present as an impurity remaining from the synthesis precursor. However, as discussed above, it is possible that Au(I) impurities might be present in AuNPs. These might originate from degradation processes taking place when AuNPs remain in solution over longer periods of time.[126]

NMR spectroscopy was used for this purpose to examine Au1.4MS. A ^{31}P -NMR spectrum of a concentrated solution of Au1.4MS in D_2O gave signals at $\delta = 15.6 \text{ ppm}$, 33.0 ppm , 37.5 ppm , 45.7 ppm (major signal), 55.4 ppm and 58.0 ppm (fig. 3.23). Not all signals could be assigned, but obviously impurities are present. The material was further purified.

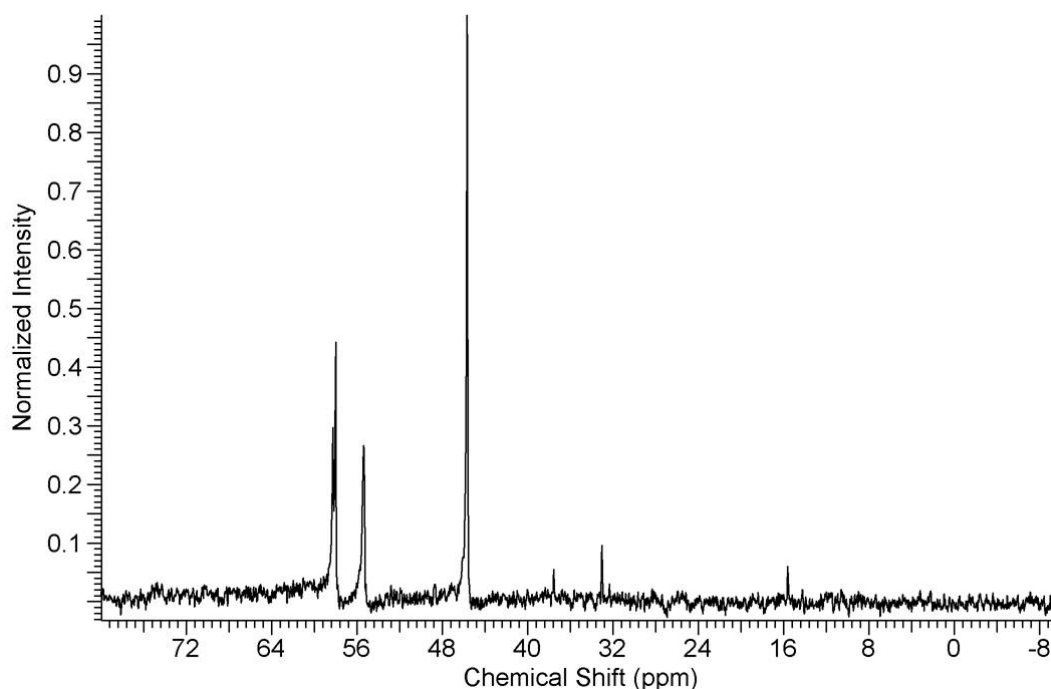


Figure 3.23: ^{31}P -NMR spectrum of Au1.4MS in H_2O .

After column chromatography over cellulose with ethanol and H_2O (4:1), the product was measured in a mixture of deuterated methanol and D_2O . Three signals remained (slightly shifted due to different solvent: 33.9 ppm, 45.3 ppm, 57.2 ppm), but the integrals and thus the concentrations were affected (fig. 3.24). The signal at 45.3 ppm is still the signal with highest intensity (approximately 77 %), and the other two remaining signals are of minor intensity.

TPPMS-Au(I)-Cl gives a ^{31}P -NMR signal at 32.1 ppm in this solvent mixture. Free TPPMS results in a signal at -6 ppm and is not visible at all. On the other hand, TPPMS in aqueous solution is prone to oxidation, and the oxidation product of TPPMS, sodium 3-(diphenylphosphoryl)benzenesulfonate (abbreviated as TPPMS=O), shows a ^{31}P -NMR signal at 36.5 ppm. It shows very low cytotoxicity ($\text{IC}_{50} = 4677 \mu\text{M}$). The three species are shown in fig. 3.25.

The signal at 45 ppm refers to the TPPMS ligand molecules bound to AuNPs of 1.4 nm diameter. It is slightly broadened. One reason for this broadening is that the 12 TPPMS molecules are weakly bound *via* a coordinative bond. This leads to ligand mobility on the AuNP surface and thus structural flexibility when the AuNPs are in solution, resulting in

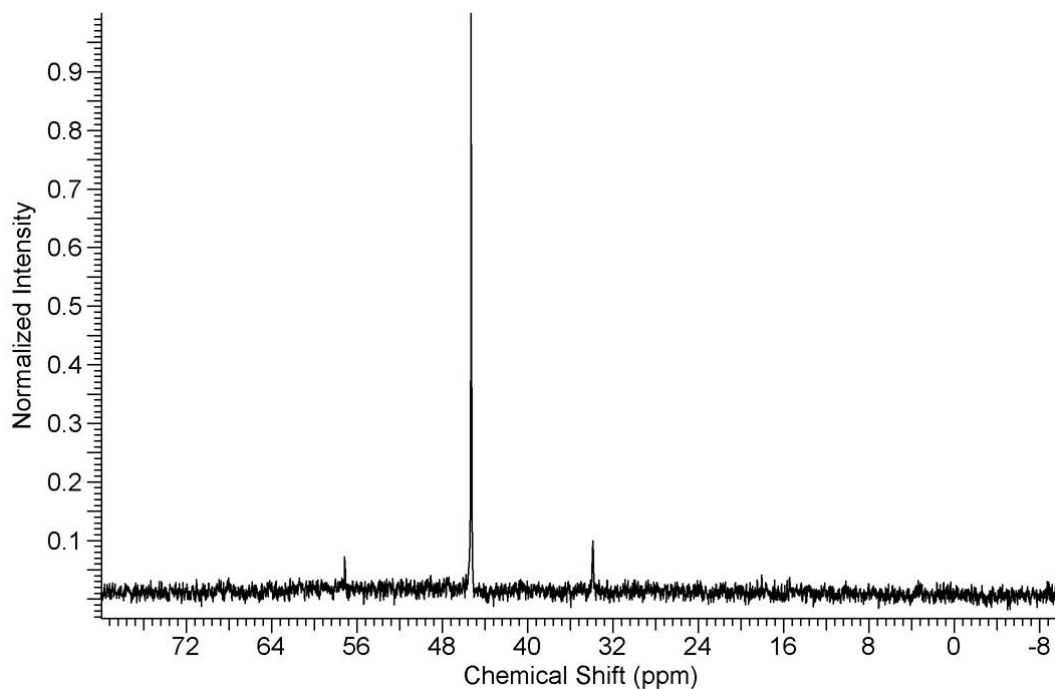


Figure 3.24: ^{31}P -NMR spectrum of Au1.4MS after column chromatography, measured in deuterated methanol/ D_2O (1:1).

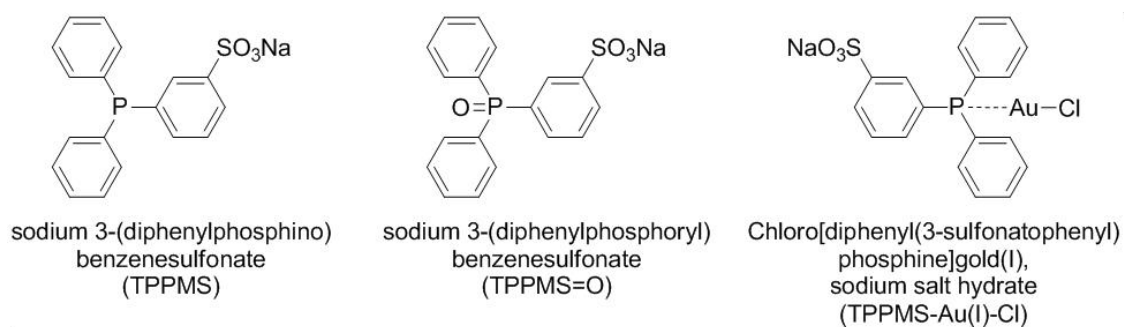


Figure 3.25: The species possibly detected in ^{31}P -NMR spectra of Au1.4MS: the ligand TPPMS, its oxidation product TPPMS=O and potentially cleaved TPPMS-Au(I)-Cl.

a broadened signal ^{31}P -NMR spectroscopy. From this spectrum, it is not definitely determinable which species causes the signal at 33.9 ppm, $\text{TPPMS}=\text{O}$ or the Au(I) complex, or if signals of both species overlap here. The signal at 57.2 ppm is probably caused by small phosphine-stabilized gold clusters. A signal for free TPPMS which would be visible at -6 ppm is not seen at all.

It is possible to purify Au1.4MS by column chromatography. The IC_{50} value for such purified material was similar to non-purified Au1.4MS judged by MTT assays in HeLa cells. The cytotoxicity therefore most likely was due to the Au1.4MS proper and not to low molecular weight impurities.

In none of the ^{31}P -NMR spectra of Au1.4MS, free TPPMS was detected. This was surprising as the TPPMS molecules are weakly bound to the AuNP surface and are expected to be in equilibrium to free TPPMS in solution. On the other hand, studies of the non-water soluble derivative Au1.4TPP have shown that the addition of excess TPP does not lead to the detection of free TPP in the ^{31}P -NMR spectrum, but to a high field shift of the signal of Au1.4TPP.[71]

It was therefore investigated if Au1.4MS in aqueous solution shows the same effect in reaction with TPPMS. Au1.4MS was dissolved in D_2O and measured in ^{31}P -NMR. 10 eq of TPPMS were added and another measurement was performed. This was repeated up to a total amount of 118 eq TPPMS. As in the case of Au1.4TPP, a high field shift of the Au1.4MS signal was observed, and no free TPPMS was visible even in the highest amount added (see fig. 3.26).

The high field shift of the spectra was used to perform a first-order estimation of the equilibrium constant for the Au1.4MS/TPPMS system. The δ values were plotted against the concentration of additional TPPMS and approximated with a logarithmical fit (fig. 3.27).

From this, the amount of intrinsic free TPPMS (c_{diss}) was estimated, and the amount of bound TPPMS (c_{ass}) was calculated from the original sample weight with the assumption of 12 ligand molecules per particle. With these two values, a dissociation constant K_d of 4.76×10^{-7} was calculated:

$$K_d = \frac{c_{\text{diss}}}{c_{\text{ass}}}$$

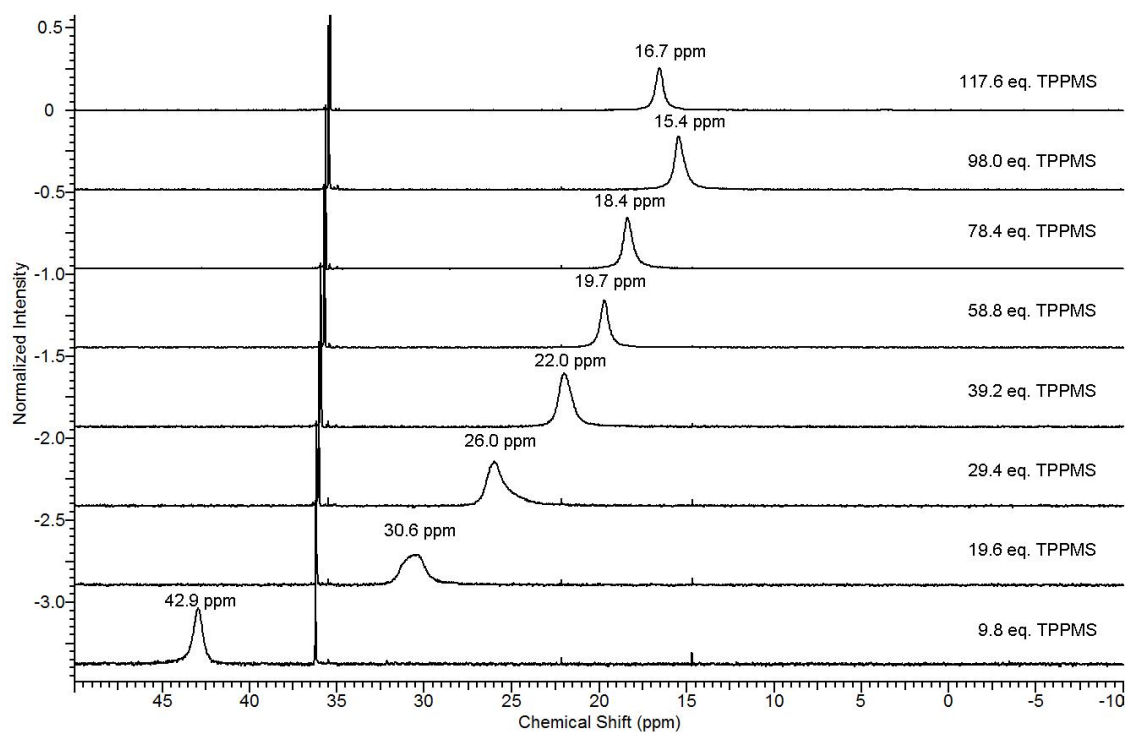


Figure 3.26: ^{31}P -NMR spectra of Au1.4MS with subsequent TPPMS addition. Signals at 36.5 ppm derive from TPPMS=O.

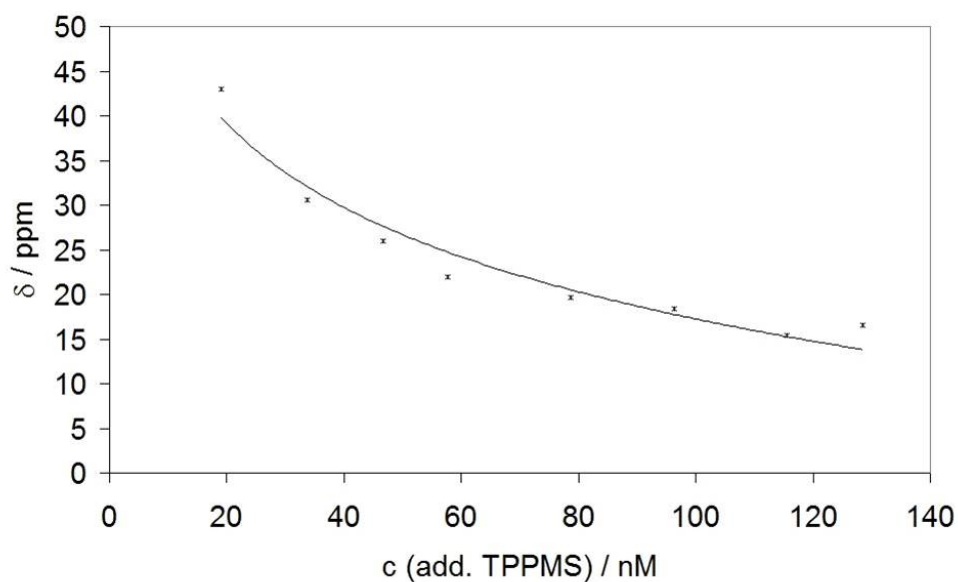


Figure 3.27: Plot of chemical shifts δ of the ^{31}P -NMR spectra of Au1.4MS depending on the addition of TPPMS.

With K_d , a Gibbs energy of $\Delta G^0 = 35.5 \text{ kJ/mol}$ was calculated:

$$\Delta G^0 = -RT \ln K_d$$

The bond strength theoretically determined for PH_3 by Häkkinen et al. was 0.93 eV, which equals to 89.7 kJ/mol.[44] The value determined by ^{31}P -NMR spectroscopy is thus significantly lower. In the theoretical calculations, solvation effects were not taken into account. Also, PH_3 is only a simple model for a phosphine ligand and not directly comparable to the bulkier and charged TPPMS.

The question remained if the detected TPPMS-Au(I)-Cl was present in the "as synthesized" material, or if it was generated in solution. Thus, a sample of Au1.4MS was investigated by solid state ^{31}P -NMR spectroscopy. A static measurement resulted in one very broad signal ranging from -100 ppm to 200 ppm without further significant characteristics and fine structures (fig. 3.28, bottom).

Next, it was measured under magic angle spinning (MAS) conditions at frequencies of 15 and 35 kHz (fig. 3.28, middle and top spectra, red). Here, the signal became narrower, but was still ranging from approximately -40 ppm to 120 ppm at a MAS frequency of 35 kHz. The MAS spectra reveal that the broad peak consists of at least three overlapping signals with an absolute maximum at $\delta = 20 \text{ ppm}$. ^1H decoupling did not influence the spectrum measured with a MAS frequency of 15 kHz (fig. 3.28, middle spectrum, green).

Furthermore, a sample of TPPMS-Au(I)-Cl was analyzed in a reference measurement (MAS with 15 kHz; fig. 3.28, middle spectrum, blue). It gave a considerably narrower signal than Au1.4MS, with a maximum at $\delta = 10 \text{ ppm}$. By superimposing the spectra of Au1.4MS and TPPMS-Au(I)-Cl it is obvious that the signal of the Au(I) complex has the same chemical shift as one of the three signals in the spectrum of Au1.4MS, visible as a shoulder of the main signal.

It is not clear what causes this shoulder in the Au1.4MS spectrum. It is possible that TPPMS-Au(I)-Cl exists as a molecular species independently besides Au1.4MS and that it was formed as the result of a degradation reaction during the synthesis of Au1.4MS. Another possibility is that TPPMS molecules bound to partially polarized Au surface atoms of a AuNP have a similar electronic environment as TPPMS in TPPMS-Au(I)-Cl and therefore

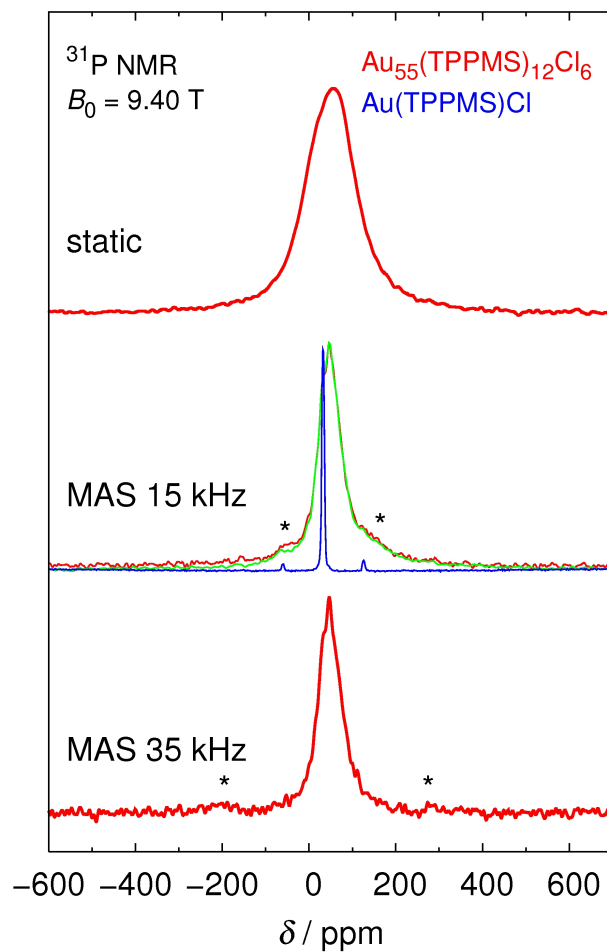


Figure 3.28: Solid state ^{31}P -NMR spectra, static (top) and with MAS frequencies of 15 (middle) and 35 kHz (bottom), from Au1.4MS (red), Au1.4MS measured with ^1H decoupling (green, with MAS at 15 kHz), and TPPMS-Au(I)-Cl (blue, with MAS at 15 kHz). Stars indicate rotational side bands in MAS measurements.

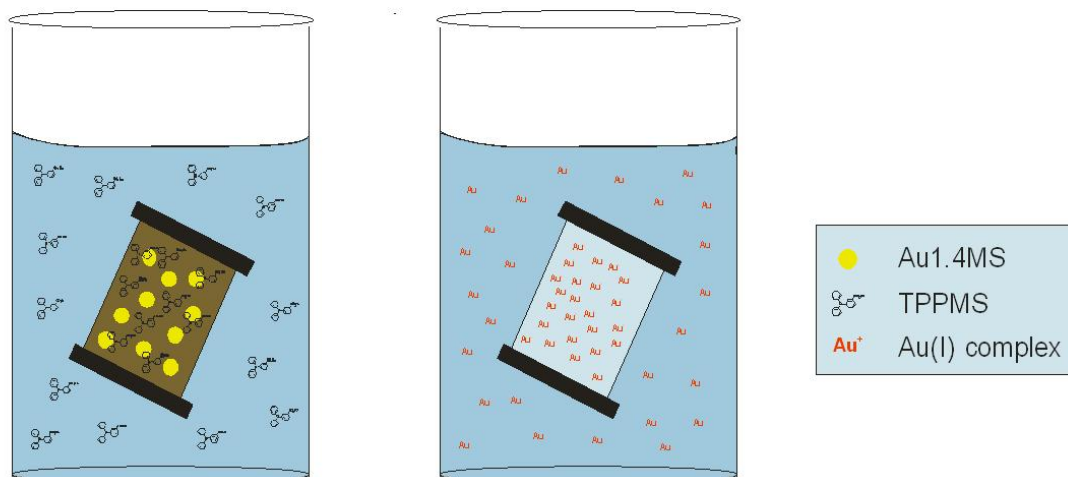


Figure 3.29: Scheme of dialysis experiments of Au1.4MS (left) and TPPMS-Au(I)-Cl as reference (right). The dried dialysates were analyzed by EDX analysis.

give a signal at the same chemical shift. From this data, no final conclusion can be drawn concerning this question. A quantification of the three overlapping signals of the spectrum of Au1.4MS by a line shape analysis could not be performed without considerable effort and was therefore not conducted.

To finally answer the question if significant amounts of TPPMS-Au(I)-Cl are present in aqueous solutions of Au1.4MS, another analysis method was chosen. A dialysis experiment with Au1.4MS was conducted (fig. 3.29).

The supernatant was dried and the resulting white residue was examined by energy dispersive X-ray (EDX) analysis. The EDX spectrum indicates that small amounts of TPPMS were shed from Au1.4MS during the dialysis, but no gold could be found. The control experiment with TPPMS-Au(I)-Cl showed that Au(I) (in whatever form) could readily traverse the dialysis membrane with a molecular weight cut off radius (MWCO) of 5 kD, as a signal for gold was found in the EDX spectrum of the white residue of this experiment.

This experiment shows that no TPPMS-Au(I)-Cl as an independent species is present in Au1.4MS in significant amounts. The contradictory results from the NMR investigations may be due to chemical compounds with similar chemical environments adsorbed to AuNPs.

3.8 Patch Clamp Experiments

In order to explore the effect of smaller particles, particularly of Au1.4MS on hERG expressing HEK 293 cells, patch clamp experiments were performed with a variety of phosphine- and thiol-stabilized AuNPs and ionic gold complexes, serving as reference materials. Parts of these results were already described in the dissertation of Dr. Yu Pan-Bartneck.[12]

HEK 293 cells transfected with the hERG gene were used in a manual patch clamp set-up. They were patched in whole-cell configuration to detect the whole cell membrane potential (fig.3.30). In the voltage protocol used the hERG channel was opened for 2 s, expressing the typical tail current characteristics. The maximum amplitude serves as a measure for decrease of the cell membrane voltage and therefore an inactivation of hERG.

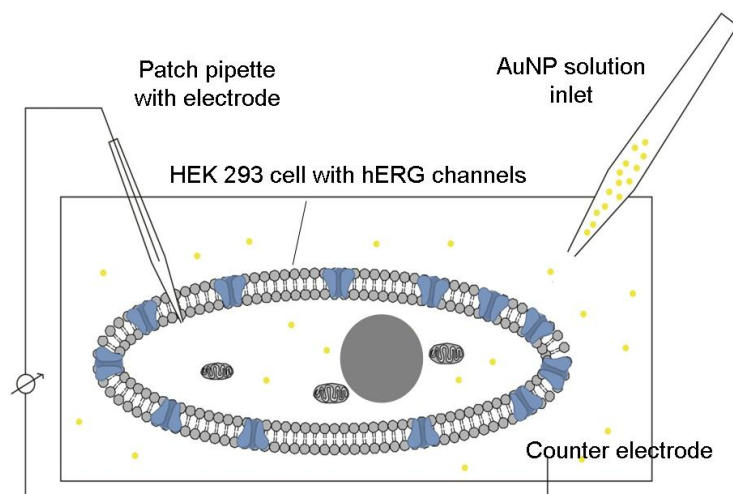


Figure 3.30: Schematic patch clamp setup of a cell in whole-cell configuration. Blue: hERG ion channels.

First, $65\text{ }\mu\text{M}$ Au1.4MS was applied to a patched cell. After a response time of approximately 2 min, the hERG current amplitude decreased significantly (fig.3.31). Compared to other well-known molecular hERG blockers such as fluvoxamin, this onset is quite slow.[127] The effect was irreversible, i.e. when the cell was perfused with extracellular buffer (EC) after the Au1.4MS incubation, the amplitude remained at its low level and did not recover to its original value.

The time scale of a typical patch clamp experiment is in the range of minutes up to a maximum of one hour, and the first detectable changes occur within a few minutes. The

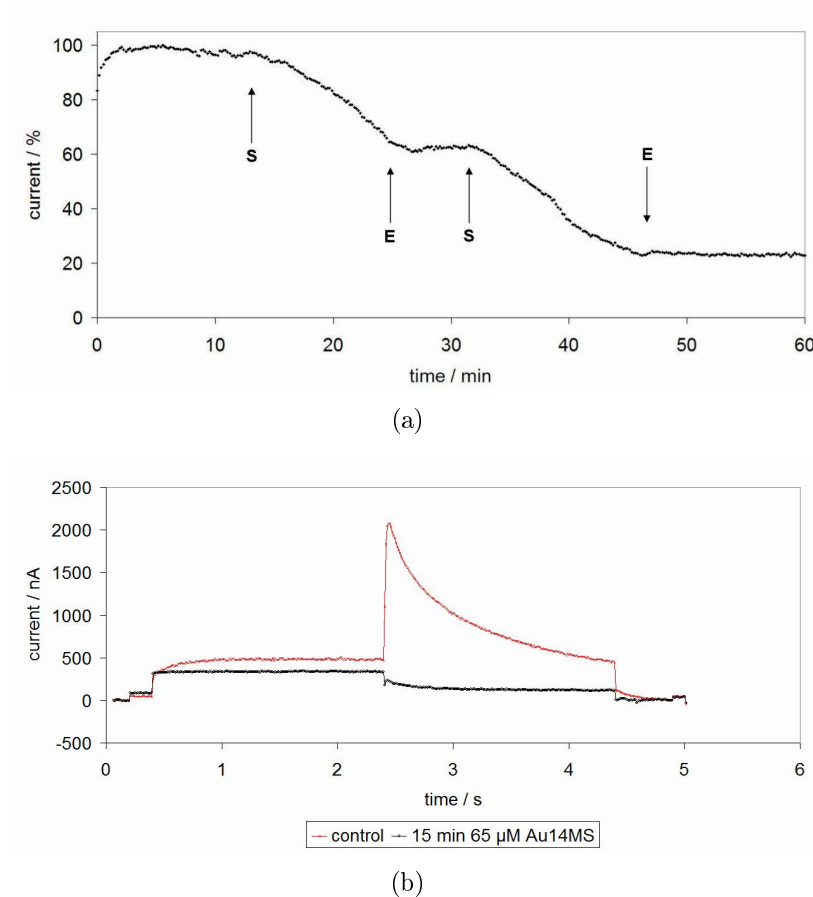


Figure 3.31: Current response of a hERG expressing cell in a patch clamp experiment during perfusion with Au1.4MS.

(a) Time response of hERG current amplitude, detected during $2\times$ perfusion of $65\text{ }\mu\text{M}$ Au1.4MS on a patched cell in whole-cell configuration for 10 min. Arrows indicate start (S) and end (E) of perfusion.

(b) hERG current before (red) and after (black) perfusion with Au1.4MS.

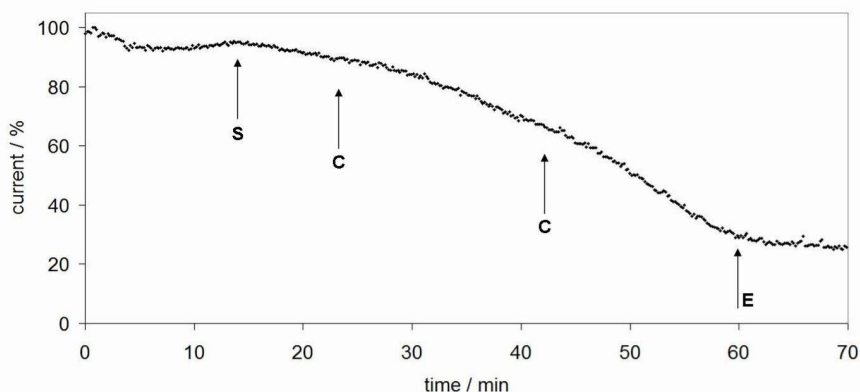


Figure 3.32: Concentration dependent response of hERG towards Au1.4MS (3.1 μM , 6.5 μM , 16.25 μM). Arrows indicate start (S), change (C) and end (E) of perfusion.

cytotoxicity of Au1.4MS in an *in vitro* cell test typically appears after a time period in the range of hours. The effect towards hERG is thus not correlated to simply induced cell death, but is probably caused by an interaction with the ion channel.

The concentration dependent behavior of Au1.4MS was investigated. Increasing concentrations of Au1.4MS were applied. The amplitude was plotted against incubation time, and the slope became steeper for higher concentrations (fig. 3.32). The lowest concentration applied was 3.1 μM . Already at this concentration (a gold atom concentration of 3.1 μM equals to a particle concentration of 56 nM), a slight decrease of amplitude was detectable.

As Au1.4MS is stabilized by TPPMS, a triphenylphosphine, an aromatic interaction between the aromatic residues within the hERG cavity and the phenyl rings is imaginable. Therefore, the effect of the TPPMS ligand alone towards hERG was tested (fig. 3.33). At concentrations in the same magnitude that was applied with the addition of Au1.4MS (12 TPPMS molecules per particle consisting of 55 gold atoms; i. e. when 3 μM Au1.4MS are applied, the TPPMS concentration is approximately 0.65 μM), no effect was detected (up to 50 μM). At a higher concentration of 100 μM , the amplitude decreased within one minute.

In contrast to the blockade of Au1.4MS, this effect was reversible when the cell was washed with EC afterwards. The blockade of TPPMS therefore obviously follows a different mechanism than the irreversible blocking of Au1.4MS.

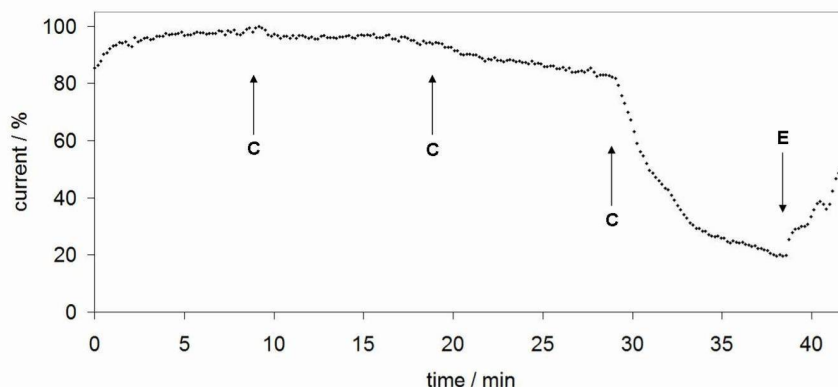


Figure 3.33: HERG response towards TPPMS in increasing concentrations (10, 50, 100, 500 μM). Arrows indicate change (C) and end (E) of perfusion. The perfusion with 10 μM TPPMS was started immediately (no arrow).

Furthermore, TPPMS was also applied intracellularly by applying it in the IC medium *via* the patch pipette. Here, no effect was measurable up to a concentration of 1 mM TPPMS. This indicates that the reversible blocking of TPPMS is related to an extracellular interaction. Also, the blocking of Au1.4MS is obviously not related to an interaction of hERG with TPPMS.

One possible mechanism for the blocking by Au1.4MS is the stripping of TPPMS in contact with the cell and an interaction of the pure gold core with the hERG channel. To prove this hypothesis, mixtures of Au1.4MS with a surplus of TPPMS in different concentrations were prepared and tested. At enhanced concentrations of free TPPMS, the equilibrium in solution between bound and dissociated TPPMS should be altered. If the accessibility of the gold core surface is crucial for the blocking mechanism of Au1.4MS, the addition of excess TPPMS will make the particle surface less accessible.

When a cell was perfused with a mixture of 20 μM Au1.4MS (a concentration that should induce a distinct blockade) together with 50 μM TPPMS, only a slight decrease in the hERG tail current amplitude was detected (fig.3.34). This slight decrease was a lot slower and less steep than the usual effect and in a non-significant scale. After 10 min, another mixture with a AuNP/TPPMS ratio of 20/25 μM was applied to the cell. Again, no obvious influence towards the hERG current was detectable. Only when the TPPMS concentration

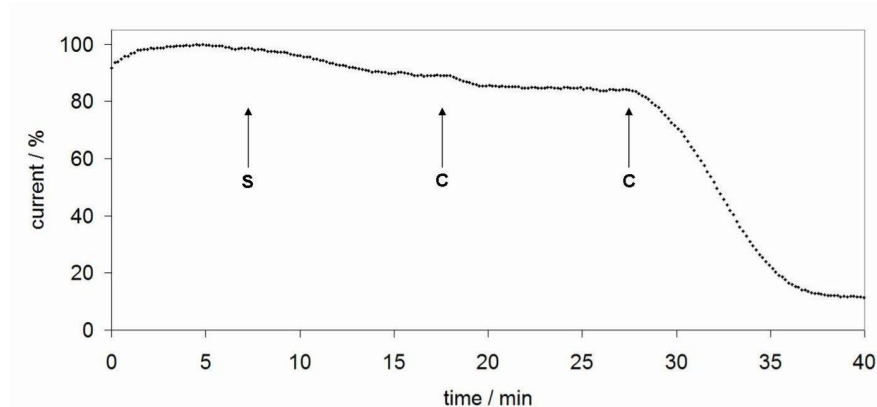


Figure 3.34: Effect of mixtures of Au1.4MS (20 μ M) pre-incubated with varied concentrations of TPPMS (50, 25, 10 μ M). Arrows indicate start (S) and change (C) of perfusion.

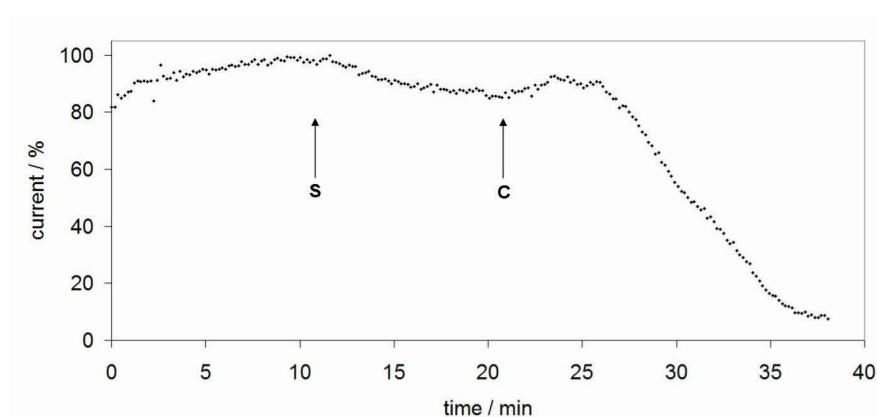


Figure 3.35: Patch clamp measurement during TPPMS application (50 μ M) and subsequent Au1.4MS application (20 μ M). Arrows indicate start (S) and change (C) of perfusion.

was further reduced and a pre-incubated mixture of 20 μ M Au1.4MS with 10 μ M TPPMS was applied, the typical reduction of tail current amplitude was found.

In a control experiment, the order of addition was changed (fig.3.35). The patched cell was pre-treated with 50 μ M TPPMS for 10 min, and then 20 μ M Au1.4MS was applied. Here, the blocking could not be prevented. A direct reaction between TPPMS and Au1.4MS is necessary to influence the ion channel blockade.

In this experiment, the response time was slightly higher compared to Au1.4MS perfused on a fresh cell. This can be explained by the excess TPPMS in the cell chamber that was still present when the addition of Au1.4MS was started.

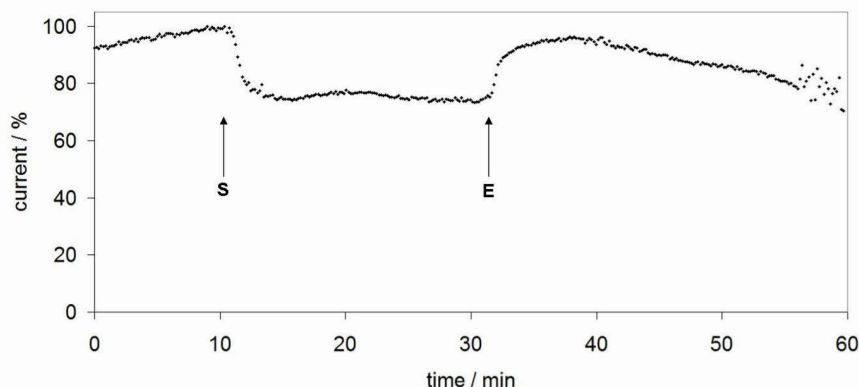


Figure 3.36: Perfusion of a patched cell with Au1.4MS (300 μ M) + GSH (455 μ M). Arrows indicate start (S) and end (E) of perfusion.

Furthermore, a mixture of 300 μ M Au1.4MS with 455 μ M GSH (final concentrations, respectively) was applied to a cell (fig. 3.36). The tail current dropped slightly (23 %), but did not decrease further. After 20 min of application the cell was washed with EC and the current amplitude recovered to its starting value. This indicates again that the surface accessibility is crucial for the blocking interaction of Au1.4MS. After the TPPMS ligands were replaced by GSH, the resulting species does not cause a complete, irreversible blockade of hERG as Au1.4MS does.

Au15MS should also be tested in patch clamp experiments. When the stock solution was diluted with EC, the AuNPs were not stable in the medium. When 10 % fetal calf serum (FCS) was added to the EC prior to dilution, the AuNPs remained stable. This solution was tested, but no effect towards the hERG amplitude was detectable.

As a reference experiment, Au1.4MS (300 μ M final concentration) was given to 10 % FCS containing EC and applied to a cell (fig. 3.37). First, the cell was pre-treated with EC + 10 % FCS which already induced a slight decrease in tail current amplitude to a stable value. When Au1.4MS in EC + 10 % FCS was added, differing from the previous experiments, this solution did not induce the expected blockade but the current amplitude remained constant. It is likely that FCS forms a protein corona around both AuNP species and thereby alters the interaction of AuNPs with the ion channel. This finding is however in contrast to the cytotoxicity investigations, where Au1.4MS was found to be toxic in the presence of FCS.

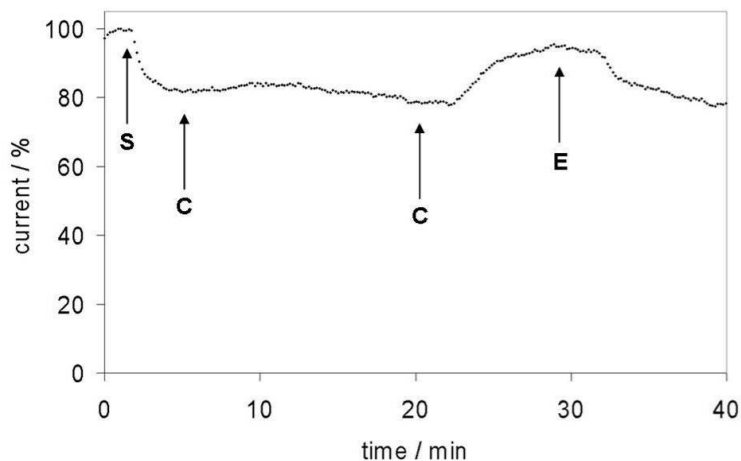


Figure 3.37: Effect of 300 μM Au1.4MS in EC containing 10 % FCS; the first arrow (S) indicates the start of FCS (10 %) perfusion. The other arrows indicate change of sample (C) to Au1.4MS + 10 % FCS and back to only 10 % FCS and end (E) of perfusion.

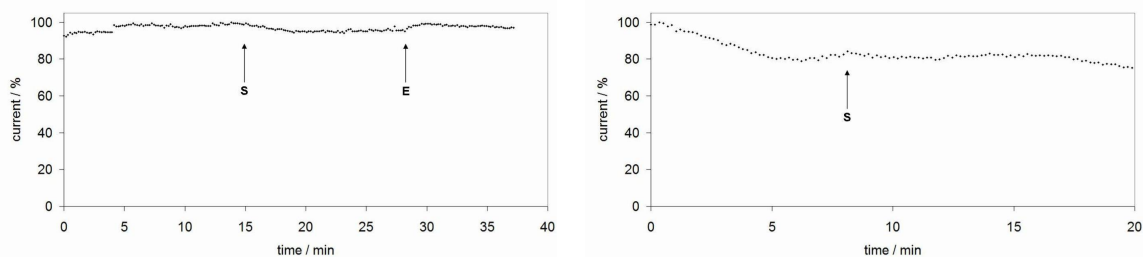


Figure 3.38: Thiol-stabilized AuNPs in patch clamp experiments, left: 300 μM Au1.1GSH, right: 300 μM Aurovist. Arrows indicate start (S) and end (E) of perfusion.

As Au15MS is not stable in EC without FCS it was not possible to investigate the pure size effect of differently sized TPPMS-stabilized AuNPs.

Two thiol-stabilized AuNP species were also tested: Au1.1GSH and AurovistTM (both in a concentration of 300 μM). No effect was detectable for both materials (fig.3.38). It can be assumed that the gold cores of the AuNPs are too strongly shielded by the respective thiol shell so that an interaction as in the case of Au1.4MS with its weaker bound phosphine ligands is disabled.

Obviously, the size difference of 1.1 nm respectively 1.9 nm does not play a role here, but the ligand shell determines the activity of AuNPs towards hERG.

Various types of ion channels are blocked by metal ions if these are applied in high micromolar and millimolar concentrations.[128] To exclude this possible pathway of gold ion blockade by potential impurities in the AuNP solutions, different gold salts and complexes were investigated.

Au(III)Cl₃ was not stable in the EC. The yellow solution turned grayish-blue within minutes, indicating the formation of large AuNPs. As the EC contains glucose, this may act as a reducing agent for Au(III). If Au(III) ions would be present as an impurity in the AuNP solutions, it can be supposed that they would react in the same way when diluted with EC. Au(III) was therefore not further investigated.

TPPMS-Au(I)-Cl was also examined. For 50 μ M or 300 μ M solutions of Au(I) complex, the cells became leaky immediately after the perfusion was started. This was reproducible in several cells. No conclusion can thus be drawn about the interaction of TPPMS-Au(I)-Cl with the hERG channel. The very rapidly induced leaking of the cells is however a different response than in the case of Au1.4MS. As it was found in the dialysis experiment (see chapter 3.7), obviously no significant amounts of Au(I) were present in a solution of Au1.4MS, as otherwise the AuNP solution should lead to leaky cells as well.

Another gold complex that was examined was Tauredon[®]. In the patch clamp experiment, no effect towards hERG could be found up to a complex concentration of 50 μ M.

Summarized, all gold salts and complexes tested gave a different response in the patch clamp experiment than Au1.4MS. The effect of Au1.4MS on hERG is obviously not induced by gold ions but by the nanoparticle species itself.

As already described, the hERG ion channel has a special structure and is very prone to channel-drug interactions, mainly because of the aromatic residues Y652 and F656 and the possibility of aromatic interaction with a variety of compounds. Thus, another ion channel (Na_v1.5) was investigated to check whether the blocking of Au1.4MS is specific to hERG. Na_v1.5 expressing CHO-K1 cells were used. The Na_v1.5 channel has a distinct gating behavior compared to hERG, leading to a different response curve with a negative current amplitude in the patch clamp experiment.

When a CHO-K1 cell was perfused with 300 μ M Au1.4MS, a strong decrease of the amplitude was observed (fig 3.39). Blocking of Au1.4MS is therefore not specific to hERG. As the

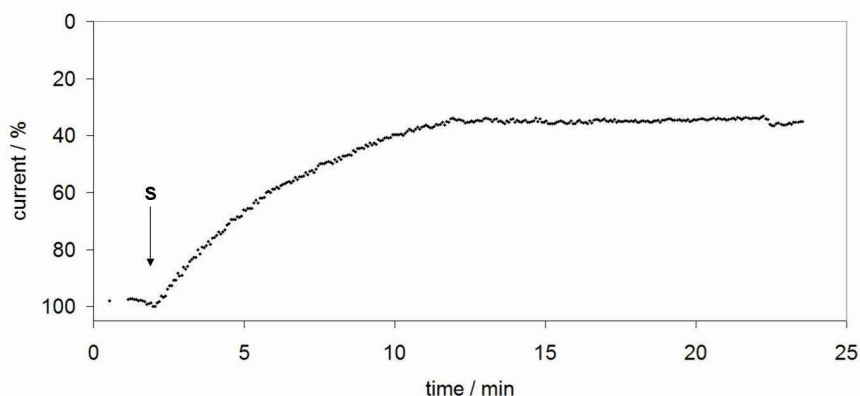


Figure 3.39: Patch clamp experiment with a $\text{Na}_V1.5$ channel expressing CHO-K1 cell exposed to $300\ \mu\text{M}$ Au1.4MS. The arrow indicates the start (S) of perfusion. Note that the compared to hERG expressing cells inverted run of the curve is caused by the distinct gating behavior of $\text{Na}_V1.5$ channels.

$\text{Na}_V1.5$ channel is, in contrast to hERG, not especially sensitive towards blocking by aromatic molecules, this result is another hint that the blocking of ion channels by Au1.4MS is not correlated to the aromatic residues inside the hERG cavity.

The investigation of the $\text{Na}_V1.5$ channel revealed another effect: the current curve showed an impaired channel inactivation. A similar behavior occurs when $\text{Na}_V1.5$ cells are incubated with different metal ions such as La^{3+} and Zn^{2+} .^[128] However, as discussed above, the blocking effect of Au1.4MS is not caused by released metal ions. Such an incomplete channel inactivation points again towards an intracellular action of Au1.4MS. What exactly leads to this effect here is not yet known.

Most so far known hERG blockers are inner cavity blockers. This means that the channel has to be in the open state to enable the blocking species to enter from the intracellular site. This open channel block leads to the characteristic kinetic features of hERG blockade: upon depolarization, the onset of channel blocking occurs quite fast, within some 100 ms, while the wash-out of blockers at hyperpolarized membrane potentials is extremely slow. In the standard voltage protocol applied before, hERG is opened for 2 s. When a different protocol (the so-called "envelope of tails"-protocol) is used, it is possible to investigate whether a species is an open channel blocker. The length of the opening time of the intracellular gate

is varied and the tail current is elucidated by activating depolarization pulses with increasing durations.

When 300 μM Au1.4MS were applied during an envelope of tails-experiment, the typical blockade of hERG could unexpectedly not be detected at all anymore. If the respective cell was further perfused with Au1.4MS and the usual voltage protocol was conducted again, the blockade occurred as expected. This points towards an intracellular blocking mechanism, as for an extracellular event the channel opening would be no prerequisite.

Furthermore, the hERG ion channel has obviously to be opened long enough for Au1.4MS to interact. There are two possible explanations for this phenomenon: either the diffusion of Au1.4MS (or, in more general, the blocking species) into the ion channel is very slow compared to other typical blocker molecules that were successfully investigated in an envelope of tails-experiment; or the postulated stripping of the TPPMS ligands from the gold core occurs only in direct interaction with the opened channel and is the rate-determining step. In cooperation with Prof. W. Wenzel from Karlsruhe Institute of Technology (KIT), the hERG structure as well as Au1.4MS were modeled and an interaction was investigated theoretically by Monte Carlo simulations. A classical force field was used for electrostatics, hydrogen bonding, Lennard-Jones potential and implicit solvent interactions in a solvent accessible surface model. The charges of Au1.4MS were calculated by DFT calculations. Au1.4MS was modeled with varying numbers of TPPMS ligands (12, 10, 8,... 0 molecules per particle). The hERG channel was based on a homology model with the crystal structure of a K^+ channel of the mammalian voltage-dependent Shaker family (pdb 2A79).

At pH 7.4 the hERG channel is negatively charged, and there is a repulsive interaction for a Au_{55} cluster with 12 TPPMS molecules which are also negatively charged. Hypothetical AuNP structures with less ligand molecules on the surface show increasing affinity towards hERG (fig. 3.40). This fits well to the experimental finding that an excess of TPPMS hinders Au1.4MS to block hERG.

Furthermore, the calculations exclude some potential points of binding. Au1.4MS will not fit into the inner cavity and will therefore not interact with the aromatic side chains as most hERG blockers do. Further, it cannot bind near the entrance of the K^+ -passage at the bottom of the extracellular channel side.

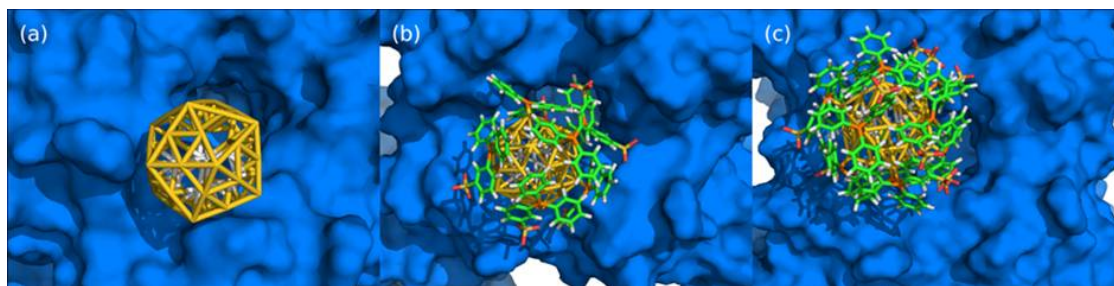


Figure 3.40: Simulations of hERG (depicted in blue) in interaction with Au1.4MS with varying numbers of TPPMS ligands: (a) pure gold core without TPPMS ligands; (b) gold core with 6 TPPMS ligands; (c) gold core with 12 TPPMS ligands. Best lowest energy conformations out of 500 simulations are shown. Models were provided by W. Wenzel, KIT.

The ligand functionalization of AuNPs, similarly as in the cytotoxicity experiments, determines the response of ion channel expressing cells. 1.4 nm phosphine-stabilized AuNPs block hERG channels in an irreversible manner, whereas thiol-stabilized AuNPs of similar sizes have no effect. It can be hypothesized that Au1.4MS strips its relatively weakly bound TPPMS ligands and a partially unprotected AuNP or the pure gold core blocks the ion channel irreversibly.

3.9 Other Monophosphine Ligands

As the ligand shell of a nanoparticle is the first entity the cell gets in contact with, the functionalities of the ligand molecules might play a crucial role in the cytotoxicity.[91] This parameter should therefore also be investigated. The phosphine ligand needs charged groups to guarantee water solubility. In the case of TPPMS, this is one sulfonate group per ligand molecule. The pK_A value of TPPMS was not determined, but the pK_A value of the respective acid H_2SO_4 is -3 , the pK_A value of a simple alkyl sulfonic acid, methanesulfonic acid (CH_3SO_3H), is still very low (-0.6), and the pK_A value of benzenesulfonic acid ($C_6H_5SO_3H$) is -2.8 . Therefore it can be presumed that TPPMS also has a low pK_A value and is fully dissociated in aqueous solution, which results in one negative charge in the dissolved state.[129, 130]

A simple modification is the use of 3,3',3''-phosphinidynetris(benzenesulfonic acid) trisodium salt (triphenylphosphine trisulfonate, TPPTS) instead of TPPMS. TPPTS is commercially

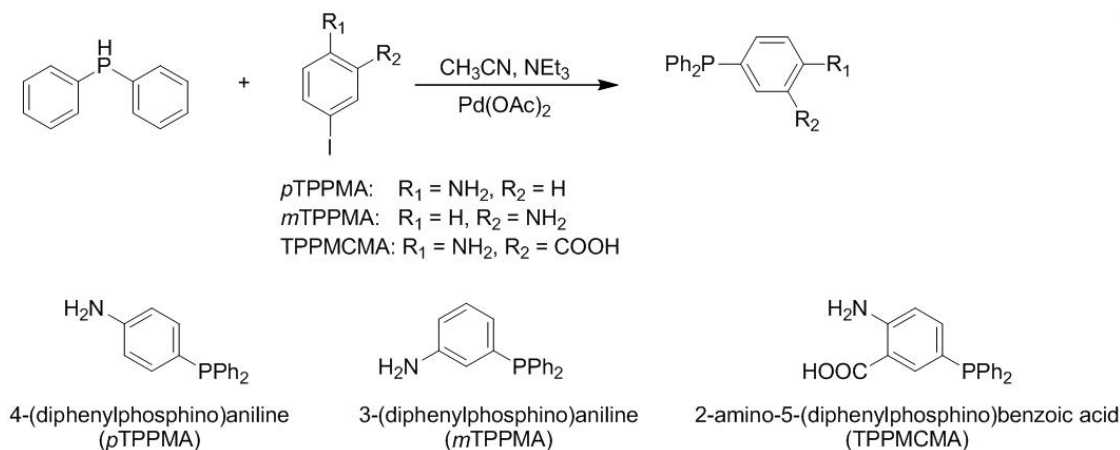


Figure 3.41: Reaction scheme of the Pd-catalyzed coupling reaction of diphenylphosphine with a iodo aryl species, and the coupling products $p\text{TPPMA}$, $m\text{TPPMA}$ and TPPMCMA .

available and has three sulfonate groups, therefore a net charge of -3 in the dissociated form in water. As the chemical composition of Au1.4MS is $\text{Au}_{55}[(\text{C}_6\text{H}_5)_2\text{P}(\text{C}_6\text{H}_4\text{SO}_3\text{Na})]_{12}\text{Cl}_6$, there are 12 ligand molecules per particle, i. e. one particle has a total charge of -12 in the fully dissociated state. There is no crystal structure of Au1.4TS available, but assuming that Au1.4TS has a ligand number of 12 as well, the total negative charge is enlarged to -42 . The precursor cluster Au1.4TPP was functionalized with TPPTS in a two-phase ligand exchange reaction and tested towards the four cell lines. Au1.4TS showed a very similar cytotoxicity as Au1.4MS ($\text{IC}_{50} = 30 \mu\text{M}$ in logarithmically growing HeLa cells), so that the increase of negative charges just by multiplying the same functional group obviously does not strongly alter the effect of the AuNPs.

Other water-soluble triphenyl phosphine derivatives were synthesized and used as ligands for Au1.4TPP . p - and m -(aminophenyl)diphenylphosphine ($p\text{TPPMA}$ and $m\text{TPPMA}$) were synthesized according to a protocol of Hessler et al.[131] Here, p - and m -iodoaniline, respectively, were coupled to diphenylphosphine in a Heck type Pd-catalyzed coupling reaction (reaction scheme see fig. 3.41).

The reaction products showed little amounts of impurities which were identified as the respective phosphine oxide species. Different routes that were tested to purify the phosphines were not successful, so the raw reaction products were used for subsequent ligand exchange reactions. Both TPPMA isomers showed only moderate solubility in H_2O . The stability of

the phosphines towards oxidation reactions was tested in a simple experiment. An NMR sample of the respective TPPMA, dissolved in deuterated dichloromethane, was left under ambient conditions for three days. The ^{31}P -NMR spectrum measured after this time period did not show any changes compared to the original spectrum. Therefore, it can be assumed that the phosphines are stable under ligand exchange reaction conditions.

Different routes were tried to exchange the ligands of Au1.4TPP against *m*TPPMA. In a first approach, similarly to TPPMS, a two phase reaction of Au1.4TPP in dichloromethane and *m*TPPMA in H_2O was tested. Due to the low solubility of *m*TPPMA in H_2O it was not possible to generate water soluble AuNPs by this method. As there are 12 ligands per particle, Au1.4TPPMA might potentially be better soluble in water than the pure ligand. This might be due to the formation of a micelle-like structure, with a nonpolar core consisting of gold and the hydrophobic parts of TPPMA, and a polar outer surface of 12 amine functionalities. Au1.4TPP and *m*TPPMA were therefore both dissolved in dichloromethane. This mixture was stirred at room temperature for several days, dried, and it was tried to redisperse the residue in H_2O . The H_2O phase remained completely colorless, indicating that the residue was insoluble in H_2O . It was not possible to generate Au1.4TPPMA *via* these routes.

To enhance water solubility of the phosphine ligand, 2-amino-5-(diphenylphosphino)benzoic acid (TPPMCMA) with one amino and one carboxylic acid function was chosen as another candidate. It was synthesized analogously to TPPMA from diphenylphosphine and 2-amino-5-iodobenzoic acid in a Pd-catalyzed P-C coupling reaction. Au1.4TPPMCMA was synthesized by a two phase ligand exchange reaction from Au1.4TPP. The H_2O phase became brown after 1.5 h so that the reaction was stopped and the product was purified by ultracentrifugation. Water soluble AuNPs with a mean particle diameter of 1.5 ± 0.4 nm were obtained. The UV/Vis spectrum showed a slightly more pronounced shoulder around 500 nm than Au1.4MS (fig. 3.42), which corresponds to the few larger particles visible in the STEM micrograph (fig. 3.43).

In cell culture medium, Au1.4TPPMCMA was not stable and showed aggregation to some extent. Therefore it was not possible to determine an IC_{50} value. The instability might be

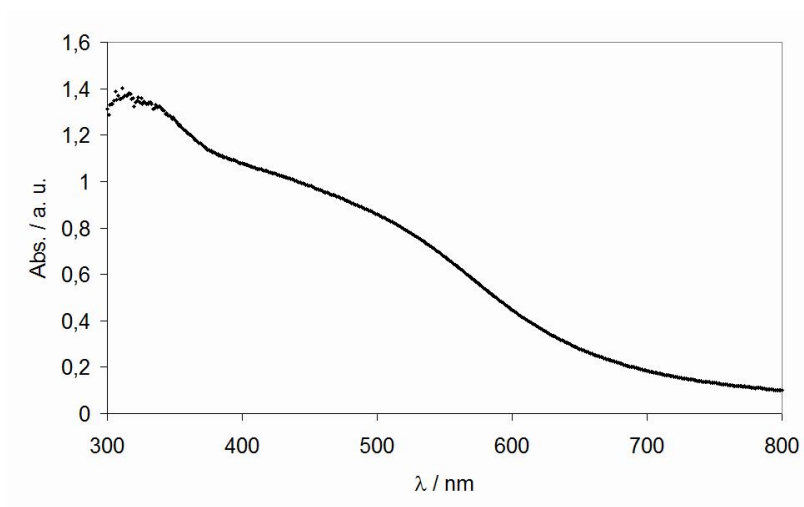


Figure 3.42: UV/Vis spectrum of Au1.4TPPMCMA.

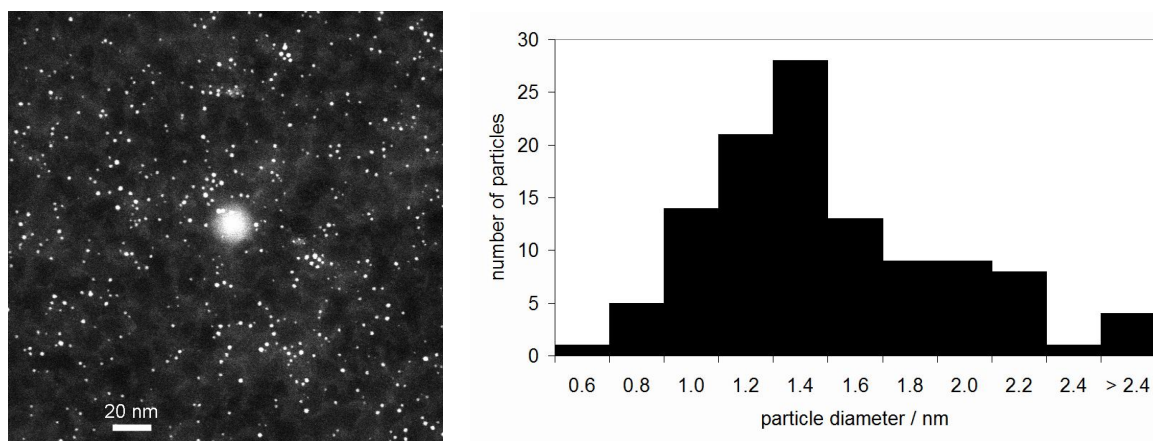


Figure 3.43: STEM micrograph (left) and histogram (right) of Au1.4TPPMCMA.

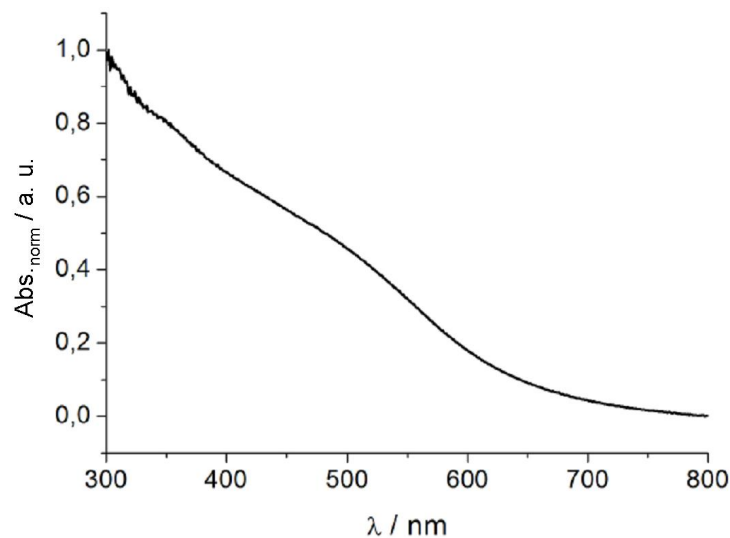


Figure 3.44: UV/Vis spectrum of Au1.4TPPMC.

due to the slightly basic pH of 7.4 of cell culture medium, or because of the (compared to ultrapure water) high salt concentration.

Furthermore, 4-(diphenylphosphino)benzoic acid (TPPMC) with one carboxylic acid functionality and Au1.4TPPMC particles were synthesized in the same way. The UV/Vis spectrum does not show significant features as expected for AuNPs of the desired size (fig. 3.44). This was confirmed by STEM analysis, as AuNPs with a mean diameter of 1.4 ± 0.2 nm with only few larger particles were visible (fig. 3.45).

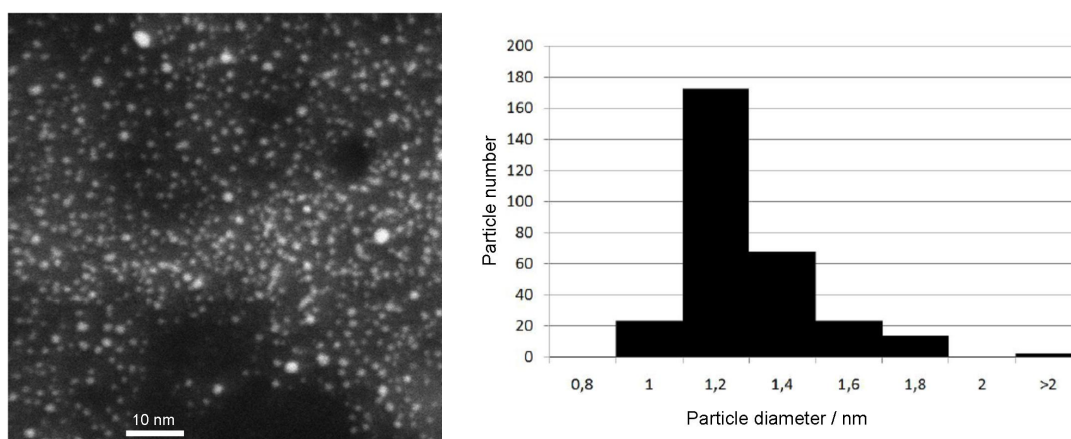


Figure 3.45: STEM micrograph (left) and histogram (right) of Au1.4TPPMC.

The EA revealed slightly higher C and H contents than theoretically expected (table 3.1). Dialysis of the sample improved the results a little.

Table 3.1: Results of EA of Au1.4TPPMC.

	C / %	H / %
Theoretical values	17.0	1.2
Measured values prior to dialysis	26.2	2.3
After dialysis	24.2	2.3

For Au1.4TPPMC, an IC_{50} value of 43 μ M was determined under standard conditions. These AuNPs were also used for further functionalization (see chapters 3.11 and 3.12).

The comparison of the results from TPPMS-, TPPTS- and TPPMC-stabilized AuNPs of 1.4 nm shows that the functional groups do not have a great influence towards the cytotoxicity. Small, phosphine-stabilized AuNPs show relatively high toxicity irrespective which functional groups the phosphine ligands have. It was not possible to generate stable AuNPs with positive charges. Here, a difference in cell uptake and therefore toxicity might be possible, as the cell membrane is negatively charged and is thus generally more sensitive towards positively charged entities.[91]

3.10 Diphosphine Ligands

As the binding strength between gold surface and ligand shell was found to influence the cytotoxicity of AuNPs (see chapter 3.3), this parameter should be further investigated. Small thiol-stabilized AuNPs were found to be less toxic than comparable phosphine-stabilized species, or even non-toxic (see chapter 3.3). Thus, AuNPs with a ligand shell that stabilizes with intermediate strength between monophosphines and thiols should be generated.

Other functionalities that are known to function as ligands for AuNPs, e.g. amines or oxygen-containing groups such as carboxylates, bind even more weakly than phosphines. Therefore, diphosphines were chosen to synthesize AuNPs with medium ligand-gold binding strength. The affinity of a molecule with two phosphine groups towards gold should be enhanced due to a chelate effect, i.e. the second phosphine of one bound molecule should be energetically favored to bind to the particle in comparison to two single monophosphine molecules. Some examples exist for diphosphine-stabilized small gold clusters (see 2.1.4).

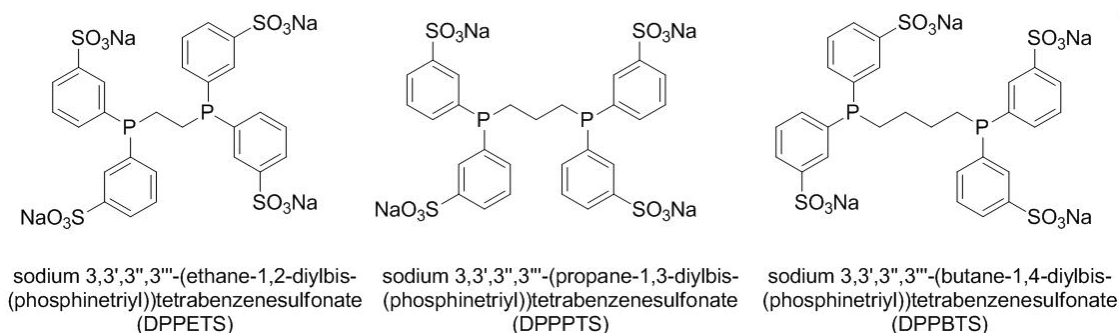


Figure 3.46: Water soluble sulfonated aryl diphosphines synthesized and investigated as AuNP ligands.

To largely exclude any effect of chemical functionalities and to cut down the effect on the binding strength of the ligand shell only, diphosphines were chosen that are as similar to the monophosphines used as possible.

Sodium 3,3',3'',3'''-(ethane-1,2-diylbis(phosphinetriyl))tetrabenzenesulfonate (DPPETS), sodium 3,3',3'',3'''-(propane-1,2-diylbis(phosphinetriyl))tetrabenzenesulfonate (DPPPTS) and sodium 3,3',3'',3'''-(butane-1,2-diylbis(phosphinetriyl))tetrabenzenesulfonate (DPPBTS) meet these requests as they are aryl phosphines with sulfonate groups (fig. 3.46). As well as the monophosphines used, these diphosphines are quite well examined in the field of catalysis, where they act as ligands for metal organic complexes of Ru, for example.[132] The sulfonated diphosphines were synthesized from the respective aryl diphosphines by sulfonation with fuming sulfuric acid (fig. 3.47).

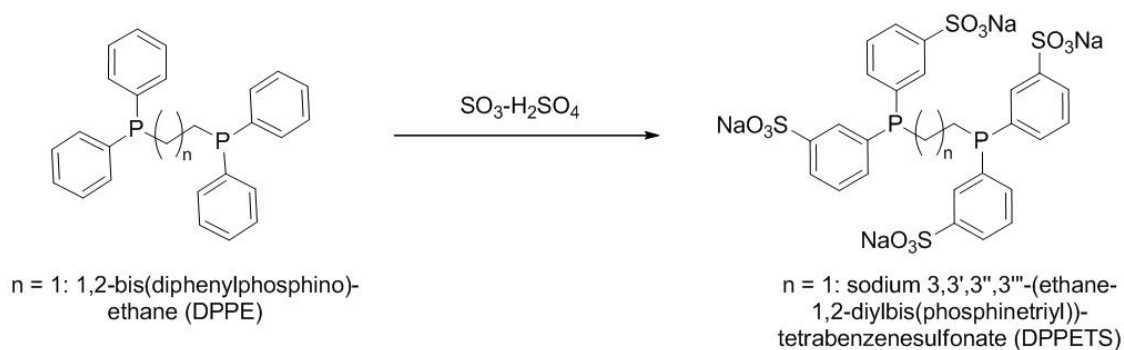


Figure 3.47: Reaction scheme of the sulfonation reaction of diphosphines. DPPE and DPPETS are exemplarily shown.

In the case of DPPETS, the purity of the raw product was only approximately 67%, estimated by ^{31}P -NMR. It was not possible to remove the phosphine oxide impurities by

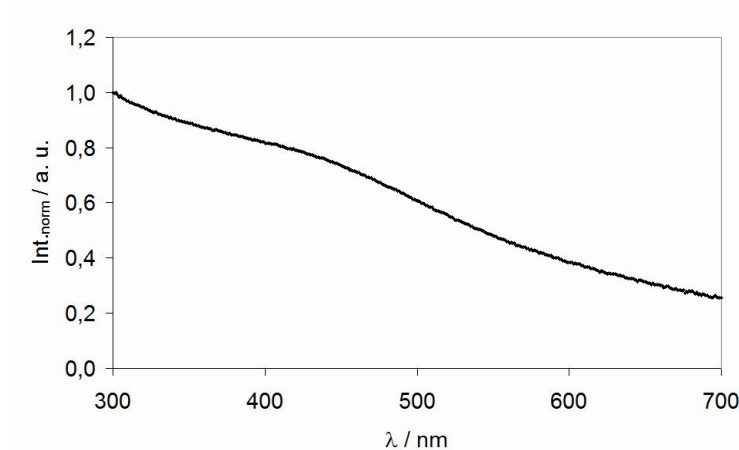


Figure 3.48: UV/Vis spectrum of Au1.4DPPETS.

standard purification techniques. As a phosphine oxide should have a lower affinity to bind to gold compared to a phosphine, the product was used as such for ligand exchange reactions. DPPPTS and DPPBTS were synthesized *via* slightly different routes, leading to higher product purities (86% for DPPPTS and 97% for DPPBTS, respectively, both determined by ^{31}P -NMR spectroscopy). For DPPETS and DPPBTS, the long term stability against oxidation was tested. The NMR sample solutions were left under atmospheric conditions for three days and then measured again. In both cases, no increase of the phosphine oxide amount was detectable.

The ligand exchange reactions were again performed as two phase systems. In the case of Au1.4DPPETS, the reaction mixture was stirred overnight. After this time, the aqueous phase had become brown, thus the reaction was stopped and the product isolated. The UV/Vis spectrum did not show a prominent shoulder (fig. 3.48); however, the STEM analysis showed several larger particles than expected and a mean diameter of $1.8 \pm 0.3 \text{ nm}$ (fig. 3.49). In the ^{31}P -NMR, no signal of free DPPETS could be detected anymore. The signals were shifted to $\delta = 20 - 23 \text{ ppm}$.

The chemical analysis revealed C and H amounts much higher than expected, reproducibly for several batches (see table 3.2).

Usually this is caused by excess ligands, but washing of the sample did not improve the results. One explanation might be that more diphosphine molecules than expected coordinated to one AuNP, possibly in a monodentate binding mode. As one phosphorus

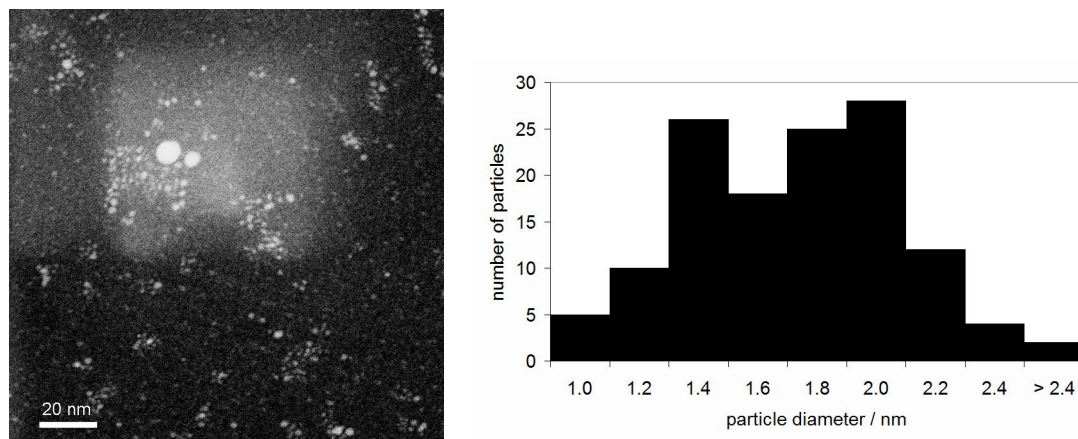


Figure 3.49: STEM micrograph (left) and histogram (right) of Au1.4DPPETS.

Table 3.2: Results of EA of Au1.4DPPETS. Theoretical values are calculated for potential chemical formulas of $\text{Au}_{55}\text{DPPETS}_6\text{Cl}_6$ (DPPETS bidentate bound) and $\text{Au}_{55}\text{DPPETS}_{12}\text{Cl}_6$ (DPPETS monodentate bound).

	C / %	H / %
Theoretical values (6 ligands)	11.8	0.8
Theoretical values (12 ligands)	18.0	1.2
Measured values	40.99	3.42
After 2 nd washing	40.82	4.24

atom is surrounded by only two phenyl rings and one alkyl chain, it is sterically less bulky than the TPPMS with its three phenyl groups per phosphorus, and potentially more ligands fit around one particle. Another explanation might be the occurrence of smaller gold clusters or mononuclear gold complexes, stabilized by diphosphines. Possibly this is thermodynamically favored due to steric reasons so that the AuNP cores were partially degraded by the diphosphine excess during ligand exchange.

With another batch of AuNPs, some stability experiments concerning the ligand-AuNP bond were performed. The chemical stability of the material was tested by the addition of KCN to a Au1.4DPPETS solution and time-dependent UV/Vis spectroscopy. In the presence of KCN, elemental gold is oxidized by oxygen according to the reaction shown in scheme 3.50.

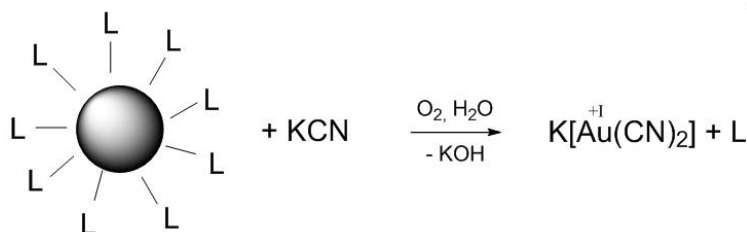


Figure 3.50: Oxidative degradation of AuNPs in the presence of KCN.

The degradation rate of the AuNPs by KCN depends on the ability of a ligand to shield the AuNP surface.[47] Au1.4DPPETS and as a reference Au1.4MS were both analyzed for 2 h. The intensity of absorbance at $\lambda = 430 \text{ nm}$ was plotted against time (fig. 3.51).

Interestingly, the decay is steeper in the case of Au1.4DPPETS than it is for Au1.4MS. This greater sensitivity of Au1.4DPPETS against KCN degradation might be a hint that DPPETS only acts as a monodentate ligand and not, as it was expected, as a bidentate one. In that case, the behavior towards degradation can possibly again be related to the fact that each phosphorus atom in DPPETS has only two phenyl rings and one alkyl chain. From a steric point of view, it is conceivable that the AuNP surface is therefore better accessible than in the case of a TPPMS-stabilized AuNP.

To investigate whether DPPETS acts as a mono- or a bidentate ligand, atom distances of the ligand and the gold cluster were theoretically estimated. They were based on the Au_{55} cluster as this was the precursor species for the ligand exchange reaction. In Au_{55} , the

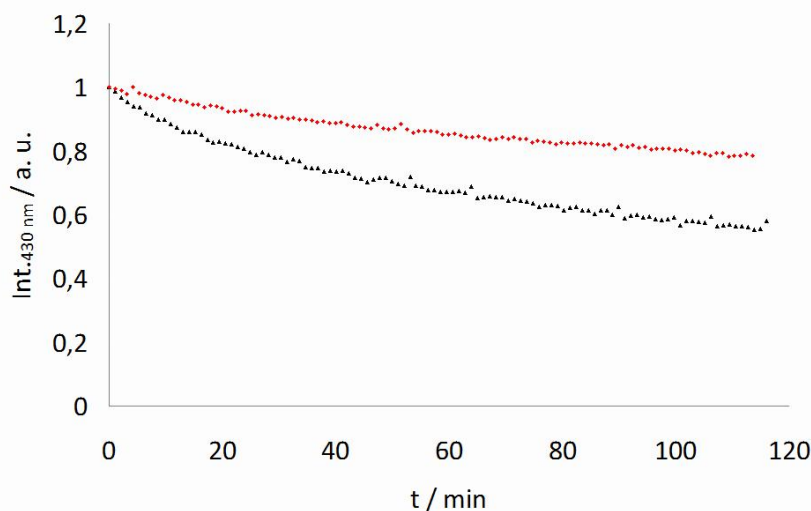


Figure 3.51: Time-dependent plot from the UV/Vis spectra of the KCN degradation of Au1.4DPPETS (black) and Au1.4MS (red), followed at 430 nm.

distance of two vertex atoms, to which the TPPMS molecules are bound, is approximately 0.86 nm. The P–P distance in a DPPETS molecule is approximately 0.45 nm, as assessed with the program *ChemBio3D* (*CambridgeSoft*, version 12.0). The molecule is therefore not appropriate to bind to a Au₅₅ cluster in the expected way. Still, one DPPETS molecule could possibly bind to two adjacent gold atoms or even to the same gold atom. More sophisticated calculations were not performed in that direction, but the insufficient chain length of DPPETS might be the explanation for the unexpected behavior of Au1.4DPPETS in the KCN experiment.

As another method, differential scanning calorimetry (DSC) was applied to analyze Au1.4DPPETS and Au1.4MS (fig. 3.52). The ligands, DPPETS and TPPMS, were measured first and showed no thermal degradation up to 400 °C.

The measurement of Au1.4MS showed a sharp signal at 240 °C which may indicate the loss of the TPPMS shell. This is comparable to a thermogravimetric analysis of 1.5 nm sized, TPP-stabilized AuNPs.[133] These showed a mass loss of 24.5 % in a temperature range of 200 – 250 °C which is assigned to the organic fraction of the AuNPs.

For Au1.4DPPETS on the other hand, no sharp signal is found, but a steady decay above 320 °C, indicating a higher stability than Au1.4MS. Compared to the KCN degradation experiment which focuses on the chemical stability, DSC is a method to investigate material

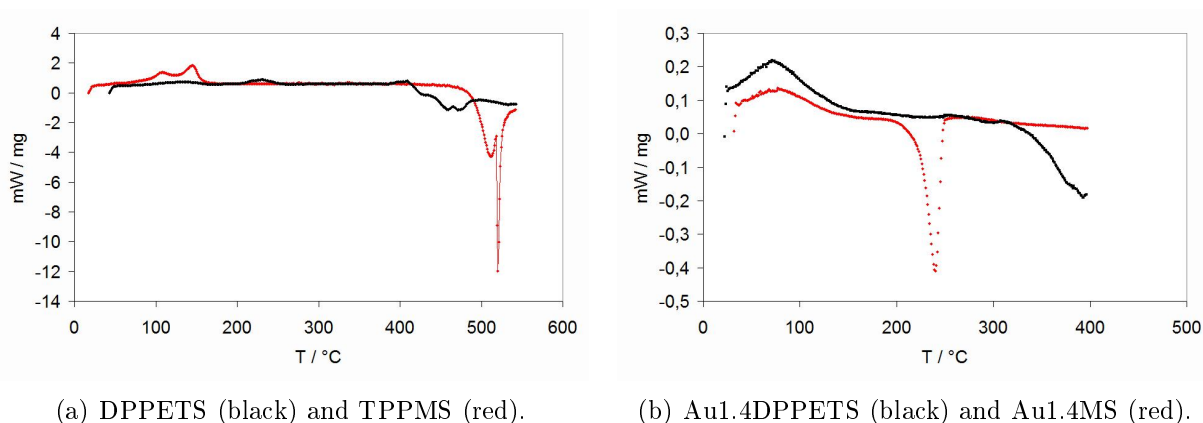


Figure 3.52: DSC measurements of the ligands (a) and the AuNPs (b).

properties such as melting, vaporization and sublimation. Furthermore, it is performed with the solid material in contrast to the KCN experiment in solution. These differences might explain why the results from both methods are contradictory and DSC points towards a higher stability of Au1.4DPPETS compared to Au1.4MS.

As the theoretical investigation of DPPETS as a ligand for Au₅₅ showed that the alkyl chain between the two phosphorus atoms might be too short, the ligands DPPPTS and DPPBTS were used for ligand exchange reactions. The reaction times were prolonged to 4 days to increase the yields of water soluble product.

For Au1.4DPPPTS, the ligand exchange reaction seemed to be partially successful, as a moderately colored water phase could be obtained after one week of reaction. A chemical analysis however showed, similar as for Au1.4DPPETS, higher C and H values than expected (see table 3.3).

Table 3.3: Results of EA of Au1.4DPPPTS.

	C / %	H / %
Theoretical values	12.24	0.98
Measured values	27.41	2.73

During a further purification by dialysis, the AuNPs aggregated. In general, the particles showed low stability in aqueous solution, thus, no further analytics in solution were performed. The low stability of DPPPTS-stabilized AuNPs might also stem from the still too short P–P distance of the molecule, still being too short to act as a bidentate ligand. When

the diphosphines bind as monodentate ligands to the particle surface, they have a lower steric hindrance than TPPMS and are thus weaker stabilizing ligands.

The synthesis of Au1.4DPPBTS was partially successful. As for the other two diphosphine-stabilized AuNP species, the elemental analysis revealed a higher fraction of hydrocarbons than the theoretical values for Au1.4DPPBTS with 6 or 12 ligand molecules (see table 3.4). Further purification by dialysis did not affect this fact: 40 mg of Au1.4DPPBTS were dissolved in H₂O and dialyzed for three days. 15 mg product were retrieved, of which the EA showed even slightly higher amounts of C and H than prior to the dialysis. This might be due to some aggregation that occurred during the dialysis, and parts of the released ligands from aggregated AuNPs might have increased the ligand excess in the product.

Table 3.4: Results of EA of Au1.4DPPBTS.

	C / %	H / %
Theoretical values	12.65	1.05
Measured values	26.73	2.75
After dialysis	29.30	3.30

For further analytics, the non-dialyzed raw product was used. A STEM analysis showed that the AuNPs had a mean diameter of 1.4 ± 0.2 nm (fig. 3.53).

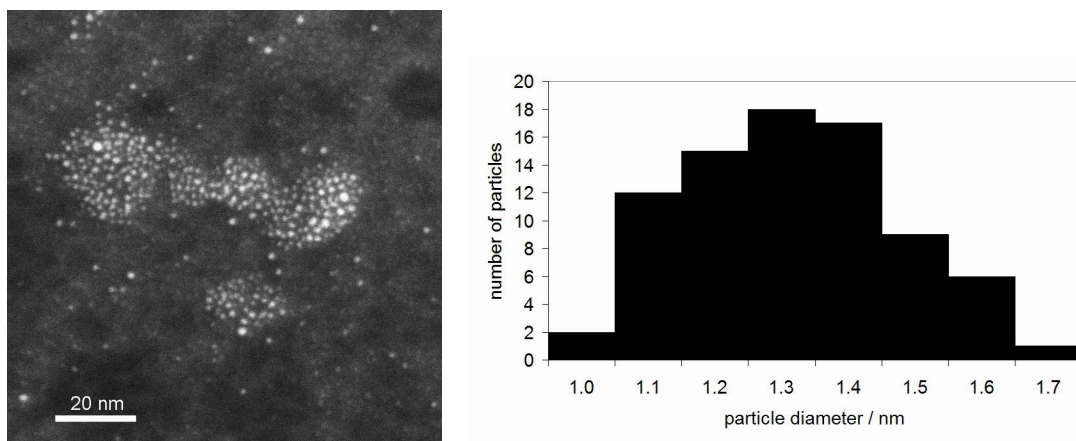


Figure 3.53: STEM micrograph (left) and histogram (right) of Au1.4DPPBTS.

A ³¹P-NMR spectrum showed only two broadened signals at 40.8 and 43.5 ppm. No signal at −12.1 ppm from the free ligand was detected. The signal at 40.8 ppm can be assigned

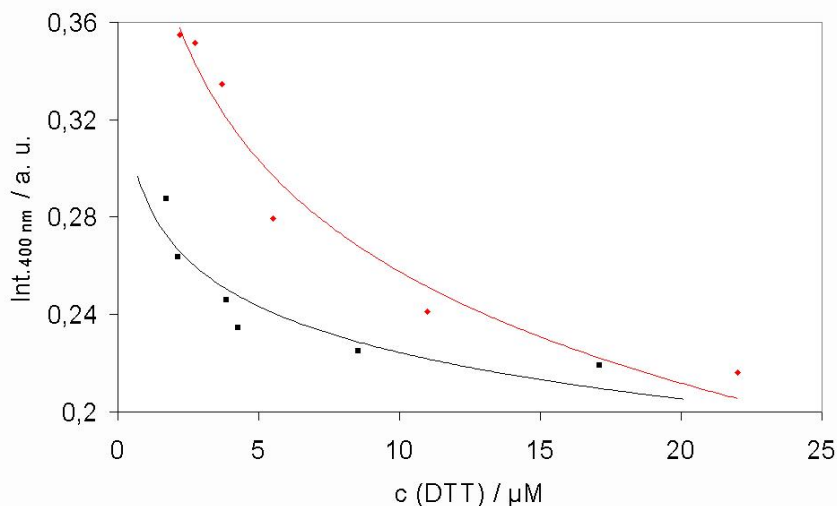


Figure 3.54: Stability test with increasing concentrations of DTT. Plotted are the intensities at 400 nm of UV/Vis spectra from Au1.4DPPBTS (black) and Au1.4MS (red) with the respective logarithmic fit curves.

to phosphine oxide impurities, whereas the signal at 43.5 ppm indicates a phosphine–gold interaction.

A different experiment was performed to test the binding strength of DPPBTS to AuNPs. The reaction with dithiothreitol (DTT) with two thiol functions as a competing ligand was shown to be useful to induce ligand release.[134] Here, it was used to test ligand dependent stability. Dispersions of Au1.4DPPBTS were mixed with increasing concentrations of aqueous DTT solutions. Au1.4MS was processed in the same way. The AuNP starting concentrations were not identical. This impedes a direct comparison. However, when the absorbances at 400 nm are plotted against DTT concentration, the logarithmic fit curve for Au1.4MS shows a steeper decrease, indicating a higher stability of the diphosphine-stabilized species against competing ligands (fig.3.54).

Table 3.5 summarizes all successfully performed ligand exchange reactions with Au1.4TPP. Within this work, it was not possible to synthesize diphosphine-stabilized small AuNPs that were long-term stable, especially in other media than H_2O such as cell culture medium with high ionic strength. One problem could be the ability of bi-functional molecules to bridge two particles and therefore induce the occurrence of networks and aggregation of the AuNPs.

Table 3.5: Two-phase ligand exchange reactions performed with Au1.4TPP (discussed in chapters 3.9 and 3.10).

Particle species	Ligand	Starting mass/mg	Yield/mg	Size ^a /nm
Au1.4MS	TPPMS	35	10.7	1.3 ± 0.2
Au1.4TS	TPPTS	163	15	1.4 ± 0.2
Au1.4TPPMCMA	TPPMCMA	50	n. d. ^b	1.5 ± 0.4
Au1.4TPPMC	TPPMC	50	10.7	1.4 ± 0.2
Au1.4DPPETS	DPPETS	50	27	1.8 ± 0.3
Au1.4DPPBTS	DPPBTS	100	144 ^c	1.1 ± 0.2

^a Determined by STEM. ^b Not determined. ^c Before further purification.

Due to this lack of stability, no cell tests could be performed so far to verify the hypothesis that diphosphine-stabilized AuNPs are less toxic than the respective monophosphine-stabilized AuNPs. Within the cooperation project, there are on-going studies in this field to enable the synthesis of stable diphosphine-stabilized AuNPs and allow the toxicological investigation of such compounds.[135]

To check whether the synthesized diphosphines are suitable ligands for AuNPs in general, they were used to functionalize larger citrate-stabilized gold colloids. Different batches of citrate-stabilized AuNPs with slightly differing mean diameters were used.

DPPETS was mixed with 13 nm sized citrate-stabilized AuNPs. The plasmon resonance maximum in the UV/Vis spectrum shifted from 522 nm to 524 nm, indicating a different dielectric environment and therefore a successful ligand exchange (fig. 3.55). The STEM analysis showed that the AuNP size was not altered (13 ± 1.4 nm, see fig. 3.56). In the ³¹P-NMR spectrum of the sample, no free DPPETS around -12 ppm was detected, only one signal at 41 ppm, indicating phosphine groups bound to gold.

From Au11Citrate with a plasmon resonance peak at 519 nm, Au11DPPPTS ($\lambda_{\max} = 520$ nm) and Au12DPPBTS ($\lambda_{\max} = 519$ nm) were synthesized (fig. 3.55). The STEM analytics resulted in mean particle diameters of 11 ± 0.7 nm and 12 ± 1.2 nm for the two samples, respectively (fig. 3.56).

DLS measurements were conducted to investigate the hydrodynamic radii of the AuNPs (fig. 3.57). The precursor colloids Au11Citrate showed a hydrodynamic particle size of 19.1 nm. As with DLS not only the metal core is measured but the particle including

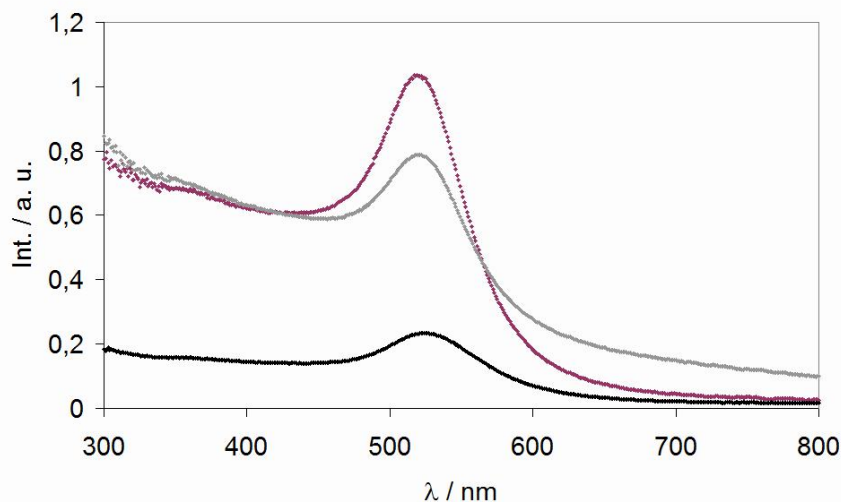


Figure 3.55: UV/Vis spectra of Au13DPPETS (black), Au11DPPPTS (gray) and Au12DPPBTS (purple).

its ligand shell and the hydrate shell, it is reasonable that the value is higher than the diameter determined from STEM micrographs.

For Au11DPPPTS and Au12DPPBTS, hydrodynamic diameters of 21.0 nm and 19.9 nm were determined. A comparison of the DLS measurements of all species shows that the hydrodynamic radii are slightly increased during ligand exchange. DPPPTS and DPPBTS are both sterically bulkier than citrate. The DLS data reflect this as both diphosphine-stabilized AuNPs have increased hydrodynamic radii compared to Au11Citrate. The difference between Au11DPPPTS and Au12DPPBTS is thus surprising, as DPPBTS is the larger molecule but the resulting hydrodynamic diameters of the AuNPs are smaller. The histogram reveals that Au11DPPPTS has a broader size distribution, therefore the here determined diameter might be more defective than the value from Au12DPPBTS.

The stability of all three species was investigated with the KCN degradation experiment (fig. 3.58). Within the accuracy of the experiments, no significant differences in the decay of absorbance was observable for the diphosphine species Au13DPPETS, Au11DPPPTS and Au12DPPBTS. In contrast to that, a batch of Au13MS showed a clearly faster reaction towards KCN. Au11Citrate was degraded even faster and was almost completely decomposed after 20 min.

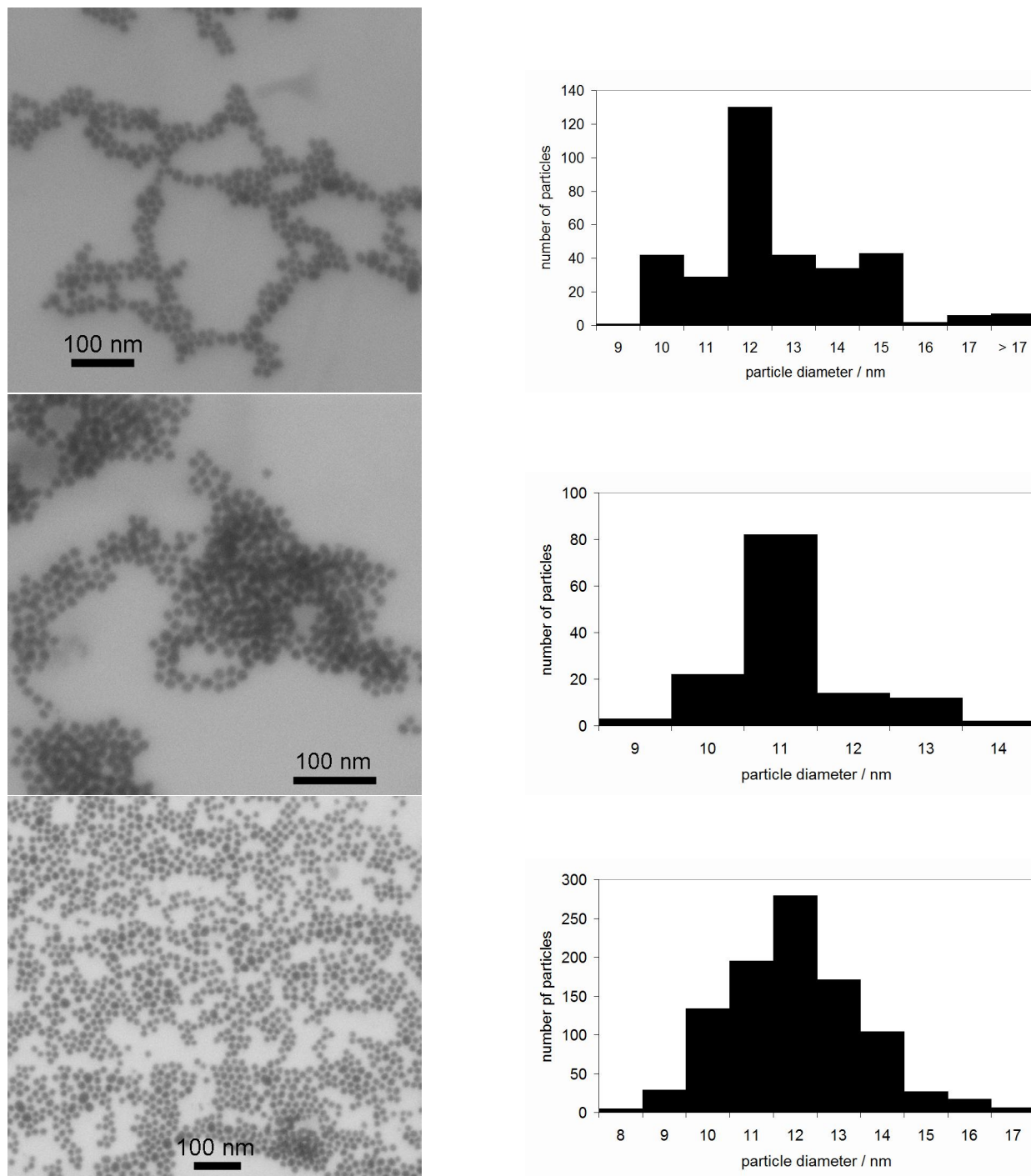


Figure 3.56: STEM micrographs and histograms of Au13DPPETS (top), Au11DPPPTS (middle) and Au12DPPBTS (bottom).

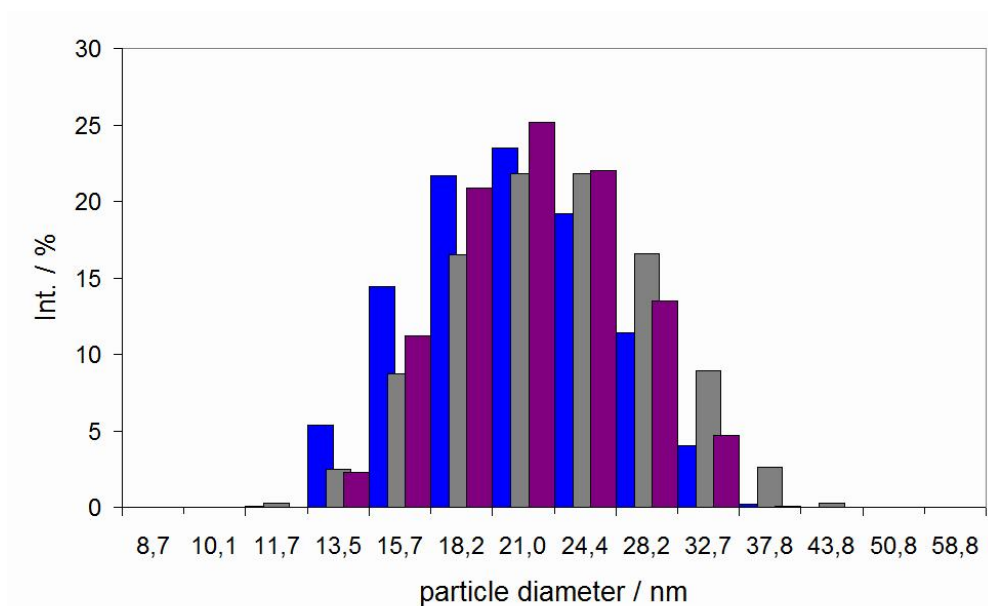


Figure 3.57: Histograms of DLS measurements (intensity weighted) of Au11Citrate (blue), Au11DPPPTS (gray) and Au12DPPBTS (purple).

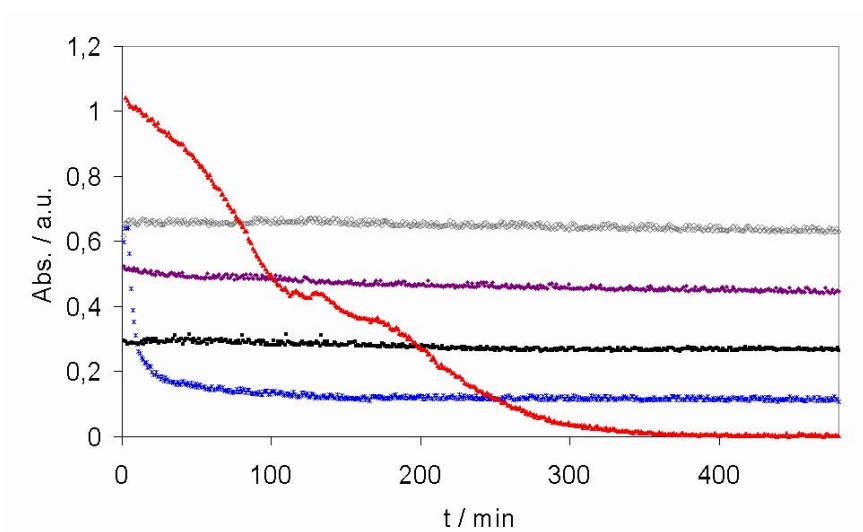


Figure 3.58: Plots of time-dependently measured UV/Vis spectra at respective absorbance maxima during KCN degradation (0.1 M).

Black: Au13DPPETS (plotted at 524 nm); gray: Au11DPPPTS (520 nm); purple: Au12DPPBTS (520 nm); red: Au13MS (524 nm); blue: Au11Citrate (520 nm). Note that starting intensities were not the same for the different AuNP solutions, and for better visualization, the spectra were not normalized.

Diphosphines are obviously suitable molecules as AuNP ligands in the case of colloids. They stabilize gold colloids more strongly against chemical degradation than weaker ligands such as monophosphines or citrate. No effect was found regarding the chain length of diphosphine ligand molecules in the case of colloids above a diameter of 10 nm. This can be explained by the surface curvature of larger AuNPs. On a molecular level, the gold atoms to which one diphosphine molecule binds are almost in one plane. Therefore, the binding situation is completely different, and the resulting strain is obviously not strongly influenced by the chain length of the investigated diphosphines.

Because Au15MS was nontoxic in cell tests, the diphosphine-stabilized gold colloids were not tested in cell experiments as the same result is expected here.

3.11 Labeling Au1.4 with (Lys³)-bombesin

The cytotoxicity of Au1.4MS opens possibilities for therapeutic applications. By binding a target molecule to the AuNP, a selective toxic compound can be generated, for example for use as a cytotoxic drug in cancer therapy.

The concept chosen was the functionalization with bombesin. Bombesin is an oligopeptide that binds to the gastrin-releasing peptide receptor (GRPR) which is expressed mainly in the pancreas. The structural formula is shown below (fig. 3.62).

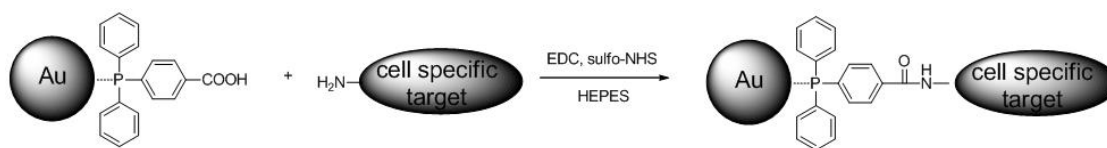


Figure 3.59: Coupling reaction scheme of a cell specific target molecule to Au1.4TPPMC.

As Au1.4TPPMC shows almost the same toxicity as Au1.4MS ($IC_{50} = 43 \mu M$, see chapter 3.9), it was used as the precursor entity (fig. 3.59). The carboxylic acid function enables different routes to bind target molecules. An EDC/sulfo-NHS coupling was chosen (fig. 3.60). When Au1.4TPPMC was functionalized with bombesin, the resulting AuNPs showed mediocre solubility in H_2O and in cell culture medium (pH 7.4). They were well soluble

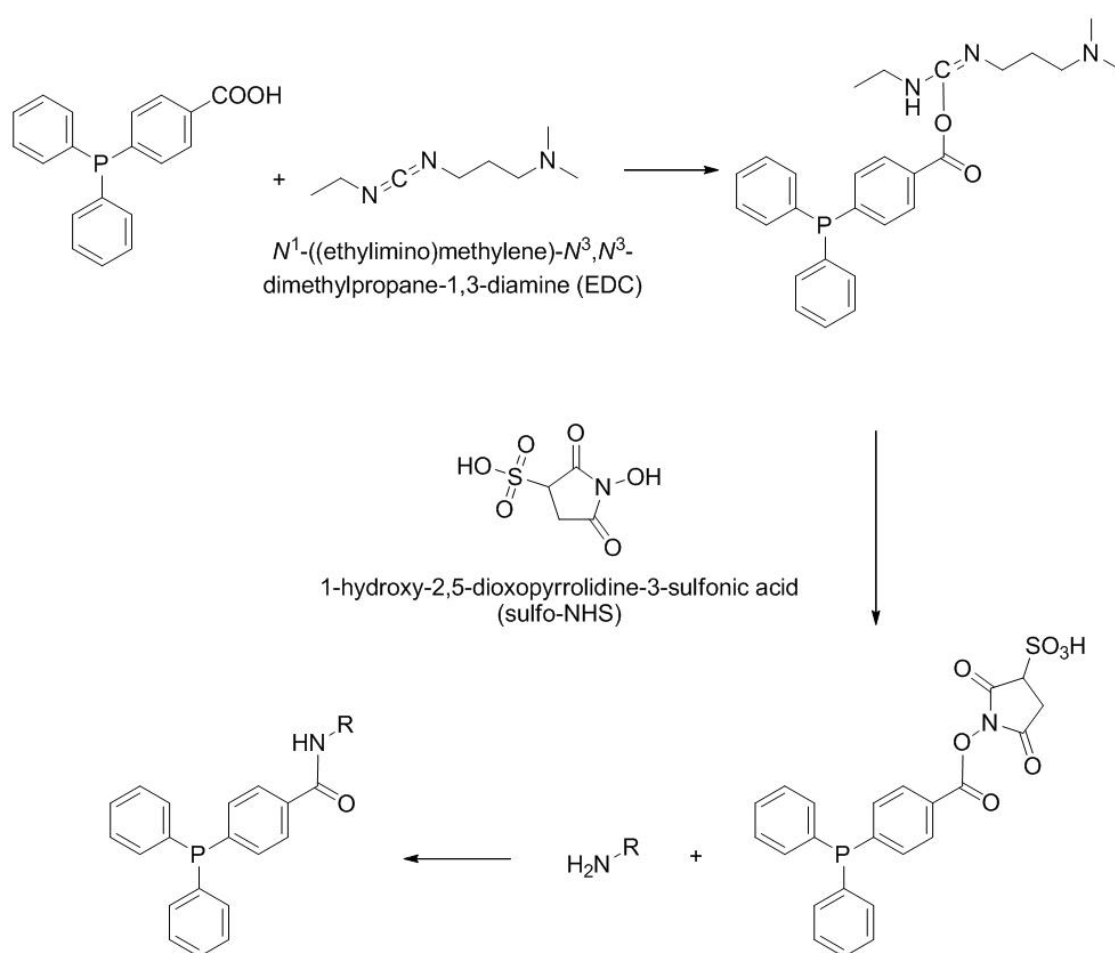


Figure 3.60: EDC/sulfo-NHS coupling reaction of an amine $R-NH_2$, indicating bombesin or (Lys³)-bombesin, to TPPMC. The carboxylic acid function is first activated by EDC, reacts with sulfo-NHS to a temporarily stable sulfo-NHS-ester, and then reacts further with the amine, generating an amide bond.

in acidified solutions. Acidic conditions are not applicable in cell tests though, and neither in later *in vivo* applications.

However, the product was characterized. The different solubility behavior was a first hint for a successful functionalization. Furthermore, the AuNPs were treated with dithiothreitol (DTT), a dithiol with a strong binding affinity towards gold and the ability to cross-link AuNPs (fig. 3.61). The aggregates were removed by centrifugation, the supernatant was dried and analyzed by mass spectroscopy. A signal for the TPPMC-bombesin adduct at $m/z = 1907.9$ could be confirmed.

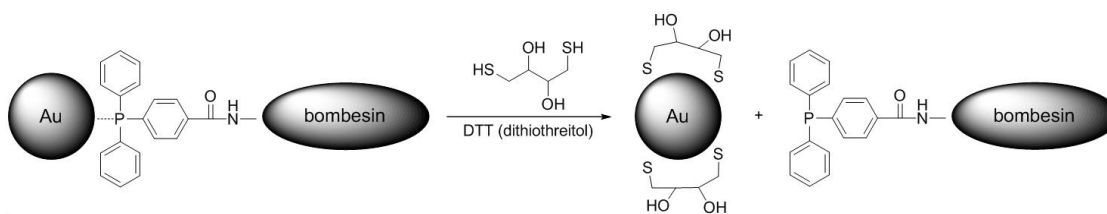


Figure 3.61: DTT ligand exchange reaction with bombesin-functionalized AuNPs. The supernatant was subsequently analyzed by MS.

Different derivatives of the peptide bombesin are available that are equally effective in binding assays and clinical studies. To facilitate the coupling reaction, (Lys³)-bombesin with a lysine residue instead of arginine on third position of the peptide structure was chosen for further experiments (fig. 3.62). The primary amine of lysine ($pK_B = 10.5$) is more prone for a coupling reaction than the amine of the guanidinium group of arginine ($pK_B = 12.5$).^[136] The use of (Lys³)-bombesin instead of bombesin should not affect the binding affinity towards GRP receptors.^[111]

To enhance solubility and stability, AuNPs with a mixed ligand shell of TPPMS and TPPMC were synthesized (Au1.4MS/MC). The optimal ratio concerning solubility and stability was determined to be a TPPMS:TPPMC molar ratio of 7:1. This is the ratio that was initially used for the ligand exchange reaction; the final exact ratio that was present on the AuNPs was not evaluated.

Characterization of Au1.4MS/MC showed typical UV/Vis spectra without specific features (fig. 3.63), identical for two synthesis batches. The STEM analytics showed AuNPs with narrow size distribution and a mean diameter of 1.4 ± 0.2 nm (fig. 3.64). The standard MTT assay revealed cytotoxicity in the same magnitude as Au1.4MS ($IC_{50} = 30.1 \mu M$).

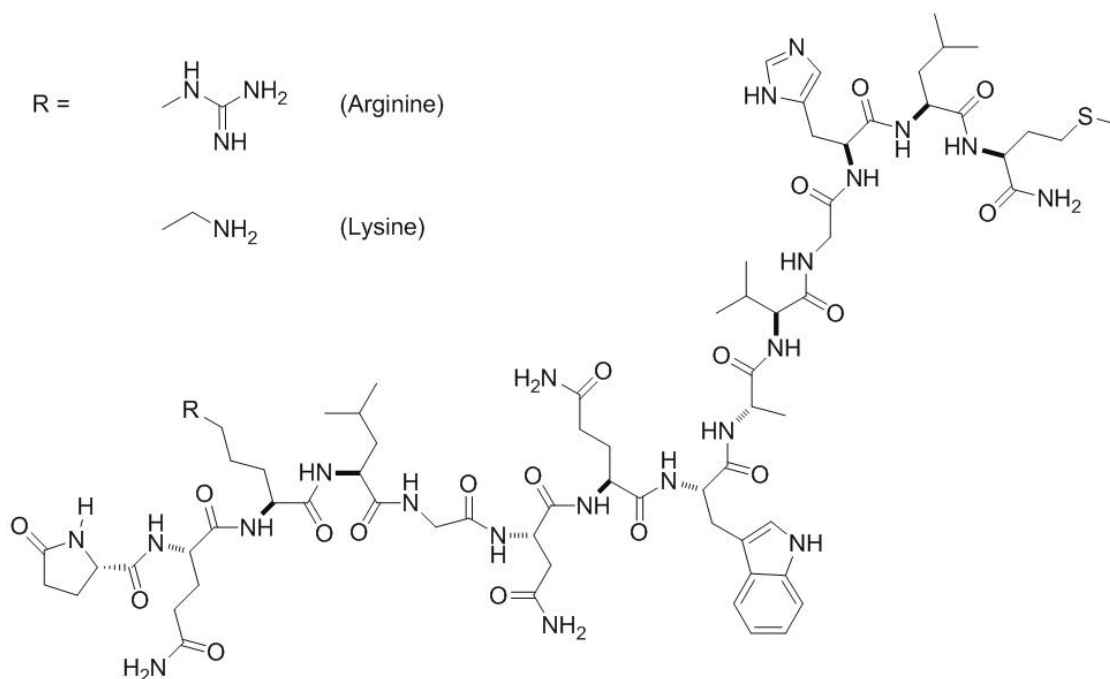


Figure 3.62: Bombesin, an oligopeptide consisting of 14 amino acids. Natural bombesin has an arginine group at third position, which is replaced by lysine in (Lys³)-bombesin.

The ligand shell of Au1.4MS contains 12 ligands. As TPPMC has a very similar chemical structure to TPPMS, the same number of ligand molecules per particle can be assumed.

With a statistical ratio of 7:1 (TPPMS:TPPMC), one to two ligand molecules per AuNP have a carboxylic acid function, suitable for the coupling of (Lys³)-bombesin. The coupling was successfully performed, resulting in (Lys³)-bombesin-functionalized AuNPs (Au1.4MS/MC-(Lys³)-bombesin) with approximately one or two bombesin molecules per particle. Therefore, no cooperative effect can be expected, i.e. a higher affinity per particle because of an increased number of agonists to GRPR and thus binding events. On the other hand, it is probable that the binding efficacy of one single bombesin molecule attached to one AuNP is not impaired in this surface density. The product was purified by ultracentrifugation to ensure the absence of free bombesin molecules.

The product was well dispersible in H₂O and stable in cell culture medium. It was characterized by UV/Vis spectroscopy, STEM and IR spectroscopy. The UV/Vis spectrum did not show a defined peak which would be a hint of aggregates in a size range above 3 nm

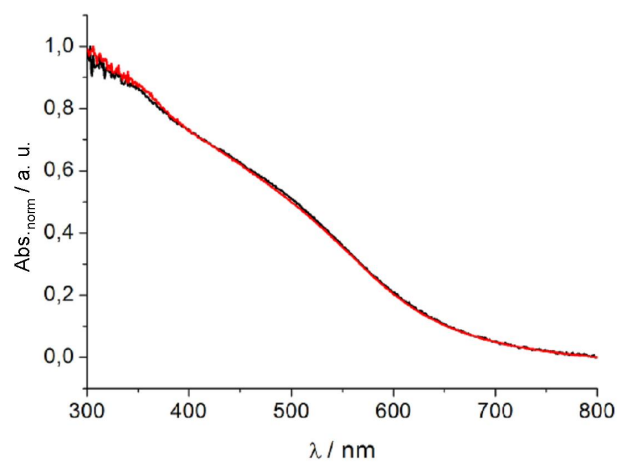


Figure 3.63: UV/Vis spectra of two batches of Au1.4MS/MC.

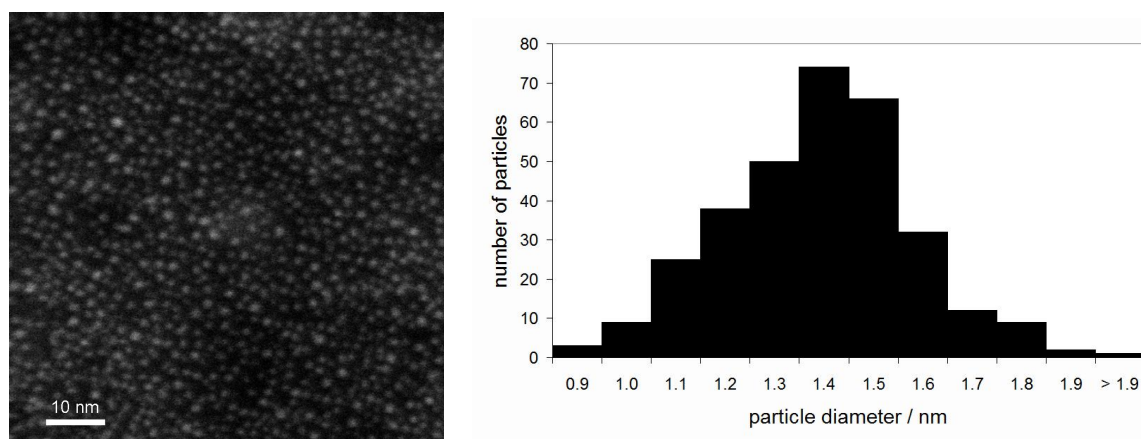


Figure 3.64: STEM micrograph (left) and histogram (right) of Au1.4MS/MC.

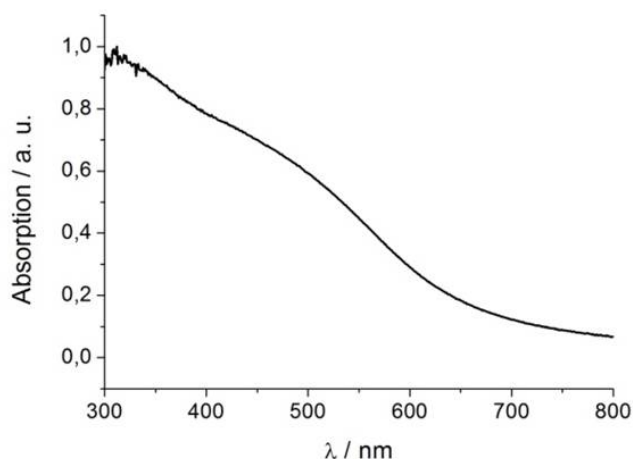


Figure 3.65: UV/Vis spectrum of Au1.4MS/MC-(Lys³)-bombesin.

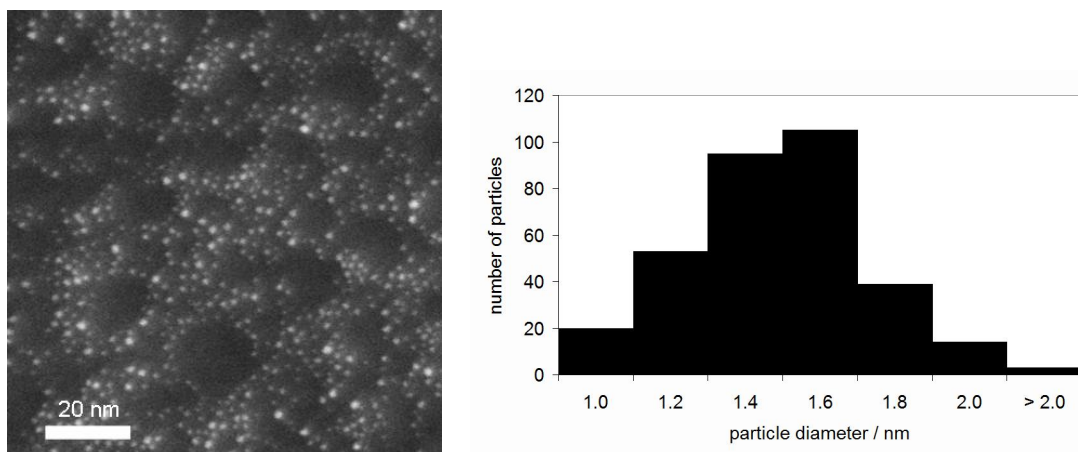


Figure 3.66: STEM micrograph (left) and histogram (right) of Au1.4MS/MC-(Lys³)-bombesin.

(fig. 3.65). The STEM analysis confirmed this as no aggregates were visible, and a mean diameter of $1.5 \text{ nm} \pm 0.2 \text{ nm}$ was determined (see fig. 3.66).

In the IR spectrum of Au1.4MS/MC-(Lys³)-bombesin, the characteristic absorption band for amides was clearly visible at 1643 cm^{-1} (fig. 3.67). This band is thus probably induced by both, the new formed amide bond between TPPMC and the amine functionality of (Lys³)-bombesin as well as the peptide bonds within the latter.

When the product was dried and redispersed in H₂O, the solubility was impaired. Therefore, the afterwards synthesized batches were not dried and stored as solid, but kept in solution. As such, they were stable over months.

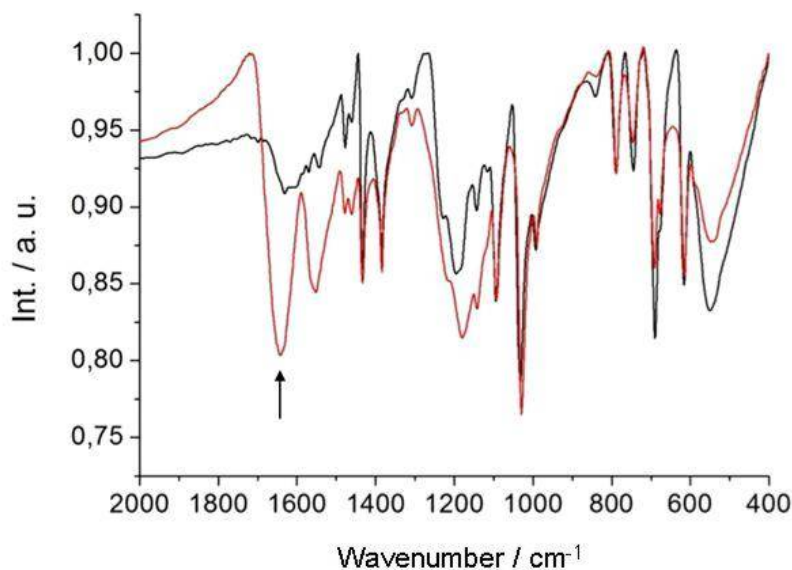


Figure 3.67: IR spectra of Au1.4MS/MC (black) and Au1.4MS/MC-(Lys³)-bombesin (red). The arrow indicates the characteristic amide absorption band at 1643 cm⁻¹.

As the analytics showed AuNPs of the desired size and the functionalization could be proven by IR spectroscopy, cell tests were performed. The MTT assay showed that the functionalization of 1.4 nm sized AuNPs with (Lys³)-bombesin did not alter the cytotoxicity ($IC_{50} = 59 \mu M$).

GeneBLAzer® GRPR-NFAT-bla CHO-K1 cells, purchased from Invitrogen™, were used to analyze if the (Lys³)-bombesin attached to the AuNPs was still active. The cells contain a β -lactamase (bla) reporter gene under control of a NFAT response element. In the case of a receptor-agonist interaction, the production of bla is triggered. As a substrate, coumarin-lactam-fluorescein is added which shows fluorescence at 520 nm from the fluorescein entity. The coumarin fluorescence is transferred by a Förster resonance energy transfer (FRET) to the fluorescein entity in this adduct. Bla cleaves the lactam bridge between the two fluorophores. An interaction with GRPR therefore induces an increase of the coumarin fluorescence at 447 nm, which can be quantified by a fluorescence microplate reader or detected by fluorescence microscopy of cell cultures.

To prove the specific functionalization of Au1.4MS/MC-(Lys³)-bombesin, distinguished from a reaction by potential residual free (Lys³)-bombesin in the sample, the supernatant from the last ultracentrifugation step was also tested as a reference sample. This supernatant visibly contained a low concentration of not centrifuged Au1.4MS/MC-(Lys³)-bombesin. To exclude effects from these particles, the supernatant was dialyzed prior to testing, and the dialysis water was concentrated to a low volume and used.

The effect of Au1.4MS/MC-(Lys³)-bombesin towards the GRPR containing cells was first analyzed visually. Under the microscope, the cytotoxicity of Au1.4MS/MC-(Lys³)-bombesin could be confirmed, whereas pure (Lys³)-bombesin did not cause cell death.

The GRPR cells were then analyzed in a fluorescence reader. For Au1.4MS/MC-(Lys³)-bombesin, increasing fluorescence could be determined, indicating an interaction between the bound (Lys³)-bombesin and the GRP receptors. Pure (Lys³)-bombesin which was tested as reference showed the same effect. Au1.4MS and the ultracentrifugation supernatant, on the other hand, gave no fluorescence signal. This proves that (Lys³)-bombesin could successfully be coupled to Au1.4MS/MC and be purified without any impairment of the (Lys³)-bombesin receptor affinity.

A not expected phenomenon was that even at very low concentrations, there was still an increased fluorescence detectable for Au1.4MS/MC-(Lys³)-bombesin and for the (Lys³)-bombesin reference. A possible explanation is that the bombesin is sticky and was therefore accidentally pipetted in the dilution series in higher concentrations than intended. Although this result is not well understood so far, the trends of all samples show the expected results and point towards covalently to AuNPs attached (Lys³)-bombesin that is still receptor active.

To further confirm these results, the cells were investigated by fluorescence microscopy by Prof. G. Müller-Newen (UKA). Like the fluorescence quantification, the detected fluorescence intensities in the micrographs confirm the effective functionalization of the AuNPs.

As can be seen in fig. 3.68, Au1.4MS does not induce an enhanced coumarin fluorescence and the cells are only stained with the uncleaved substrate (the fluorescence at 520 nm from the adduct is shown in red). (Lys³)-bombesin on the other hand leads to an increased fluorescence at 447 nm, shown as yellow fluorescence here. Au1.4MS/MC-(Lys³)-bombesin

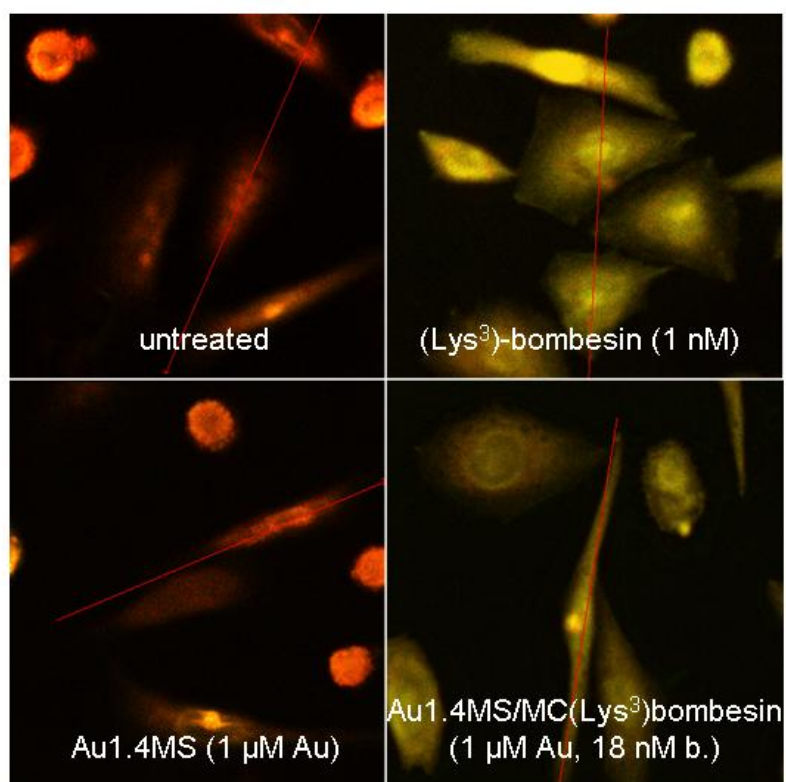


Figure 3.68: GeneBLAzer GRPR-NFAT-bla CHO-K1 cells in fluorescence micrographs. Cells were untreated (up left), treated with 1 nM (Lys³)-bombesin as positive control (up right), with 1 µM Au1.4MS as negative control (down left) and with 1 µM Au1.4MS/MC-(Lys³)-bombesin (down right). Au1.4MS/MC-(Lys³)-bombesin induces enhanced fluorescence at 447 nm as indicated by the yellow color. Figures were provided by G. Müller-Newen, UKA.

has the same effect. The (Lys³)-bombesin bound to AuNPs is still active, can bind to the GRP receptor and trigger the release of coumarin.

In tissue consisting of healthy cells and cancerous cells expressing GRPR, interaction of Au1.4MS/MC-(Lys³)-bombesin with cancer cells is possibly amplified and the functionalized AuNPs will affect mainly those. This would finally lead to a potential cytotoxic drug with reduced side effects.

3.12 Labeling Au1.4 with 5-Aminofluorescein

It could be shown that the ligand binding strength plays a crucial role in AuNP cytotoxicity (3.3). Furthermore, in the patch clamp experiments it became obvious that the equilibrium of bound and free ligands has a great influence on the interaction with ion channels (3.8). From these findings it can be assumed that the ligand shell of Au1.4MS is partially or completely stripped at some point of the interaction with a cell.

Until now, there is no clarity about this stripping event, i.e. the time point and the spatial circumstance and which cell organelles or molecular entities might be involved. Also, the uptake mechanism of small AuNPs could not be verified so far. The uptake of Au15MS *via* endocytosis and the fate of these AuNPs in vesicles within the cells could be shown by TEM. Au1.4MS is however too small to be clearly visualized in the organic material.

To learn more about the interaction of Au1.4MS with a cell and its membrane and to follow the TPPMS ligand shell, it would be helpful to have a probe that can easily be visualized. The use of fluorescence markers would allow further investigation.

The fluorescence of fluorophores that are bound closely to the surface of metal nanoparticles is quenched due to resonant energy transfer. This effect depends of the AuNP size and the spacer length, determining the distance between fluorophore and nanoparticle.[74] A species consisting of a 1.4 nm gold core and a phosphine ligand shell labeled with a fluorophore would allow to follow the fate of the ligand molecules within the cell by fluorescence microscopy. In the moment of ligand stripping, the until then quenched fluorophore should light up.

5-Aminofluorescein was chosen for this purpose (fig. 3.69). It was attached to Au1.4MS/MC by an EDC/sulfo-NHS coupling under the same conditions as (Lys³)-bombesin (fig. 3.70,

see also chapter 3.11), resulting in Au1.4MS/MC-Aminofluorescein comprising the adduct TPPMC-AF.

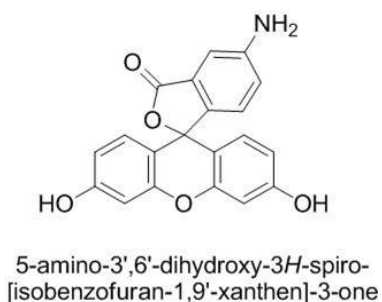


Figure 3.69: Chemical structure of the fluorophore 5-aminofluorescein.

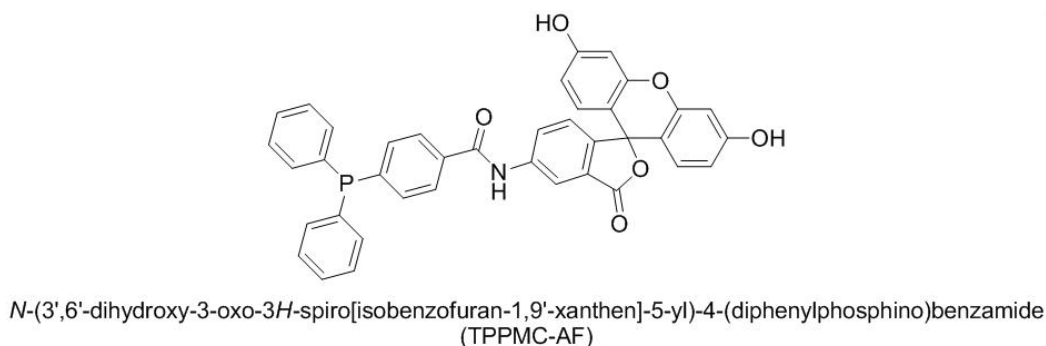


Figure 3.70: 5-Aminofluorescein, coupled to TPPMC *via* an amide bond.

The UV/Vis spectrum of the product showed a distinct peak at 484 nm (fig. 3.71). A comparison to the UV/Vis spectrum of pure 5-aminofluorescein revealed the origin for this peak, as it showed high absorbance at this wavelength.

The STEM analysis showed that the particle functionalization had not altered the AuNP size distribution much (mean diameter $1.5 \text{ nm} \pm 0.2 \text{ nm}$; see fig. 3.72).

An IR spectrum of the product confirmed the positive functionalization, as the characteristic bands at 1630 cm^{-1} and 1385 cm^{-1} from the spectrum of 5-aminofluorescein were clearly visible here as well (fig. 3.73).

Next, the ability for monitoring the ligand binding and unbinding was evaluated. Au1.4MS/MC-Aminofluorescein was treated with DTT to release TPPMC-AF from the AuNP surface. Fluorescence spectroscopy measurements of the stock solution before treatment and of the supernatant after DTT induced aggregation were conducted.

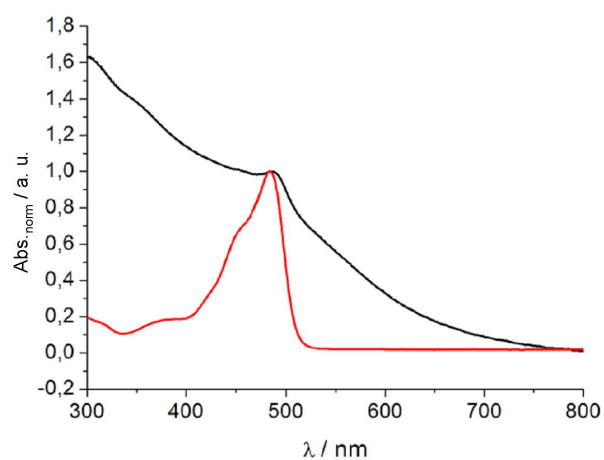


Figure 3.71: UV/Vis spectra of Au1.4MS/MC-Aminofluorescein (black) and 5-aminofluorescein (red).

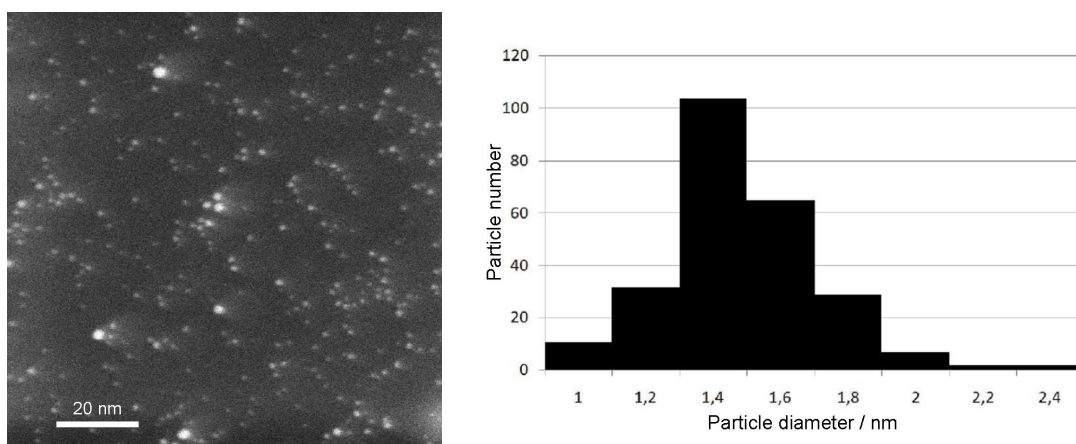


Figure 3.72: STEM micrograph (left) and histogram (right) of Au1.4MS/MC-Aminofluorescein.

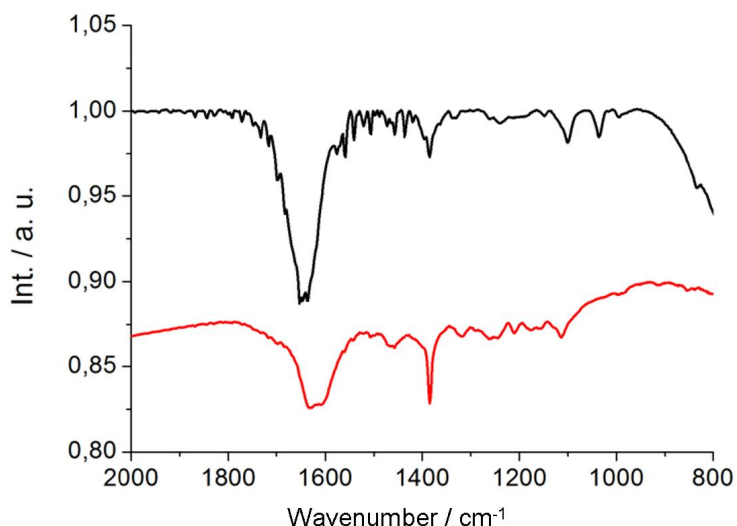


Figure 3.73: IR spectra of Au1.4MS/MC-Aminofluorescein (black) and 5-aminofluorescein (red).

The measurements gave contradicting results. The fluorescence intensity at 520 nm (fluorescence maximum for 5-aminofluorescein) did not change strongly. After the reaction with DTT the signal was even slightly weaker, opposed to what was expected (fig. 3.74).

Possibly, AuNPs with a mean diameter of 1.4 nm are too small for efficient fluorescence quenching, and the 5-aminofluorescein attached to the particles already gave a full intensity signal. Another explanation for this finding is an excess of unbound 5-aminofluorescein in the AuNP stock solution. This is however not probable, as the wash supernatants of the sample after synthesis showed decreasing fluorescence, indicating efficient washing (fig. 3.75). Within the first three washing steps, fluorescence increased, probably due to subsequent release of unspecifically bound 5-aminofluorescein. In washing steps 4 and 5, the fluorescence decreases. This was interpreted as successful washing.

If the insufficient quenching efficacy of 1.4 nm sized AuNPs is the reason for the fluorescence spectroscopy results, a different concept instead of using attached 5-aminofluorescein has to be applied to visualize ligand desorption.

The standard cell test was performed nonetheless, giving a similar IC_{50} as non-functionalized Au1.4MS ($IC_{50} = 32 \mu M$). This result suggests that the functionalization of Au1.4MS/MC with 5-aminofluorescein does not alter the interaction with cells.

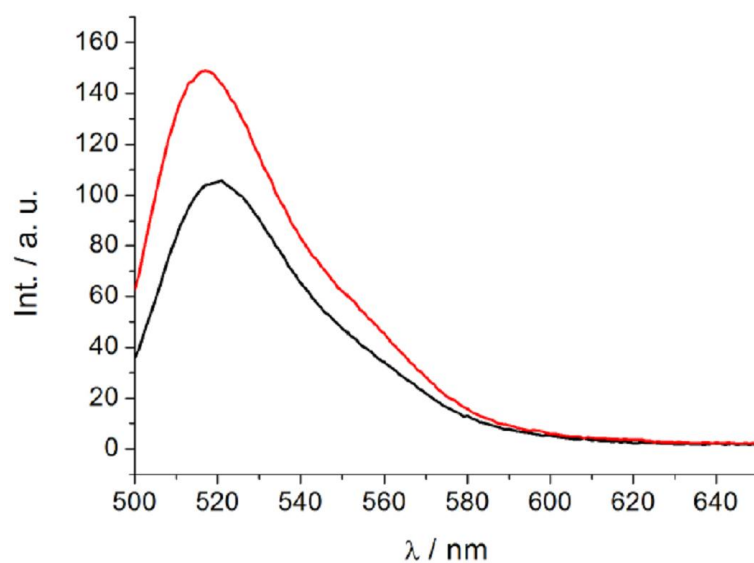


Figure 3.74: Fluorescence spectra of a Au1.4MS/MC-Aminofluorescein solution before (red) and after (black) reaction with DTT.

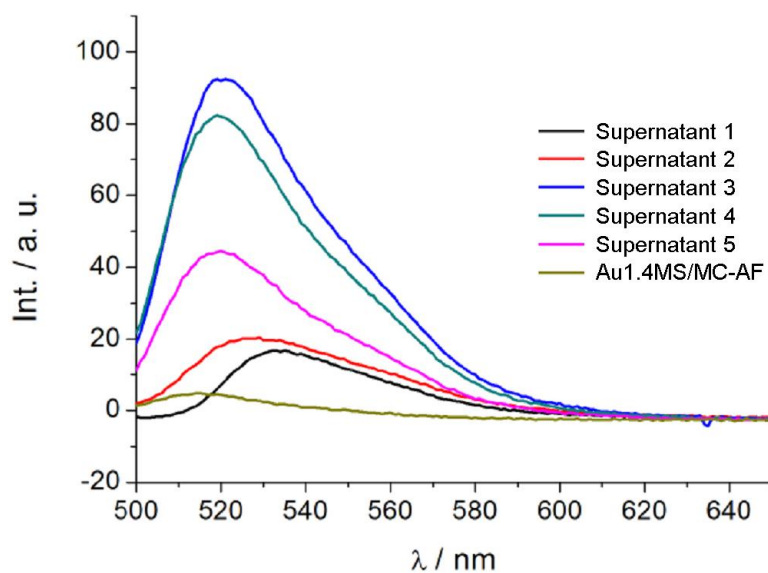


Figure 3.75: Fluorescence spectra of the washing supernatants from the coupling product Au1.4MS/MC-Aminofluorescein.

4 Summary and Outlook

The biological activity of a variety of AuNPs was examined in detail. For this, diverse water soluble AuNPs have been synthesized and characterized for subsequent cytotoxicity investigations. Following the first of the initially formulated parameters, AuNPs of different sizes up to 15 nm were synthesized. They were all functionalized with TPPMS for a ligand independent size effect determination which resulted in the identification of Au1.4MS as the most toxic AuNP species.

A toxicity dependence of gold–ligand binding strength was revealed by synthesis and further analysis of GSH-stabilized AuNPs. The stronger binding thiol ligands could clearly reduce the AuNP toxicity. This pointed towards an influence of the accessibility of the AuNP surface.

Mechanistic aspects concerning the Au1.4MS toxicity were examined. These AuNPs mainly induce necrosis in cells. Furthermore, they activate the expression of heat shock and stress related genes. A fluorophore dye based flow cytometry analysis indicated a correlation with oxidative stress. This could partially be confirmed by the protecting effect of anti-oxidants. However, this was obviously more related to a binding reaction to the AuNPs and not directly to an antioxidative effect, as ascorbic acid without gold affine functional groups had a significantly different effect than GSH, NAC and TPPMS.

A hypothesized correlation between cytotoxicity and catalytic activity towards oxidation reactions could not be confirmed when Amino-TEMPO was used as oxidation substrate for EPR studies. Only non-toxic citrate-stabilized gold colloids were able to quench the Amino-TEMPO signal whereas all other differently stabilized AuNPs (with TPPMS or GSH, respectively) had no effect on the substrate signal intensity, thus no oxidation activity.

The experiments concerning genotoxicity of AuNPs gave unexpected results. DNA damage was investigated by quantification of DNA base lesions *via* GC/MS in the presence of isotopically labeled oxidation products. Here, Au1.4MS and Au1.1GSH showed a very similar behavior despite an opposite toxicity profile. Furthermore it was found that the concentrations of two lesions, FapyAde and FapyGua, were decreased. This was not expected and is still under further investigation for a deeper understanding.

A toxic effect by potentially present TPPMS-Au(I)-Cl could be ruled out. Although the Au(I) complex shows high cytotoxicity, it was proven in a dialysis experiment that only TPPMS shows desorption of Au1.4MS to some extent, but no gold could be detected by EDX analysis of the supernatant residue. The adsorption/desorption equilibrium of TPPMS on Au1.4MS was analyzed by ^{31}P -NMR spectroscopy, resulting in an equilibrium constant of $K_d = 4.76 \times 10^{-7}$ and a free Gibbs energy of 35.5 kJ/mol.

This effect plays obviously also a role in the interaction of Au1.4MS with potassium ion channels. Patch clamp experiments identified Au1.4MS as an irreversibly acting hERG channel blocker. No other AuNP material tested showed this effect, and for Au1.4MS it could be inhibited by the addition of FCS, GSH or TPPMS. Again, ligand stripping of TPPMS as a crucial factor for feasible interaction was postulated and could be corroborated by docking simulations, conducted by the Wenzel group (KIT, Karlsruhe).

In agreement to this, variation of the phosphine functionalities (TPPTS, TPPMC) did not alter the toxicity of Au1.4MS. Obviously, the interaction strength with the AuNP surface is the dominating factor whereas the influence of outer ligand functionalities can be neglected. However, it was not possible to synthesize stable positively charged AuNPs of 1.4 nm size, which may potentially show a different cell interaction.

The effort to synthesize diphosphine-stabilized 1.4 nm sized AuNPs was not successful. This would be an interesting species with potentially intermediate binding affinity between monophosphines and thiols. Different diphosphine-stabilized gold colloids, stabilized with DPPETS, DPPPTS and DPPBTS, with an average size of 12 nm were successfully synthesized and showed all a higher stability in a KCN degradation experiment than TPPMS-stabilized AuNPs.

The functionalization of Au1.4MS/MC with (Lys³)-bombesin could be realized by an EDC/sulfo-NHS coupling reaction. The functionalization was proven by IR spectroscopy. Cell tests showed that both the IC₅₀ value of the AuNPs as well as the receptor affinity of (Lys³)-bombesin could be retained. This proof of concept shows high potential for a further application in cancer therapy.

Via the same route, 5-aminofluorescein functionalized AuNPs could be synthesized. Nevertheless, they were not applicable for ligand visualization in cells due to unspecific ligand desorption and therefore fluorophore release already in ultrapure water.

Summarized, the biological effects of diverse AuNP materials were investigated in detail. A size- as well as a ligand-dependent toxicity were observed, with Au1.4MS as the most toxic species. Some hypotheses concerning its mechanism could be validated, others be disproven. The high cytotoxicity of Au1.4MS could neither be directly connected with DNA transcription inhibition, nor with direct oxidation catalysis. A side effect by Au(I) species could also be ruled out. The understanding of toxicity behavior still requires further mechanistic studies.

In future, it might be interesting to use sophisticated cell analytics regarding specific sub-cellular structures and reactions to gain deeper insight into the exact mechanism of the cytotoxicity of Au1.4MS. *In vitro* EPR spectroscopy is a method to visualize ROS in cells and could therefore help to answer the questions concerning time point of action and cell organelle(s) involved, i. e. when and where oxidative stress occurs.

The genotoxicity studies should be further conducted. The investigation of other DNA repair enzymes besides NEIL1 could lead to the identification of an enzyme that can be activated by AuNPs. As the non-toxic Au1.1GSH also led to an decrease of certain DNA lesions, this species would be an interesting candidate for potential medical applications to enhance DNA repair.

The synthesis of diphosphine-stabilized, small AuNPs with long-term stability was found to be challenging. However, species of this type would be interesting for cytotoxicity investigations. Variation of the reaction conditions and testing of further diphosphines could potentially lead to success here.

A system of phosphine-stabilized, 1.4 nm sized AuNPs with a fluorophore marker that does not readily desorb from the AuNPs would be an interesting probe for fluorescence microscopy investigations in cells. Possibly this can be achieved by varying the reaction and purification conditions for the synthesis of Au1.4MS/MC-Aminofluorescein. Alternatively, a combination of this approach with the use of diphosphine ligands could solve this problem. The desorption of the ligand shell is most probably a crucial step in the AuNP/cell interaction pathway and deserves further investigation.

The functionalization of AuNPs with bombesin gave encouraging first results. These particles are very promising candidates for further tests, potentially *in vivo* in a tumor model to investigate whether the AuNPs show increased uptake in tumor cells besides healthy tissue. The organ distribution of Au1.4MS in an *in vivo* rat model was already investigated. 24 h after intravenous injection, the highest concentration ($\sim 50\%$) was found in the liver due to clearance effects. 19.3% were present in the carcass (which refers to the entire body of the animal without the organs and tissues that were removed). This reflects a uniform distribution of Au1.4MS throughout the whole body. No specific uptake in any organs could be observed, but significant amounts of the injected dose (3.7%) circulated in the blood. For a potential application of a targeted species it is interesting to notice that Au1.4MS was not cleared completely within 24 h, in opposite to larger AuNPs of 18 nm diameter.[137]

In a more recent study, the size dependence of AuNP biodistribution was further investigated. 5 differently sized, TPPMS-stabilized AuNPs were intravenously injected in rats in low doses to exclude acute toxicity, and the distribution after 24 h was analyzed by using radio-labeled AuNPs with ^{198}Au . Au1.4MS was not accumulated in the liver to the same extent as all other, larger AuNPs (51% compared to $> 80\%$). Further, Au1.4MS showed highest percentage of retention in blood (8%) and highest clearance *via* urine (4.7%) of all AuNPs tested.[138] These findings confirm that Au1.4MS is well distributed *in vivo* and also that slow clearance is possible, which is crucial for a potential therapeutic use.

Administration of the same library of AuNPs to rats by oral ingestion led to a generally low absorption across intestinal membranes, showing that the administration pathway is an important parameter, but again Au1.4MS showed highest uptake of all AuNPs tested (0.37%).[139]

This field could also be further expanded by using other targeting entities, such as CPPs or NLS peptides. There are numerous receptors on cells that are interesting target structures.[106]

Besides the here investigated toxicity dependence on size and ligand functionalization of spherical AuNPs, the influence of shape could be examined, as for example gold nanorods and hollow gold nanospheres have interesting optical properties with application potential in imaging and treatment of diseases which makes the toxicological analysis indispensable. Apart from AuNPs, various other metal nanoparticles have valuable properties with potential applications for biomedical purposes, such as superparamagnetic FePt nanoparticles. Synthesis of water-soluble species and systematic toxicology investigations would open the door to new developments in diverse nanomaterial based applications.

5 Experimental Part

5.1 Chemicals and Solvents

5.1.1 Precursor Chemicals

Chemicals were available at the Institute of Inorganic Chemistry (IAC), RWTH Aachen University, at the Cytocentrics AG, Rostock, or at the National Institute of Standards and Technology (NIST), Gaithersburg, MD, USA, or purchased from diverse commercial suppliers. If not stated explicitly differently, chemicals were used as received.

Table 5.1: Chemicals, solvents and suppliers.

Substance, grade/concentration	Supplier
Acetic acid	Riedel de Haen
Acetonitrile	Merck
5-Aminofluorescein	Fluka
2-Amino-5-iodobenzoic acid	Fluka
4-Amino-2,2,6,6-tetramethylpiperidine-1-oxyl (Amino-TEMPO)	Aldrich
Benzene, p. a.	AppliChem
BF ₃ · OEt ₂	Aldrich
1,4-Bis(diphenylphosphino)butane (DPPB), 98 %	Aldrich
1,2-Bis(diphenylphosphino)ethane (DPPE), 99 %	Aldrich
Continued on next page	

Substance, grade/concentration	Supplier
1,3-Bis(diphenylphosphino)propane (DPPP), 97 %	Aldrich
Bis(2-methoxyethyl)ether (diglyme), 99 %	Acros
CaCl ₂	Grüssing
Chlorodiphenylphosphine (Ph ₂ PCl)	Aldrich
Chloro[diphenyl(3-sulfonatophenyl)phosphine] gold(I), sodium salt, 98 %	ABCR
Dichloromethane, p. a.	VWR
Diethyl ether	Riedel de Hæn
4-(Diphenylphosphino)benzoic acid (TPPMC), 97.0 %	TCI Europe
Dithiothreitol (DTT)	Aldrich
D ₂ O	Aldrich
Dodecylamine	Sigma-Aldrich
Ethanol	Grüssing
GeO ₂	Schuchardt
Glutathione (GSH), 98. %	Fisher BioReagents
HAuCl ₄ · 3 H ₂ O, ACS reagent	Sigma-Aldrich
HCl, 37 %	KMF
H ₃ PO ₄	Merck
H ₂ SO ₄ , 20 %	Riedel de Hæn
H ₂ SO ₄ , 65 %	Merck
4-(2-Hydroxyethyl)piperazine-1-ethanesulfonic acid (HEPES)	Sigma
4-Iodobenzoic acid	Fluka
KBr	Sigma
KCN	Grüssing
KOH	KMF
LiAlH ₄	Fluka

| Continued on next page | |

Substance, grade/concentration	Supplier
(Lys ³)-Bombesin, 98 %	Bachem
Methanol, p. a.	VWR
MgSO ₄	Grüssing
<i>M</i> -iodoaniline	Fluka
NaBH ₄ , , purum p. a.	Aldrich
NaOH	Geyer
<i>N</i> -(3-Dimethylaminopropyl)- <i>N</i> '-ethylcarbodiimide (EDC)	Fluka
<i>N</i> -Hydroxysulfosuccinimide sodium salt (sulfo-NHS)	Fluka
Palladium(II) acetate	Fluka
<i>P</i> -iodoaniline	Sigma-Aldrich
Pentane	Grüssing
Petroleum ether	Merck
Sodium auro(I)thiomalate hydrate (Tauredon®)	Aldrich
Tetrakis(triphenylphosphine)palladium	Merck
Toluene	Merck
TPPTS	Fluka
Triethylamine	Grüssing
Triphenylphosphine (TPP), 99+ %	Alfa Aesar
Trisodium citrate dihydrate	Fluka

H₂O was obtained from an *ELGA Purelab Plus* water purification system.

5.1.2 Commercially Purchased or Provided AuNPs

Au1.2MS and Au1.8MS were kindly provided by *STREM Chemicals Inc.*

AurovistTM was purchased from *Nanoprobes*.

5.2 General Comments on Preparative Work

As phosphines are sensitive towards oxidation, most syntheses including phosphines were performed in inert atmosphere (N_2 or Argon).

All glassware, magnetic stir bars and other materials used for AuNPs were cleaned with *aqua regia* and thoroughly washed with de-ionized H_2O prior to usage. When AuNPs were kept in solution over longer periods of time (in reactions or for storage), this was done under exclusion from light to prevent light induced aggregation.

Centrifugation was performed with a *Biofuge fresco* centrifuge (*Heraeus*). Ultracentrifugation was performed at the Institute of Physical Chemistry, RWTH Aachen University, with a *Sorvall Discovery 90SE*. Drying of solutions in *Eppendorf* tubes was performed with a *miVac DNA concentrator* (*Genevac*). To filter AuNP solutions, *Anotop* filters (*Millipore*®, pore diameter 20 nm) were used. For dialysis experiments, dialysis membranes made of regenerated cellulose with a molecular weight cut-off (MWCO) of 5 kD (*ZelluTrans*, *Roth*, V series) were used.

5.3 General Comments on Analytics

5.3.1 UV/Vis Spectroscopy

UV/Vis measurements were performed on a *J & M TIDAS* microspectrometer in PMMA cuvettes for aqueous solutions and fused quartz glass cuvettes for organic solvents in a spectral range from $\lambda = 300 - 800$ nm. Low concentrated AuNP solutions were used (maximal absorbance ≤ 1), and the respective solvent was measured as a reference. For long-term measurements, fused quartz glass cuvettes were used and tempered to 23 °C.

5.3.2 Scanning Transmission Electron Microscopy (STEM)

Low concentrated AuNP solutions were used. A drop of 5 μL was placed on a carbon-coated copper grid (S160, *Plano*) and dried.

A *STEM FEI Tecnai G2 F20* with a High Angle Annular Dark Field (HAADF) detector (Ernst Ruska-Centre Jülich), operated at 200 kV, or a *FE-SEM Leo/Zeiss Supra 35 VP* (IAC), operated at 20 kV, were used.

Grids measured in Jülich were cleaned in a *Fishione Model 1020* Plasma Cleaner with a 25 % oxygen and 75 % argon plasma (Ernst Ruska-Centre Jülich) before they were analysed. The statistical analysis of the micrographs was performed with a Visual Basic tool for *CorelDraw*, developed by Dr. T. Koplin (IAC, RWTH Aachen University).

5.3.3 Scanning Electron Microscopy (SEM) and Energy-Dispersive X-Ray Spectroscopy (EDX)

For AuNP solutions, low concentrated solutions were used. A drop of 5 μL was placed on a clean silicon wafer and dried. For solids, a small part of the respective sample was fixed on a conductive adhesive carbon tab attached to a pin stub. A *FE-SEM Leo/Zeiss Supra 35 VP* with an integrated EDX system (Oxford, *INCA Energy 200* with SiLi crystal, 133 eV, 10 mm²) was used.

5.3.4 Elemental Analysis (EA)

For an elemental analysis (elements C, H, N), 3 mg of a solid sample was investigated on a *Elementar Vario EL* in the Institute of Organic Chemistry, RWTH Aachen University.

5.3.5 Atomic Absorption Spectroscopy (AAS)

For concentration determinations of AuNP solutions, 100 μL of the respective sample was diluted with 400 μL H₂O, oxidized with *aqua regia* and measured on a *Shimadzu AA-6200*. Concentrations of AuNP solutions are therefore always given as gold atom concentrations, if not stated differently.

5.3.6 Electron Paramagnetic Resonance (EPR)

The EPR measurements were performed on a *magnettech MiniScope MS100* EPR spectrometer (Forschungszentrum Jülich). They were measured with a B_0 field of 3380 G, a magnetic field variation of 140 G, a modulation of 205 mG and a microwave damping of 6 dB. Concentrated solutions of AuNPs, Amino-TEMPO and Oxo-TEMPO stock solutions were saturated with O_2 or Ar by bubbling with gas for at least 10 min. For the measurements, solutions were filled into *Blaubrand intraMARK* micropipettes (50 μ L volume) and closed with paramagnetic silicon paste.

5.3.7 Gas chromatography / mass spectrometry (GC/MS)

The GC/MS experiments were conducted at the NIST, Gaithersburg, MD, USA. A mass spectrometer (*Hewlett-Packard Model 5989A MS Engine*) interfaced to a gas chromatograph (*Hewlett-Packard Model 5890 Series II*), equipped with an automatic injector, was used.

5.3.8 Nuclear Magnetic Resonance Spectroscopy (NMR)

5.3.8.1 Solution NMR

For organic samples, 10 mg of the sample was dissolved in 700 μ L deuterated solvent and measured on a *Bruker Avnt II 400* (400 MHz) or a *Mercury 200B* (200 MHz). The chemical shifts are given as δ in ppm and are referenced to the respective solvent (for ^1H -NMR) or to H_3PO_4 as external standard (for ^{31}P -NMR).

For AuNP solutions, highly concentrated solutions were used (for small particles, 15 mg of the respective sample was dissolved in 300 μ L D_2O ; solutions of AuNPs > 5 nm were concentrated by centrifugation). For aqueous solutions, FEP sample tube liners (Wilmad®) were used. The number of scans and the delay time were individually fitted for each experiment.

5.3.8.2 Solid State NMR

Static and magic angle spinning (MAS) solid state ^{31}P -NMR investigations were carried out with a *Bruker AVANCE III* spectrometer with a magnetic field of 9.40 T equipped with a

standard *Bruker* 4.0 and 2.5 mm MAS probe, respectively. The corresponding frequency of ^{31}P is 161.988 MHz. ^{31}P -NMR signals of Au1.4MS were recorded using a Hahn echo sequence with pulses of 2.0 μs and an interpulse delay of 100 μs for the static measurements. Rotor synchronized interpulse delays were applied under MAS conditions of 15 and 35 kHz, respectively. A cycle delay of 5.4 s was used to ensure full recovery of the magnetization. ^1H decoupling was achieved throughout a Spinal64 sequence with pulses of 5.0 μs . For the NMR measurements of TPPMS-Au(I)-Cl, a ^1H decoupled (Spinal64, 5.4 μs) single pulse sequence with pulses of 3.4 μs and a cycle delay of 64 s was applied. The ^{31}P -NMR signals are referred to H_3PO_4 .

5.3.9 Patch Clamp Experiments

The patch clamp experiments were performed at the Cytocentrics AG, Rostock, together with Dr. Olaf Scheel, Dr. Yu Pan-Bartneck and Frank Schiefer. The recordings were performed on a patch clamp setup:

Patch clamp amplifier: EPC-10, *HEKA Elektronik*; Software: PatchMaster, *HEKA Elektronik*, v2.15; Tube pump: ISM830, *Ismatec*; Bath chamber: RC-25 with platform P-3, *Warner Instruments*, with glass cover slips; patch clamp pipettes: pipette resistance between 1.5 and 4 M Ω . The pipette electrode was built of a chlorinated silver wire in IC. As reference electrode a Ag/AgCl pellet electrode (*Warner Instruments*) was used. Patch clamp data were recorded and analyzed using the *HEKA patchmaster* software. Further analysis was performed with *Microsoft Excel*. The peak amplitude of the hERG tail current was corrected by the value of the leak current determined with the -50 mV pulse before the depolarizing activation pulse giving the hERG tail current value.

5.3.10 Differential Scanning Calorimetry (DSC)

Samples of 5- 20 mg were weighted exactly and investigated on a *NETZSCH DSC 204*.

5.3.11 Dynamic light scattering (DLS) and ζ potential measurements

DLS measurements and ζ potential measurements were performed with low concentrated solutions in 10 mM or 100 mM HEPES buffer with a pH of 8 in folded capillary cells (clear polycarbonate) on a *Malvern ZETA SIZER ZS* with a laser of the wavelength $\lambda = 632.8$ nm.

5.3.12 Mass Spectrometry (MS)

The MS measurements at the IAC were performed on a *Finnigan MAT95*. FAB-SIMS spectra were recorded in a glycerine/thioglycerine matrix and in a 1,4-dithioerythritol/*DL*-dithiothreitol (DTE/DTT) matrix.

5.3.13 Infrared Spectroscopy (IR)

Samples were either mixed as a powder (1 mg) with 200 mg pre-dried KBr, or 5 μ L of a concentrated AuNP solution was added to 200 mg KBr and dried. This mixture was pestled and then pressed in a molding press. The pellet was measured on a *FT-IR Bruker Vertex 70* spectrometer.

The spectra were processed with the *OPUS 6.5* program. A baseline correction and a CO₂ correction were performed.

5.3.14 Fluorescence Spectroscopy

Low concentrated solutions were measured in PMMA cuvettes with four clear sides in a *Jasco FP-6300* fluorescence spectrometer.

5.3.15 Cell Experiments

All other, not so far mentioned cell experiments described in this work were performed at the UKA and are described in detail in the PhD thesis of Dr. Yu Pan-Bartneck.[12] To prepare test compound solutions, the AuNP solutions of small AuNPs (< 5 nm) were always

filtered with an *Anotop* filter after redispersion. A small portion of each sample was taken for the measurement of the concentration by AAS.

5.4 Syntheses

5.4.1 Ligands

5.4.1.1 TPPMS

To a mixture of 4.8 mL 20 % fuming sulfuric acid and 0.2 mL 65 % fuming sulfuric acid, 2.5 g (9.5 mmol) TPP were added slowly under stirring and cooling with an ice bath. After the dissolution of the TPP, the solution was heated to 90 °C. After 30 min, the reaction was stopped and cooled to room temperature. The solution was poured into 200 mL H₂O and neutralized with saturated NaOH. The product precipitated as fine white platelets. It was filtered, recrystallized from ethanol and dried.

5.4.1.2 Diphenylphosphine (precursor)

3.1 g LiAlH₄ were added to 50 mL dry diethyl ether. 25 mL Ph₂PCl in 50 mL diethyl ether were added drop wise with a dropping funnel under stirring and cooling with an ice bath. After complete addition, the solution was refluxed for 1 h. A white suspension formed. 13 mL H₂O were added drop wise and the solution was refluxed for further 2 h. A white precipitate formed. It was filtered, and the solid was dissolved in 60 mL diethyl ether. The solution was dried over CaCl₂, then the ether was removed. The product remained as a yellow viscous liquid.

5.4.1.3 *p*TPPMA, *m*TPPMA

1.31 g (5.95 mmol) *p*-Iodoaniline, or *m*-iodoaniline respectively, and 0.61 g (5.95 mmol) triethylamine were mixed in 15 mL acetonitrile. The solution was degassed, and 1.11 g (5.95 mmol) diphenylphosphine were added. The solution was heated to reflux, and 7 mg tetrakis-(triphenylphosphine)palladium in 5 mL acetonitrile and 5 mL H₂O were added. The reaction was refluxed for 60 h. Afterwards, the solvent was removed and the residue was

dissolved in 5 mL H₂O. 5 mL dichloromethane were added and the mixture was poured in a separation funnel. The organic phase was separated and discarded, the H₂O was removed and the remaining yellowish product was dried.

5.4.1.4 TPPMCMA

3.53 g (13.4 mmol) 2-Amino-5-iodobenzoic acid, 3.8 mL triethylamine and 2 mg (9 μ mol) palladium(II) acetate were dissolved in 30 mL acetonitrile. After the addition of 2 mL (11.5 mmol) diphenylphosphine, the reaction mixture was refluxed for 48 h. The solution was dried and the residue was dissolved in 30 mL 1 M KOH. The aqueous phase was washed with dry diethyl ether (4 \times 30 mL) and once with 30 mL petroleum ether. The aqueous phase was cooled to 5 °C and acidified to a pH of 2 with 2 M HCl. A yellowish precipitate formed. It was filtered, dissolved in dry diethyl ether, washed with 20 mL H₂O and dried over MgSO₄. After removal of the ether, the product remained as a yellow-orange solid.

5.4.1.5 TPPMC

1.96 g (7.9 mmol) 4-Iodobenzoic acid, 2.3 mL (16 mmol) triethylamine and 2 mg (9 μ mol) palladium(II) acetate were mixed in 24 mL acetonitrile. After the addition of 1.2 mL (7.9 mmol) diphenylphosphine, the reaction mixture was heated to 85 °C for 12 h. The color of the solution changed from red to yellow-green during that time. Afterwards, the solvents were removed and the residue was dissolved in 20 mL H₂O with 1.06 g (16 mmol) KOH. The solution was washed 3 \times with dry diethyl ether and then acidified with 5 mL 2 M HCl. Afterwards, the product was extracted from the aqueous phase with diethyl ether (3 \times 30 mL), the combined ether fractions were washed with 20 mL H₂O and dried over MgSO₄. After removal of the ether, the product remained as a yellowish powder.

5.4.1.6 DPPETS

2.0 g (5.0 mmol) 1,2-bis(diphenylphosphino)ethane (DPPE) were dissolved in 25 mL 20 % fuming sulfuric acid. The reaction mixture was stirred for 90 h at 0 °C, while the temperature was kept constant with a cryostate. After this time, the solution was slowly neutralized with 120 mL 25 % NaOH. The H₂O was removed. 160 mL methanol were added and the

solution was refluxed for 1 h. It was filtered hot and washed in portions with 50 mL of a hot methanol/H₂O mixture (4:1). The filtrate was dried, then dissolved in methanol/H₂O (10:1) and stored in the refrigerator overnight to recrystallize. The solvents were removed and the product was dried.

5.4.1.7 DPPPTS, DPPBTS

32.5 mL 30 % fuming sulfuric acid was cooled to 0 °C. 2.5 g of DPPP (6.0 mmol), respectively DPPB (5.9 mmol), were dissolved in 8 mL cold sulfuric acid and then added *via* a dropping funnel to the fuming sulfuric acid. The dropping speed was adjusted so that a temperature of 5 °C was not exceeded. After the addition, additional 10 mL 30 % fuming sulfuric acid were added *via* the dropping funnel. The reaction mixture was stirred for 48 h at room temperature. After this time, the solution was slowly poured into 250 mL H₂O while a temperature of 10 °C was not exceeded. Afterwards, the pH of the solution was adjusted to 2 with saturated NaOH. 175 mL methanol were added, and the Na₂SO₄ formed was removed. The filtrate was dried, and the remaining solid was dissolved in H₂O. The pH was brought to 7, and 125 mL methanol were added. The solid was filtered and the filtrate was dried. DPPPTS remained as a light brown solid, DPPBTS as a beige solid.

5.4.2 Gold Nanoparticles

5.4.2.1 Au1.4TPP

Au1.4TPP (with the chemical structure Au₅₅[(C₆H₅)₃P]₁₂Cl₆) was synthesized according to the literature.[33] Briefly, 3.907 g (7.9 mmol) TPP-Au(I)-Cl was dispersed in 200 mL benzene in inert atmosphere. B₂H₆ was generated *in situ* from 20 g (529 mmol) NaBH₄ in 100 mL diglyme and 100 mL BF₃ · OEt₂, slowly added *via* a dropping funnel, and bubbled through the Au(I) dispersion which was heated to 50 °C. The gas flow rate and temperature were kept constant for 40 min, while the solution turned from turbid to colorless and clear to dark brown. After the reaction, the solution was cooled to room temperature, the dark brown solid formed was filtered and washed with benzene and pentane. It was redispersed

in dichloromethane and filtered through an *Anotop* filter. After removal of the solvent, the product remained as a dark brown solid.

5.4.2.2 Au1.4MS

Au1.4MS (with the chemical structure $\text{Au}_{55}[(\text{C}_6\text{H}_5)_2\text{P}(\text{C}_4\text{H}_4\text{SO}_3\text{Na})]_{12}\text{Cl}_6$) was synthesized according to the literature.[34] 163 mg (0.01 mmol) Au1.4TPP was dissolved in 10 mL dichloromethane and covered with a solution of 62 mg (0.17 mmol) TPPMS in 50 mL H_2O . This two-phase system was stirred at room temperature to the exclusion of light for three days. After this time, the H_2O phase had become dark brown, indicating the phase transfer by a ligand exchange reaction. The two phases were separated, the H_2O was removed, the obtained solid was washed $3\times$ with 20 mL dichloromethane and $3\times$ with 20 mL ethanol to remove excess TPPMS, and dried. It was redispersed in H_2O and filtered through an *Anotop* filter. After removal of the solvent, the product remained as a dark brown solid.

5.4.2.3 Au5.6MS

56 mg (165 μmol) $\text{HAuCl}_4 \cdot 3 \text{H}_2\text{O}$ were dissolved in 12.5 mL H_2O and 12.5 mL toluene. 287 mg (1.5 mmol) dodecylamine in 12.5 mL toluene were added. A yellowish precipitate formed. 82.5 mg (2.2 mmol) NaBH_4 were dissolved in 12.5 mL H_2O and directly added drop wise to the reaction mixture over a period of 5 min. The solution turned black. It was stirred at room temperature for 7 h. Afterwards, the aqueous phase was separated and discarded and the volume of the organic phase was reduced to 5 mL. 60 mL ethanol were added, and the solution was kept at -25°C overnight. It was warmed up to room temperature, the black precipitate formed was centrifuged, washed with ethanol and resuspended in 1 mL dichloromethane.

The red AuNP solution was mixed with 12.8 mL TPPMS in 10 mL H_2O and stirred for 2 h at room temperature. The organic phase was removed, and the red aqueous phase was centrifuged (15 min at 8000 rev/min). The supernatant was taken and further used.

5.4.2.4 Au15MS

Au15Citrate was synthesized in allusion to a route known from literature.[32] The ligand exchange reaction was performed according to the literature.[115] 17 mg (40 μmol) $\text{HAuCl}_4 \cdot 3 \text{H}_2\text{O}$ were dissolved in 5 mL H_2O (solution I), 42 mg (1.4 mmol) trisodium citrate dihydrate were dissolved in 15 mL H_2O (solution II). 85 mL H_2O were brought to boil, and solution I and II were added consecutively under vigorous stirring. After a few minutes, a color change from yellow over dark blue to red was visible. When the color of the solution remained constant, the solution was heated for further 10 min and then cooled to room temperature. The size of AuNPs synthesized *via* this route is very sensitive towards the starting concentrations of the precursors and towards reaction conditions. Therefore, not all batches synthesized gave AuNPs of exactly 15 nm. If the size of a certain batch differed, it is stated at the respective part.

To 100 mL of the AuNP solution, 10 mg (27 μmol) TPPMS were added. The solution was stirred for 5 min at room temperature and then kept in the refrigerator overnight. In small portions (1.5 mL per tube), it was centrifuged (15 min, 5 °C, 10000 rev/min). The supernatants (1.4 mL per tube) were discarded and the tubes were refilled with H_2O (1.4 mL). The centrifugation was repeated, the supernatants were again discarded, and afterwards, the concentrated solutions (100 μL per tube) were collected.

5.4.2.5 Au1.1GSH, Au1.5GSH

Au1.1GSH was synthesized in allusion to a route known from literature.[39] 100 mg (0.25 mmol) $\text{HAuCl}_4 \cdot 3 \text{H}_2\text{O}$ was dissolved in 50 mL methanol. 154 mg (0.5 mmol) glutathione (GSH) were added. The solution was cooled to 0 °C. 12.5 mL of a freshly prepared NaBH_4 solution (0.2 M, 95 mg, 2.5 mmol) were added drop wise over 5 min. The yellowish solution turned dark brown. It was stirred for 30 min, and the precipitate formed was filtered. It was first washed with a mixture of H_2O and methanol (1:10) and then with methanol. The solid was resuspended in H_2O and the dispersion was filtered through an *Anotop* filter. After removal of the solvent, the product remained as a dark brown solid.

In different batches, slightly different particle sizes were obtained (1.1-1.5 nm). The mean diameter, determined by STEM, of the corresponding AuNPs is stated at the respective part.

5.4.2.6 Au1.4GSH by Ligand Exchange

7 mg (0.45 μmol) Au1.4MS and 75.6 mg (246 μmol) GSH were dissolved in 0.7 mL H_2O and kept 24 h at 37 °C. Afterwards, the solution was centrifuged (30 min, 5 °C, 13000 rev/min) and washed 3 \times with ethanol. The remaining residue was redispersed in 1 mL H_2O plus 50 μL 10 % NaOH, filtered through an *Anotop* filter and used for a ζ potential measurement. Another batch was not redispersed but used as a powder for IR spectroscopy.

5.4.2.7 Au1.4TS

Au1.4TS was synthesized analogously to Au1.4MS. 163 mg (0.01 mmol) Au1.4TPP was dissolved in 10 mL dichloromethane and covered with a solution of 97 mg (0.17 mmol) TPPTS in 50 mL H_2O . This two-phase system was stirred at room temperature to the exclusion of light for ten days. After this time, the H_2O phase had become dark brown, indicating the phase transfer by a ligand exchange reaction. The two phases were separated, the H_2O was removed, the solid was washed 3 \times with 20 mL dichloromethane and 3 \times with 20 mL ethanol to remove excess TPPTS, and dried. It was redispersed in H_2O and filtered through an *Anotop* filter. After removal of the solvent, the product remained as a dark brown solid.

5.4.2.8 Au1.4TPPMCMA

50 mg (3.5 μmol) Au1.4TPP were dissolved in 3.5 mL dichloromethane. A solution of 16.1 mg (52 μmol) TPPMCMA in 10 mL H_2O and 300 μL 2 M NaOH was added. The mixture was stirred for 1.5 h at room temperature. After this time, the aqueous phase was dark brown. The organic phase was separated and discarded. The aqueous phase was centrifuged in an ultracentrifuge (4 h, 20 °C, 50000 rev/min). The supernatant was discarded, and the pellet at the bottom of the centrifuge tube was washed 3 \times with H_2O by redispersion and centrifugation under the same conditions. After the last centrifugation step the pellet was

dried. It was redispersed in H₂O and filtered through an *Anotop* filter. After removal of the solvent, the product remained as a dark brown solid.

5.4.2.9 Au1.4TPPMC

100 mg (7 μ mol) Au1.4TPP were dissolved in 8 mL dichloromethane. A solution of 46.1 mg (0.16 mmol) TPPMC in 10 mL H₂O and 20 mL 0.1 M NaOH was added. The mixture was stirred for 2 h at room temperature. After this time, the aqueous phase was dark brown. The organic phase was separated and discarded. The aqueous phase was centrifuged in an ultracentrifuge (4 h, 20 °C, 50000 rev/min). The supernatant was discarded, and the pellet at the bottom of the centrifuge tube was washed 3 \times with H₂O by redispersion and centrifugation under the same conditions. After the last centrifugation step the pellet was dried. It was redispersed in H₂O and filtered through an *Anotop* filter. After removal of the solvent, the product remained as a dark brown solid.

5.4.2.10 Au1.4DPPETS

50 mg (3.5 μ mol) Au1.4TPP were dissolved in 4 mL dichloromethane. A solution of 48 mg (0.06 mmol) DPPETS in 20 mL H₂O was added. The mixture was stirred for 15 h at room temperature. The two phases were separated, the H₂O was removed, the obtained solid was washed with dichloromethane once and 3 \times with ethanol to remove excess DPPETS, and dried. It was redispersed in H₂O and filtered through an *Anotop* filter. After removal of the solvent, the product remained as a dark brown solid.

5.4.2.11 Au1.4DPPPTS

100 mg (7 μ mol) Au1.4MS were dissolved in 8 mL dichloromethane. A solution of 158.5 mg (0.175 mmol) DPPPTS in 60 mL H₂O was added. The mixture was stirred for 4 days at room temperature. The two phases were separated, the H₂O was removed, the obtained solid was washed 2 \times with dichloromethane and once with ethanol to remove excess DPPPTS, and dried.

5.4.2.12 Au1.4DPPBTS

100 mg (7 μ mol) Au1.4MS were dissolved in 8 mL dichloromethane. A solution of 160.6 mg (0.175 mmol) DPPBTS in 60 mL H₂O was added. The mixture was stirred for 4 days at room temperature. The two phases were separated, the H₂O was removed, the obtained solid was washed 2 \times with dichloromethane and once with ethanol to remove excess DPPBTS, and dried. For a further purification, 40 mg of the product were redispersed in 4.5 mL H₂O and dialyzed for 3 days (MWCO of 5 kD), while the wash water (400 mL) was exchanged 3 \times a day.

5.4.2.13 Au13DPPETS

As a precursor, citrate-stabilized gold colloids were synthesized as described above (see 5.4.2.4). To 25 mL of this AuNP solution, 5.5 mg (6.8 μ mol) of DPPETS were added. The solution was stirred at room temperature for 1 h and then left in the refrigerator overnight. In small portions (1.5 mL per tube), it was centrifuged (15 min, 5 $^{\circ}$ C, 10000 rev/min). The supernatants (1.4 mL per tube) were discarded and the tubes were refilled with H₂O (1.4 mL). The centrifugation was repeated, the supernatants were again discarded, and afterwards, the concentrated solutions (100 μ L per tube) were collected.

5.4.2.14 Au11DPPPTS

As a precursor, citrate-stabilized gold colloids were synthesized as described above (see 5.4.2.4). To 30 mL of this AuNP solution, 5.9 mg (7.2 μ mol) of DPPPTS were added. The solution was stirred at room temperature for 10 min, left in the refrigerator overnight and centrifuged under the same conditions as described above (see 5.4.2.13).

5.4.2.15 Au12DPPBTS

Au12DPPBTS was synthesized analogously to Au11DPPPTS (see 5.4.2.14) using 6.0 mg (7.2 μ mol) DPPBTS.

5.4.2.16 Degradation of Diphosphine-Stab. AuNPs with KCN

The stability against KCN degradation of Au1.4MS, Au1.4DPPETS, Au11Citrate, Au13MS, Au13DPPETS, Au11DPPPTS and Au12DPPBTS was analyzed by time-dependent UV/Vis spectroscopy. For Au1.4MS and Au1.4DPPETS, a AuNP stock solution of 9.8 mg AuNPs in 3 mL H₂O was used. For larger gold colloids, highly concentrated solutions, concentrated by centrifugation, were used.

To 1 mL AuNP solution in a fused quartz glass cuvette, 0.17 mL 0.1 M KCN was added. The cuvette was tempered to 23 °C and UV/Vis spectra were taken over a time period of 8 h (1 spectrum/min).

5.4.2.17 DTT Exchange with Au1.4DPPBTS

8 mg Au1.4DPPBTS were redispersed in 10 mL H₂O. For each experiment, 900 µL of this stock solution were taken and mixed with 100 µL of differently concentrated DTT solutions (2.2 µM - 22 µM). The mixtures were heated to 60 °C for 5 min. After cooling to room temperature, UV/Vis spectra were taken and the absorbance at $\lambda = 400$ nm was determined. In a reference experiment, 3 mg Au1.4MS were redispersed in 10 mL H₂O, and samples were prepared and measured as described above.

5.4.2.18 Au1.4MS/MC

180 mg (0.01 mmol) Au1.4TPP were dissolved in 12 mL dichloromethane. 10.6 mg (35 µmol) TPPMC and 88.7 mg (243 µmol) TPPMS (molar ratio TPPMC:TPPMS 1:7) were dissolved in 25 mL H₂O and 25 mL 0.1 M NaOH. This two-phase system was stirred for 24 h. The organic phase was separated and discarded. The H₂O was removed, the obtained solid was washed 2× with dichloromethane and once with ethanol to remove excess ligands, and the product was dried. It was redispersed in H₂O, filtered through an *Anotop* filter and further purified by dialysis for 24 h (MWCO of 5 kD), while the wash water (400 mL) was exchanged 3×. The dialyzed solution was dried, and the product remained as a dark brown solid.

5.4.2.19 Au1.4MS/MC-(Lys³)-bombesin

50 mg (3.3 μ mol) Au1.4MS/MC were dissolved in 8 mL H₂O. 43.4 mg (0.2 mmol, final concentration 20 mM) sulfo-NHS and 77.6 mg (0.5 mmol, final concentration 50 mM) were dissolved in 2 mL HEPES buffer (100 mM, pH 8), filtered through an *Anotop* filter and added to the AuNP solution. It was stirred for 30 min at room temperature, then 5 mg (3.1 μ mol) (Lys³)-bombesin were added. The solution was stirred for 20 h at room temperature, transferred into Eppendorf tubes and centrifuged (30 min, 5 °C, 13000 rev/min) to remove aggregates. The supernatant was transferred into centrifugation tubes and ultracentrifuged (2 h, 20 °C, 50000 rev/min). The supernatant was discarded, the pellets were redispersed in H₂O and centrifuged once more. The supernatant was collected and was used as a reference after a further dialysis step. The pellet of Au1.4MS/MC-(Lys³)-bombesin was stored as a highly concentrated AuNP solution.

5.4.2.20 Au1.4MC-bombesin

Under similar conditions, bombesin was coupled to Au1.4MC. This product was only soluble in acidic solvents and had a poor stability in cell culture medium (pH 7.4). For cell experiments, Au1.4MS/MC-(Lys³)-bombesin was therefore used. However, Au1.4MC-bombesin was used for a DTT ligand exchange reaction (see 5.4.2.21 below).

5.4.2.21 DTT Exchange with Au1.4MC-bombesin

10 mg of Au1.4MC-bombesin were redispersed in 2 mL of diluted acetic acid. 2 mL of acetic DTT solution (0.5 M) were added, and the mixture was heated to 60 °C for 5 min. Afterwards, it was stirred for 1 h at room temperature. The precipitate was centrifuged, and the supernatant was dried. The residue was analyzed by MS.

5.4.2.22 Au1.4MS/MC-Aminofluorescein

The functionalization of Au1.4MS/MC with 5-Aminofluorescein was conducted under similar conditions as the coupling reaction with (Lys³)-Bombesin (5.4.2.19).

40 mg (2.6 μmol) Au1.4MS/MC were dispersed in 6.4 mL H_2O . 34.8 mg (160 μmol) sulfo-NHS and 62.1 mg (400 μmol) EDC were dissolved in 1.6 mL HEPES buffer (100 mM, pH 8). The two solutions were mixed and stirred for 30 min at room temperature. Afterwards, 2.0 mg (5.8 μmol) 5-Aminofluorescein was added and the solution was stirred for further 20 h. The solution was transferred to Eppendorf tubes, centrifuged and washed once with ethanol. The product was dried in a *miVac DNA concentrator*. The residue was dispersed in diluted NaOH (pH 7.5) by shaking overnight. The insoluble residue was separated by centrifugation and discarded.

5.5 Measurements with AuNPs

5.5.1 EPR Measurements

All solutions used were saturated with Ar or O_2 , respectively, before they were diluted and mixed. The aqueous AuNP stock solutions were diluted in different ratios to a total volume of 100 μL , respectively (for concentrations see table 5.2). They were then mixed with 100 μL of a 4-Amino-2,2,6,6-tetramethylpiperidine-1-oxyl (Amino-TEMPO) solution (30 μM) directly prior to the measurements. The pH was adjusted to 8-9 with 50 mM NaOH.

Table 5.2: Concentrations of AuNP solutions for EPR spectroscopy.

AuNP species	conc. stock solution / mM	final conc. / mM
Au15Citrate	18.2	2.3
Au15MS	32.7	8.2
Au1.4MS	18.6	4.7
Au1.5GSH	21.6	5.4

5.5.2 GC/MS Measurements

DNA samples were prepared by Dr. Yu Pan-Bartneck (UKA). Au1.4MS, Au1.1GSH, and Au15MS (50 μM , respectively; Au1.4MS was also applied in 20 μM) were used to incubate

HeLa cells (incubation times 3 h, 24 h, 72 h), followed by subsequent DNA extraction (sample set 1). As a positive control, cells were also treated with 0.3 % H_2O_2 for 30 min.

Furthermore, DNA was isolated from untreated HeLa cells and the pure DNA was incubated (incubation times 3 h, 24 h, 72 h) with Au1.4MS, Au1.1GSH, and Au15MS (50 μM , respectively) as well (sample set 2).

Further treatment of the samples and GC/MS measurements were performed at the NIST, Gaithersburg, MD, USA, together with Dr. Bryant Nelson and Dr. Elijah Petersen. All DNA pellets were washed several times ($2\times$ 70 % ethanol, $1\times$ 100 % ethanol). Then the exact DNA concentrations were determined with a *NanoDrop* spectrometer. 50 μg DNA was taken of each sample (except for the few samples that contained less DNA). Isotopically labeled internal standards (FapyAde, FapyGua, 8OHGua, 5OHCyt, 5OHUra, TG, and 5OH5MeHyd) were added. After that, the DNA was enzymatically digested by Endo III/Nth and Fpg enzymes. The samples were freeze dried, and bis(trimethylsilyl)trifluoroacetamide (BSTFA) was added to derivatize the DNA bases to their silyl ester analogues. GC/MS measurements were performed. For the data analysis, the signals were integrated manually with the *MSD Productivity ChemStation* (Agilent) and further processed for statistical analysis with *GraphPad Prism*.

5.5.3 NMR and EDX Experiments

5.5.3.1 Au1.4MS + TPPMS

15 mg (0.95 μmol) Au1.4MS were dissolved in 300 μL D_2O and the ^1H and ^{31}P -NMR spectra were measured (400 MHz). 3.2 mg (8.7 μmol , 9.8 eq) TPPMS were dissolved in 60 μL D_2O and added. The NMR measurements were repeated. Successively, more TPPMS was added (see table 5.3), and the NMR measurements were repeated after each addition.

The δ values of the ^{31}P -NMR spectra were plotted against the concentration of additionally added TPPMS. A logarithmic fit was performed with *Microsoft Excel*. The first measurement value was neglected as the added concentration of TPPMS was in the same regime as the calculated concentration of intrinsically present TPPMS (which is not taken into account in the fit). Therefore, this first measurement point is not feasible for a fit.

Table 5.3: TPPMS amounts for ^{31}P -NMR analysis.

Measurement No.	m (TPPMS) / mg	eq (TPPMS)	δ / ppm
1	0	0	44.95
2	3.2	9.8	42.95
3	3.2	19.6	30.56
4	3.2	29.4	25.98
5	3.2	39.2	21.98
6	6.4	58.8	19.70
7	6.4	78.4	18.38
8	6.4	98.0	15.44
9	6.4	117.6	16.56

The δ value for pure Au1.4MS (measurement no. 1) was used to approximate the amount of dissociated TPPMS ligands in a Au1.4MS solution (c_{diss}).

5.5.3.2 Solid State NMR of Au1.4MS

Fine powdered samples of Au1.4MS and TPPMS-Au(I)-Cl were diluted with GeO_2 in a ratio of approximately 1 : 5 and mounted in a 4.0 and 2.5 mm ZrO_2 rotor.

5.5.3.3 Dialysis and EDX of Au1.4MS

6 mg (0.38 μmol) Au1.4MS were dissolved in 6 mL H_2O and filled in a dialysis membrane (MWCO of 5 kD). The membrane was put in a beaker filled with 400 mL H_2O and the AuNP solution was dialyzed under slow stirring at room temperature for 2 h. Afterwards the supernatant was reduced to dryness and the remaining residue was examined by EDX analysis. In the control experiment, 12.4 mg (0.38 μmol) TPPMS-Au(I)-Cl was dialyzed under the same conditions and the dialysate was examined.

For the EDX investigation, the solid samples were fixed on a conductive adhesive carbon tab attached to a pin stub.

5.5.4 Patch Clamp Experiments

HEK 293 cells, stably transfected with the hERG ion channel gene, or CHO-K1 cells transfected with the gene encoding the sodium ion channel $\text{Na}_v1.5$, were used. These cells were

stored in liquid nitrogen and were ready-to-use directly after thawing without any cultivation. After thawing, the cells were resuspended in extracellular buffer and kept in the *Cytocentricks* Cell Reservoir as a cell suspension at a density of 2.0 millions/mL in extracellular buffer at room temperature and were used for 4 h after thawing.

The extracellular buffer (EC) was used for thawing the cells, the storage in the Cell Reservoir and the preparation of the working concentrations of the test and reference compounds. The extracellular buffer consists of: 140 mM NaCl, 2.5 mM KCl, 2 mM MgCl₂, 2 mM CaCl₂, 10 mM HEPES, 10 mM glucose, 15 mM sucrose. The buffer was adjusted to a pH of 7.4 ± 0.1 ; osmolality 320 ± 5 mOsmol/kg. The buffer was stored at 4 °C and heated up to room temperature prior to usage. The intracellular buffer (IC) consists of: 100 mM K-gluconate, 20 mM KCl, 1 mM CaCl₂, 1 mM MgCl₂, 10 mM HEPES, 11 mM EGTA-KOH, 4 mM ATP-Mg²⁺, 3 mM phosphocreatine-Na₂-H₂O, 9 mM sucrose. The buffer was adjusted to a pH of 7.2 ± 0.1 ; osmolality 295 ± 5 mOsmol/kg. Aliquots were stored at -20 °C. Prior to usage an aliquot IC was thawed and used no longer than for 4 h.

The different AuNPs were dissolved in H₂O as stock solutions and diluted with EC in the concentrations needed for the experiments directly prior to the experiments. When Au1.4MS was pre-incubated with TPPMS or GSH, both compounds were diluted in EC to the respective concentrations, mixed and kept at 37 °C for 3 h.

For patch clamp recordings, cells were seeded in the bath chamber filled with EC. After approx. 5 min in which the cells attached to the cover slips the seal process was started. After gigaseal formation the membrane patch under the tip of the glass pipette was opened by a short suction pulse to gain electrical access from the pipette electrode to the cytosol (whole cell configuration). Then the cell was lifted from the cover slip with the pipette and positioned close to the perfusion entry of the bath chamber and perfusion with EC was started. To activate hERG currents the voltage protocol was repeated every 10 s. The hERG currents were then recorded for 10 min upon EC perfusion to assure that stable recording conditions were established. Only cells with tail current amplitude of more than 400 pA were used. After the control phase the test compounds were applied. Application time was in general 10 min per concentration. Recordings in which the whole cell membrane resistance

decreased below 500 M Ω m without recovery (leaky) were stopped and not taken into the analysis from here. All measurements were done at room temperature.

The typical pulse protocol that was applied was: 0.2 s, -80 mV; 0.2 s, -50 mV; 2 s, +40 mV; 2 s, -50 mV; 0.2 s, -80 mV.

5.5.5 Cell Experiments

All other cell experiments were performed by Dr. Yu Pan-Bartneck at the UKA and are described elsewhere.[12]

6 Abbreviations

AAS	Atomic absorption spectroscopy
AF	5-Aminofluorescein
Amino-TEMPO	4-Amino-2,2,6,6-tetramethylpiperidine-1-oxyl
ANOVA	Analysis of variance
ATP	Adenosine-5'-triphosphate
AuNPs	Gold nanoparticles
BINAP	2,2'-bis(diphenylphosphino)-1,1'-binaphthyl
bla	β -lactamase
BLM	Human melanoma cell line
ccp	cubic close-packed
cDNA	complementary DNA
CHO-K1	Chinese hamster ovary cell line
ct-DNA	calf thymus DNA
CM-H ₂ DCFDA	5-(and-6)-chloromethyl-2',7'-dichlorodihydro-fluorescein diacetate, acetyl ester
COS-1	Cell line ("CV-1 (simian) in Origin, and carrying the SV40 genetic material")
CPP	Cell penetrating peptide
DFT	Density functional theory
DNA	Deoxyribonucleic acid
DLS	Dynamic light scattering
DPPB	1,2-Bis(diphenylphosphino)butane
DPPBTS	1,2-Bis(diphenylphosphino)butane tetrasulfonate
DPPE	1,2-Bis(diphenylphosphino)ethane
DPPETS	1,2-Bis(diphenylphosphino)ethane tetrasulfonate

Continued on next page

DPPP	1,2-Bis(diphenylphosphino)propane
DPPPTS	1,2-Bis(diphenylphosphino)propane tetrasulfonate
DSC	Differential scanning calorimetry
DTE	Dithioerythritol
DTT	Dithiothreitol
EA	Elemental analysis
EC	Extracellular buffer
EDC	1-Ethyl-3-(3-dimethylaminopropyl) carbodiimide
EDX	Energy-dispersive x-ray spectroscopy
EGTA	Ethylene glycol tetraacetic acid
ELISA	Enzyme-linked immunosorbent assay
EM	Electron microscopy
EPR	Electron paramagnetic resonance
eq	Equivalents
FBS	Fetal bovine serum
FCS	Fetal calf serum
FEP	Fluorinated ethylene propylene
FRET	Förster resonance energy transfer
GC/MS	Gas chromatography / mass spectrometry
GRPR	Gastrin releasing peptide receptor
GSH	Glutathione
HAADF	High angle annular dark field
HEK 293	Human embryonic kidney cell line
HeLa	HeLa cervix carcinoma epithelial cell line
HEPES	4-(2-Hydroxyethyl)-1-piperazineethanesulfonic acid
HepG2	Hepatocellular carcinoma cell line
hERG	Human ether-à-go-go related gene
HPLC	High-performance liquid chromatography
IAC	Institute of Inorganic Chemistry (RWTH Aachen University)
IC	Intracellular buffer
ICP-OES	Induced coupled plasma-optical emission spectroscopy

Continued on next page

IC ₅₀	half maximal inhibitory concentration
IR	Infrared
IUPAC	International Union of Pure and Applied Chemistry
J774A1	Mouse monocytic/macrophage cell line
KIT	Karlsruhe Institute of Technology
L929	L929 mouse fibroblast cell line
LC/MS/MS	Liquid chromatography / tandem mass spectrometry
Lys	Lysine
MAS	Magic angle spinning
MDCK	Madine darby canine, kidney cell line
mRNA	Messenger ribonucleic acid
MS	Mass spectrometry
MTT	Dimethyl thiazolyl diphenyl tetrazolium salt
MWCO	Molecular weight cut off radius
NAA	Neutron activation analysis
NAC	<i>N</i> -acetylcysteine
NEIL1	Enzyme encoded by nei endonuclease VIII-like 1 gene
NIST	Natinal Institute of Standards and Technology
NLS	Nuclear localizing signal
NMR	Nuclear magnetic resonance
NP	nanoparticle
8-OH-dG	8-Oxo-2'-deoxyguanosine
Oxo-TEMPO	4-Oxo-2,2,6,6-tetramethyl-1-piperidinyloxy
PEG	Poly(ethylene glycol)
PMMA	Poly(methyl methacrylate)
PVP	Poly(vinylpyrrolidone)
ROS	Reactive oxygen species
RWTH	Rheinisch-Westfälische Technische Hochschule
SAM	Self-assembled monolayer
SK-Mel-28	SK-Mel-28 melanoma cell line

Continued on next page

STEM	Scanning transmission electron microscopy
Sulfo-NHS	N-Hydroxysuccinimide sulfonate
Tat	Trans-activator of transcription
TEG	Tetra(ethylene glycol)
TEM	Transmission electron microscopy
TPP	Triphenylphosphine
TPPMA	Triphenylphosphine monoamine
TPPMC	Triphenylphosphine monocarboxylate
TPPMCMA	Triphenylphosphine monocarboxylate monoamine
TPPMS	Triphenylphosphine monosulfonate
TPPMS=O	Sodium 3-(diphenylphosphoryl)benzenesulfonate
TPPTS	Triphenylphosphine trisulfonate
UKA	University Hospital Aachen
UV/Vis	Ultraviolet/Visible
XPS	X-ray photoelectron spectroscopy
XRD	X-ray diffractometry

Bibliography

- [1] G. M. Whitesides. Nanoscience, Nanotechnology, and Chemistry. *Small*, **1**(2), 172 (2005). 1
- [2] C. Minelli, S. B. Lowe and M. M. Stevens. Engineering Nanocomposite Materials for Cancer Therapy. *Small*, **6**(21), 2336 (2010). 1
- [3] D. Giljohann, D. Seferos, W. Daniel, M. Massich, P. Patel and C. Mirkin. Gold Nanoparticles for Biology and Medicine. *Angewandte Chemie International Edition*, **49**(19), 3280 (2010). 1
- [4] C. M. Niemeyer. Nanoparticles, Proteins, and Nucleic Acids: Biotechnology Meets Materials Science. *Angewandte Chemie International Edition*, **40**(22), 4128 (2001). 1
- [5] H. F. Krug and P. Wick. Nanotoxicology: An Interdisciplinary Challenge. *Angewandte Chemie International Edition*, **50**(6), 1260 (2011). 1, 48
- [6] N. Lewinski, V. Colvin and R. Drezek. Cytotoxicity of Nanoparticles. *Small*, **4**(1), 26 (2008). 1, 22, 24
- [7] W. Jahnen-Dechent and U. Simon. Function follows form: shape complementarity and nanoparticle toxicity. *Nanomedicine*, **3**(5), 601 (2008). 2
- [8] M. Tsoli, H. Kuhn, W. Brandau, H. Esche and G. Schmid. Cellular Uptake and Toxicity of Au₅₅ Clusters. *Small*, **1**(8–9), 841 (2005). 2, 25, 55
- [9] Y. Liu, W. Meyer-Zaika, S. Franzka, G. Schmid, M. Tsoli and H. Kuhn. Goldcluster-Abbau durch den Übergang von B-DNA in A-DNA und Bildung von Nanodrähten. *Angewandte Chemie*, **115**, 2959 (2003). 2, 38
- [10] N. Pernodet, X. Fang, Y. Sun, A. Bakhtina, A. Ramakrishnan, J. Sokolov, A. Ulman and M. Rafailovich. Adverse Effects of Citrate/Gold Nanoparticles on Human Dermal Fibroblasts. *Small*, **2**(6), 766 (2006). 2, 25
- [11] E. E. Connor, J. Mwamuka, A. Gole, C. J. Murphy and M. D. Wyatt. Gold Nanoparticles Are Taken Up by Human Cells but Do Not Cause Acute Cytotoxicity. *Small*, **1**(3), 325 (2005). 2, 23, 25
- [12] Y. Pan-Bartneck. *Assessing the Toxicity of Gold Nanoparticles in Vitro and In Vivo*. Dissertation, RWTH Aachen University (2010). 2, 3, 34, 62, 70, 126, 141
- [13] A. Nel, T. Xia, L. Maedler and N. Li. Toxic Potential of Materials at the Nanolevel. *Science*, **311**, 622 (2006). 3, 26, 38

- [14] G. Schmid, S. Roberto, H. Fuchs, R. Waser and V. Vogel. *Nanotechnology*. Nanotechnology, VCH. John Wiley & Sons Inc (2009). 5
- [15] M.-C. Daniel and D. Astruc. Gold Nanoparticles: Assembly, Supramolecular Chemistry, Quantum-Size-Related Properties, and Applications toward Biology, Catalysis, and Nanotechnology. *Chemical Reviews*, **104**(1), 293 (2004). 5, 8, 11
- [16] G. Schmid. *Clusters and Colloids - From theory to application*. VCH (1994). 5, 6
- [17] G. Schmid and B. Corain. Nanoparticulated Gold: Syntheses, Structures, Electronics, and Reactivities. *Eur. J. Inorg. Chem.*, 3081 (2008). 6, 17
- [18] R. Jin, Y. Zhu and H. Qian. Quantum-Sized Gold Nanoclusters: Bridging the Gap between Organometallics and Nanocrystals. *Chemistry - A European Journal*, **17**(24), 6584 (2011). 6
- [19] F. Wen, U. Englert, B. Gutrath and U. Simon. Crystal Structure, Electrochemical and Optical Properties of $[\text{Au}_9(\text{PPh}_3)_8](\text{NO}_3)_3$. *European Journal of Inorganic Chemistry*, **2008**(1), 106 (2008). 7, 34
- [20] G. Mie. Beiträge zur Optik trüber Medien, speziell kolloidaler Metallösungen. *Ann. Phys.*, **25**, 377 (1908). 7
- [21] K. L. Kelly, E. Coronado, L. L. Zhao, and G. C. Schatz. The Optical Properties of Metal Nanoparticles: The Influence of Size, Shape, and Dielectric Environment. *J. Phys. Chem. B*, **107**(3), 668 (2003). 7
- [22] T. Huang and R. W. Murray. Visible Luminescence of Water-Soluble Monolayer-Protected Gold Clusters. *The Journal of Physical Chemistry B*, **105**(50), 12498 (2001). 7
- [23] T. Tsukuda, H. Tsunoyama and H. Sakurai. Aerobic Oxidations Catalyzed by Colloidal Nanogold. *Chemistry - An Asian Journal*, **6**(3), 736 (2011). 7
- [24] C. D. Pina, E. Falletta, L. Prati and M. Rossi. Selective oxidation using gold. *Chem. Soc. Rev.*, **37**, 2077 (2008). 7
- [25] C. D. Pina, E. Falletta and M. Rossi. Update on selective oxidation using gold. *Chem. Soc. Rev.*, **41**, 350 (2012). 7
- [26] Y. Gao, N. Shao, Y. Pei, Z. Chen and X. C. Zeng. Catalytic Activities of Subnanometer Gold Clusters (Au_{16} - Au_{18} , Au_{20} , and Au_{27} - Au_{35}) for CO Oxidation. *ACS Nano*, **5**(10), 7818 (2011). 7
- [27] M. Haruta. Catalysis of Gold Nanoparticles Deposited on Metal Oxides. *CATTECH*, **6**, 102 (2002). 8
- [28] H. Tsunoyama, N. Ichikuni, H. Sakurai and T. Tsukuda. Effect of Electronic Structures of Au Clusters Stabilized by Poly(N-vinyl-2-pyrrolidone) on Aerobic Oxidation Catalysis. *Journal of the American Chemical Society*, **131**(20), 7086 (2009). 8

-
- [29] M. Turner, V. B. Golovko, O. P. H. Vaughan, P. Abdulkin, A. Berenguer-Murcia, M. S. Tikhov, B. F. G. Johnson and R. M. Lambert. Selective oxidation with dioxygen by gold nanoparticle catalysts derived from 55-atom clusters. *Nature*, **454**, 981 (2008). 8, 50
- [30] Y. Zhu, H. Qian, B. Drake and R. Jin. Atomically Precise Au₂₅(SR)₁₈ Nanoparticles as Catalysts for the Selective Hydrogenation of α,β -Unsaturated Ketones and Aldehydes. *Angewandte Chemie International Edition*, **49**(7), 1295 (2010). 8
- [31] F. E. Kruis, H. Fissan and A. Peled. Synthesis of NPs in the gas phase for electronic, optical and magnetic applications-a review. *J. Aerosol Sci.*, **29**(5-6), 511 (1998). 8
- [32] J. Turkevitch, P. C. Stevenson and J. Hillier. A study of the nucleation and growth processes in the synthesis of colloidal gold. *Discuss. Faraday Soc.*, **11**, 55 (1951). 9, 33, 131
- [33] G. Schmid, R. Pfeil, R. Boese, F. Bandermann, S. Meyer, G. H. M. Calis and J. W. A. van der Velden. Au₅₅[P(C₆H₅)₃]₁₂Cl₆ - ein Goldcluster ungewöhnlicher Grösse. *Chemische Berichte*, **114**, 3634 (1981). 9, 18, 33, 129
- [34] G. Schmid, N. Klein, L. Korste, U. Kreibitz and D. Schönauer. Large transition metal clusters VI. Ligand exchange reactions on Au₅₅(PPh₃)₁₂Cl₆. The formation of a water soluble Au₅₅ cluster. *Polyhedron*, **7**(8), 605 (1988). 9, 33, 34, 130
- [35] M. Brust, M. Walker, D. Bethell, D. J. Schiffrin and R. Whyman. Synthesis of Thiol-derivatised Gold Nanoparticles in a Two-phase Liquid-Liquid System. *J. Chem. Soc., Chem. Commun.*, 801 (1994). 9
- [36] M. Brust, J. Fink, D. Bethell, D. J. Schiffrin and C. Kiely. Synthesis and Reactions of Functionalised Gold Nanoparticles. *J. Chem. Soc., Chem. Commun.*, 1655 (1995). 9, 20
- [37] D. V. Leff, L. Brandt and J. R. Heath. Synthesis and Characterization of Hydrophobic, Organically-Soluble Gold Nanocrystals Functionalized with Primary Amines. *Langmuir*, **12**(20), 4723 (1996). 9, 14, 35
- [38] T. G. Schaaff, G. Knight, M. N. Shafigullin, R. F. Borkman and R. L. Whetten. Isolation and Selected Properties of a 10.4 kDa Gold:Glutathione Cluster Compound. *The Journal of Physical Chemistry B*, **102**(52), 10643 (1998). 10
- [39] Y. Negishi, Y. Takasugi, S. Sato, H. Yao, K. Kimura and T. Tsukuda. Magic-Numbered Au_n Clusters Protected by Glutathione Monolayers (n = 18, 21, 25, 28, 32, 39): Isolation and Spectroscopic Characterization. *Journal of the American Chemical Society*, **126**(21), 6518 (2004). 10, 39, 131
- [40] R. A. Sperling and W. J. Parak. Surface modification, functionalization and bioconjugation of colloidal inorganic nanoparticles. *Phil. Trans. R. Soc. A.*, **368**, 1333 (2010). 10, 12, 29
-

- [41] J. C. Love, L. A. Estroff, J. K. Kriebel, R. G. Nuzzo and G. M. Whitesides. Self-Assembled Monolayers of Thiolates on Metals as a Form of Nanotechnology. *Chemical Reviews*, **105**(4), 1103 (2005). 10
- [42] L. A. Porter, D. Ji, S. L. Westcott, M. Graupe, R. S. Czernuszewicz, N. J. Halas and T. R. Lee. Gold and Silver Nanoparticles Functionalized by the Adsorption of Dialkyl Disulfides. *Langmuir*, **14**(26), 7378 (1998). 10
- [43] X.-M. Li, M. R. d. Jong, K. Inoue, S. Shinkai, J. Huskens and D. N. Reinhoudt. Formation of gold colloids using thioether derivatives as stabilizing ligands. *J. Mater. Chem.*, **11**, 1919 (2001). 10
- [44] H. Häkkinen, M. Walter and H. Grönbeck. Divide and Protect: Capping Gold Nanoparticles with Molecular Gold-Thiolate Rings. *J. Phys. Chem. B*, **110**, 9927 (2006). 10, 39, 67
- [45] P. Selvakannan, S. Mandal, S. Phadtare, R. Pasricha and M. Sastry. Capping of Gold Nanoparticles by the Amino Acid Lysine Renders Them Water-Dispersible. *Langmuir*, **19**(8), 3545 (2003). 11
- [46] S. Perumal, A. Hofmann, N. Scholz, E. Rühl and C. Graf. Kinetics Study of the Binding of Multivalent Ligands on Size-Selected Gold Nanoparticles. *Langmuir*, **27**(8), 4456 (2011). 11
- [47] L.-O. Srisombat, J.-S. Park, S. Zhang and T. R. Lee. Preparation, Characterization, and Chemical Stability of Gold Nanoparticles Coated with Mono-, Bis-, and Tris-Chelating Alkanethiols. *Langmuir*, **24**(15), 7750 (2008). 11, 89
- [48] M. Tamura and H. Fujihara. Chiral Bisphosphine BINAP-Stabilized Gold and Palladium Nanoparticles with Small Size and Their Palladium Nanoparticle-Catalyzed Asymmetric Reaction. *Journal of the American Chemical Society*, **125**(51), 15742 (2003). 11
- [49] Y. Yanagimoto, Y. Negishi, H. Fujihara and T. Tsukuda. Chiroptical Activity of BINAP-Stabilized Undecagold Clusters. *The Journal of Physical Chemistry B*, **110**(24), 11611 (2006). 12
- [50] D. E. Bergeron, O. Coskuner, J. W. Hudgens and C. A. Gonzalez. Ligand exchange reactions in the formation of diphosphine-protected gold clusters. *Journal of Physical Chemistry C*, **112**(33), 12808 (2008). 12
- [51] M. J. Hostetler, A. C. Templeton and R. W. Murray. Dynamics of Place-Exchange Reactions on Monolayer-Protected Gold Cluster Molecules. *Langmuir*, **15**(11), 3782 (1999). 12
- [52] A. Caragheorgheopol and V. Chechik. Mechanistic aspects of ligand exchange in Au nanoparticles. *Phys. Chem. Chem. Phys.*, **10**, 5029 (2008). 12

-
- [53] J. A. Jamison, K. M. Krueger, C. T. Yavuz, J. T. Mayo, D. LeCrone, J. J. Redden and V. L. Colvin. Size-Dependent Sedimentation Properties of Nanocrystals. *ACS Nano*, **2**(2), 311 (2008). 13
- [54] C.-L. Wang, M. Fang, S.-H. Xu and Y.-P. Cui. Salts-Based Size-Selective Precipitation: Toward Mass Precipitation of Aqueous Nanoparticles. *Langmuir*, **26**(2), 633 (2010). 13
- [55] G.-T. Wei and F.-K. Liu. Separation of Nanometer Gold Particles by Size Exclusion Chromatography. *Journal of Chromatography A*, **836**(2), 253 (1999). 13
- [56] S. Gupta, H. Andresen, J. E. Ghadiali and M. M. Stevens. Kinase-Actuated Immunoaggregation of Peptide-Conjugated Gold Nanoparticles. *Small*, **6**(14), 1509 (2010). 15
- [57] D. B. Williams and C. B. Carter. *Transmission Electron Microscopy. Part 1: Basics*. Springer (2009). Second Edition. 15
- [58] S. L. Flegler, J. W. Heckman jr. and K. L. Klomparens. *Elektronenmikroskopie*. Spektrum Akademischer Verlag (1995). 15
- [59] R. Erni, M. D. Rossell, C. Kisielowski and U. Dahmen. Atomic-Resolution Imaging with a Sub-50-pm Electron Probe. *Phys. Rev. Lett.*, **102**, 096101 (2009). 15
- [60] W. D. Pyrz and D. J. Buttrey. Particle Size Determination Using TEM: A Discussion of Image Acquisition and Analysis for the Novice Microscopist. *Langmuir*, **24**(20), 11350 (2008). 16
- [61] Z. Y. Li, N. P. Young, M. D. Vece, S. Palomba, R. E. Palmer, A. L. Bleloch, B. C. Curley, R. L. Johnston, J. Jiang and J. Yuan. Three-dimensional atomic-scale structure of size-selected gold nanoclusters. *Nature*, **451**, 46 (2008). 16
- [62] G. Schmid, R. Pugin, T. Sawitowski, U. Simon and B. Marler. Transmission electron microscopic and small angle X-ray diffraction investigations of Au₅₅(PPh₃)₁₂Cl₆ microcrystals. *Chem. Commun.*, 1303 (1999). 16
- [63] P. D. Jadzinsky, G. Calero, C. J. Ackerson, D. A. Bushnell and R. D. Kornberg. Structure of a Thiol Monolayer-Protected Gold Nanoparticle at 1.1 Å Resolution. *Science*, **318**(5849), 430 (2007). 17
- [64] B. L. Berne and R. Pecora. *Dynamic Light Scattering - With Applications to Chemistry, Biology and Physics*. Wiley (2000). Dover edition. 17
- [65] R. W. O'Brien and L. R. White. Electrophoretic mobility of a spherical colloidal particle. *J. Chem. Soc., Faraday Trans. 2*, **74**, 1607 (1978). 17
- [66] B. Khlebtsov and N. Khlebtsov. On the measurement of gold nanoparticle sizes by the dynamic light scattering method. *Colloid Journal*, **73**, 118 (2011). 18
-

- [67] M. Yu, C. Zhou, J. Liu, J. D. Hankins and J. Zheng. Luminescent Gold Nanoparticles with pH-Dependent Membrane Adsorption. *Journal of the American Chemical Society*, **133**(29), 11014 (2011). 18
- [68] A. Chompoosor, G. Han and V. M. Rotello. Charge Dependence of Ligand Release and Monolayer Stability of Gold Nanoparticles by Biogenic Thiols. *Bioconjugate Chemistry*, **19**(7), 1342 (2008). 18, 31
- [69] H. Jans, X. Liu, L. Austin, G. Maes and Q. Huo. Dynamic Light Scattering as a Powerful Tool for Gold Nanoparticle Bioconjugation and Biomolecular Binding Studies. *Analytical Chemistry*, **81**(22), 9425 (2009). 18
- [70] D. D. Laws, H.-M. L. Bitter and A. Jerschow. Solid-State NMR Spectroscopic Methods in Chemistry. *Angewandte Chemie International Edition*, **41**(17), 3096 (2002). 19
- [71] G. Schmid. Developments in Transition Metal Cluster Chemistry - The Way to Large Clusters -. *Structure and Bonding*, **62**, 51 (1985). 19, 65
- [72] R. Sharma, G. P. Holland, V. C. Solomon, H. Zimmermann, S. Schiftenhaus, S. A. Amin, D. A. Buttry and J. L. Yarger. NMR Characterization of Ligand Binding and Exchange Dynamics in Triphenylphosphine-Capped Gold Nanoparticles. *The Journal of Physical Chemistry C*, **113**(37), 16387 (2009). 19, 62
- [73] N. Schaeffer, B. Tan, C. Dickinson, M. J. Rosseinsky, A. Laromaine, D. W. McComb, M. M. Stevens, Y. Wang, L. Petit, C. Barentin, D. G. Spiller, A. I. Cooper and R. Levy. Fluorescent or not? Size-dependent fluorescence switching for polymer-stabilized gold clusters in the 1.1-1.7 nm size range. *Chem. Commun.*, 3986 (2008). 20
- [74] E. Dulkeith, A. C. Morteani, T. Niedereichholz, T. A. Klar, J. Feldmann, S. A. Levi, F. C. J. M. van Veggel, D. N. Reinhoudt, M. Möller and D. I. Gittins. Fluorescence Quenching of Dye Molecules near Gold Nanoparticles: Radiative and Nonradiative Effects. *Phys. Rev. Lett.*, **89**, 203002 (2002). 20, 31, 107
- [75] D. S. Seferos, D. A. Giljohann, N. L. Rosi and C. A. Mirkin. Locked Nucleic Acid-Nanoparticle Conjugates. *ChemBioChem*, **8**(11), 1230 (2007). 20
- [76] S. D. Techane, L. J. Gamble and D. G. Castner. X-ray photoelectron spectroscopy characterization of gold nanoparticles functionalized with amine-terminated alkanethiols. *Bioninterphases*, **6**(3), 98 (2011). 21
- [77] L. J. Berliner. *In Vivo EPR (ESR). Theory and Applications*. Kluwer (2003). Biological Magnetic Resonance - Volume 18. 21
- [78] Z. Zhang, A. Berg, H. Levanon, R. W. Fessenden and D. Meisel. On the Interactions of Free Radicals with Gold Nanoparticles. *Journal of the American Chemical Society*, **125**(26), 7959 (2003). 21, 50
- [79] A. Alkilany and C. Murphy. Toxicity and cellular uptake of gold nanoparticles: what we have learned so far? *Journal of Nanoparticle Research*, **12**, 2313 (2010). 22

-
- [80] Y.-F. Li and C. Chen. Fate and Toxicity of Metallic and Metal-Containing Nanoparticles for Biomedical Applications. *Small*, **7**(21), 2965 (2011). 22
- [81] M. Mahmoudi, K. Azadmanesh, M. A. Shokrgozar, W. S. Journeay and S. Laurent. Effect of Nanoparticles on the Cell Life Cycle. *Chemical Reviews*, **111**(5), 3407 (2011). 23
- [82] A. Verma and F. Stellacci. Effect of Surface Properties on Nanoparticle-Cell Interactions. *Small*, **6**(1), 12 (2010). 23
- [83] B. D. Chithrani, A. A. Ghazani and W. C. W. Chan. Determining the Size and Shape Dependence of Gold Nanoparticle Uptake into Mammalian Cells. *Nano Letters*, **6**(4), 662 (2006). 23
- [84] E. Oh, J. B. Delehanty, K. E. Sapsford, K. Susumu, R. Goswami, J. B. Blanco-Canosa, P. E. Dawson, J. Granek, M. Shoff, Q. Zhang, P. L. Goering, A. Huston and I. L. Medintz. Cellular Uptake and Fate of PEGylated Gold Nanoparticles Is Dependent on Both Cell-Penetration Peptides and Particle Size. *ACS Nano*, **5**(8), 6434 (2011). 23
- [85] Y. Shan, S. Ma, L. Nie, X. Shang, X. Hao, Z. Tang and H. Wang. Size-dependent endocytosis of single gold nanoparticles. *Chem. Commun.*, **47**, 8091 (2011). 24
- [86] A. Verma, O. Uzun, Y. Hu, Y. Hu, H.-S. Han, N. Watson, S. Chen, D. J. Irvine and F. Stellacci. Surface-structure-regulated cell-membrane penetration by monolayer-protected nanoparticles. *Nature Mater.*, **7**, 588 (2008). 24
- [87] C. Röcker, M. Pötzl, F. Zhang, W. J. Parak and G. U. Nienhaus. A quantitative fluorescence study of protein monolayer formation on colloidal nanoparticles. *Nature Nanotechnol.*, **4**, 577 (2009). 24
- [88] S. H. De Paoli Lacerda, J. J. Park, C. Meuse, D. Pristinski, M. L. Becker, A. Karim and J. F. Douglas. Interaction of Gold Nanoparticles with Common Human Blood Proteins. *ACS Nano*, **4**(1), 365 (2010). 24
- [89] D. A. Giljohann, D. S. Seferos, P. C. Patel, J. E. Millstone, N. L. Rosi and C. A. Mirkin. Oligonucleotide Loading Determines Cellular Uptake of DNA-Modified Gold Nanoparticles. *Nano Letters*, **7**(12), 3818 (2007). 24
- [90] N. Khlebtsov and L. Dykman. Biodistribution and toxicity of engineered gold nanoparticles: a review of in vitro and in vivo studies. *Chem. Soc. Rev.*, **40**, 1647 (2011). 24
- [91] C. M. Goodman, C. D. McCusker, T. Yilmaz and V. M. Rotello. Toxicity of Gold Nanoparticles Functionalized with Cationic and Anionic Side Chains. *Bioconjugate Chemistry*, **15**, 897 (2004). 25, 80, 85
- [92] J. Ponti, R. Colognato, F. Franchini, S. Gioria, F. Simonelli, K. Abbas, C. Ubaldi, C. J. Kirkpatrick, U. Holzwarth and F. Rossi. A quantitative in vitro approach to study the intracellular fate of gold nanoparticles: from synthesis to cytotoxicity. *Nanotoxicology*, **3**(4), 296 (2009). 25
-

- [93] J. Li, L. Zou, D. Hartono, C.-N. Ong, B.-H. Bay and L.-Y. Lanry Yung. Gold Nanoparticles Induce Oxidative Damage in Lung Fibroblasts In Vitro. *Advanced Materials*, **20**(1), 138 (2008). 26
- [94] H. Y. Jia, Y. Liu, X. J. Zhang, L. Han, L. B. Du, Q. Tian and Y. C. Xu. Potential Oxidative Stress of Gold Nanoparticles by Induced-NO Releasing in Serum. *Journal of the American Chemical Society*, **131**(1), 40 (2009). 26
- [95] A. Chompoosor, K. Saha, P. S. Ghosh, D. J. Macarthy, O. R. Miranda, Z.-J. Zhu, K. F. Arcaro and V. M. Rotello. The Role of Surface Functionality on Acute Cytotoxicity, ROS Generation and DNA Damage by Cationic Gold Nanoparticles. *Small*, **6**(20), 2246 (2010). 26
- [96] R. Landsiedel, M. D. Kapp, M. Schulz, K. Wiench and F. Oesch. Genotoxicity investigations on nanomaterials: Methods, preparation and characterization of test material, potential artifacts and limitations-Many questions, some answers. *Mutation Res./Rev. in Mutation Res.*, **681**(2-3), 241 (2009). 27
- [97] M. M. Greenberg, Z. Hantosi, C. J. Wiederholt and C. D. Rithner. Studies on N4-(2-deoxy-D-pentofuranosyl)-4,6-diamino-5-formamidopyrimidine (Fapy.dA) and N6-(2-deoxy-D-pentofuranosyl)-6-diamino-5-formamido-4-hydroxypyrimidine (Fapy.dG). *Biochemistry*, **40**(51), 15856 (2001). 27
- [98] E. J. Petersen and B. C. Nelson. Mechanisms and measurements of nanomaterial-induced oxidative damage to DNA. *Analytical and Bioanalytical Chemistry*, **398**(2), 613 (2010). 27, 55
- [99] M. Dizdaroglu, P. Jaruga, M. Birincioglu and H. Rodriguez. Free radical-induced damage to DNA: mechanisms and measurement. *Free Radical Biology and Medicine*, **32**(11), 1102 (2002). 27, 57
- [100] J. Serrano, C. M. Palmeira, K. B. Wallace and D. W. Kuehl. Determination of 8-Hydroxydeoxyguanosine in Biological Tissue by Liquid Chromatography/Electrospray Ionization-Mass Spectrometry/Mass Spectrometry. *Rapid Communications in Mass Spectrometry*, **10**(14), 1789 (1996). 27
- [101] W. Redfern, L. Carlsson, A. Davis, W. Lynch, I. MacKenzie, S. Palethorpe, P. Siegl, I. Strang, A. Sullivan, R. Wallis, A. Camm and T. Hammond. Relationships between preclinical cardiac electrophysiology, clinical QT interval prolongation and torsade de pointes for a broad range of drugs: evidence for a provisional safety margin in drug development. *Cardiovasc. Res.*, **58**, 32 (2003). 28
- [102] M. C. Sanguinetti and M. Tristani-Firouzi. hERG potassium channels and cardiac arrhythmia. *Nature*, **440**, 463 (2006). 28
- [103] J. S. Mitcheson. Drug binding to HERG channels: evidence for a 'non-aromatic' binding site for fluvoxamine. *Br. J. Pharmacol.*, **139**(5), 883 (2003). 28

-
- [104] L. K. Liem, J. M. Simard, Y. Song and K. Tewari. The Patch Clamp Technique. *Neurosurgery*, **36**(2), 382 (1995). 28
- [105] C. Kirchner, T. Liedl, S. Kudera, T. Pellegrino, A. Muñoz Javier, H. E. Gaub, S. Stölzle, N. Fertig and W. J. Parak. Cytotoxicity of Colloidal CdSe and CdSe/ZnS Nanoparticles. *Nano Letters*, **5**(2), 331 (2005). 29
- [106] J. A. Barreto, W. O'Malley, M. Kubeil, B. Graham, H. Stephan and L. Spiccia. Nanomaterials: Applications in Cancer Imaging and Therapy. *Advanced Materials*, **23**(12), H18 (2011). 29, 117
- [107] Y. Liu, M. K. Shipton, J. Ryan, E. D. Kaufman, S. Franzen and D. L. Feldheim. Synthesis, Stability, and Cellular Internalization of Gold Nanoparticles Containing Mixed Peptide-Poly(ethylene glycol) Monolayers. *Anal. Chem.*, **79**, 2221 (2007). 30
- [108] J. M. de la Fuente and C. C. Berry. Tat Peptide as an Efficient Molecule to Translocate Gold Nanoparticles into the Cell Nucleus. *Bioconjugate Chem.*, **16**, 1176 (2005). 30
- [109] P. Nativio, I. A. Prior and M. Brust. Uptake and Intracellular Fate of Surface-Modified Gold Nanoparticles. *ACS Nano*, **2**(8), 1639 (2008). 30
- [110] A. Anastasi, V. Erspamer and M. Bucci. Isolation and Structure of Bombesin and Alytesin, two Analogous Active Peptides from the Skin of the European Amphibians *Bombina* and *Alytes*. *Experientia*, **27**(2), 166 (1971). 30
- [111] E. Podstawka. Investigation of Molecular Structure of Bombesin and Its Modified Analogues Nonadsorbed and Adsorbed on Electrochemically Roughened Silver Surface. *Biopolymers*, **89**(6), 506 (2007). 30, 100
- [112] H. Zhang, J. Schuhmacher, B. Waser, D. Wild, M. Eisenhut, J. Reubi and H. Maecke. DOTA-PESIN, a DOTA-conjugated bombesin derivative designed for the imaging and targeted radionuclide treatment of bombesin receptor-positive tumours. *European Journal of Nuclear Medicine and Molecular Imaging*, **34**, 1198 (2007). 30
- [113] N. Chanda, V. Kattumuri, R. Shukla, A. Zambre, K. Katti, A. Upendran, R. R. Kulkarni, P. Kan, G. M. Fent, S. W. Casteel, C. J. Smith, E. Boote, J. D. Robertson, C. Cutler, J. R. Lever, K. V. Katti and R. Kannan. Bombesin functionalized gold nanoparticles show in vitro and in vivo cancer receptor specificity. *Proceedings of the National Academy of Sciences*, **107**(19), 8760 (2010). 30
- [114] L. Hosta-Rigau, I. Olmedo, J. Arbiol, L. J. Cruz, M. J. Kogan and F. Albericio. Multifunctionalized Gold Nanoparticles with Peptides Targeted to Gastrin-Releasing Peptide Receptor of a Tumor Cell Line. *Bioconjugate Chemistry*, **21**(6), 1070 (2010). 30
- [115] G. Schmid and A. Lehnert. The Complexation of Gold Colloids. *Angewandte Chemie International Edition*, **28**(6), 780 (1989). 34, 131
-

- [116] C. F. Shaw. Gold-Based Therapeutic Agents. *Chemical Reviews*, **99**(9), 2589 (1999). 36
- [117] Y. Pan, S. Neuss, A. Leifert, M. Fischler, F. Wen, U. Simon, G. Schmid, W. Brandau and W. Jahnen-Dechent. Size-Dependent Cytotoxicity of Gold Nanoparticles. *Small*, **3**(11), 1941 (2007). 37, 43
- [118] J. Broda. *Synthese und Untersuchung der Zytotoxizität wasserlöslicher TPPMS/TPPTS-stabilisierter Goldnanopartikel*. Diploma thesis, RWTH Aachen University (2010). 36
- [119] S. Linse, C. Cabaleiro-Lago, W.-F. Xue, I. Lynch, S. Lindman, E. Thulin, S. E. Radford and K. A. Dawson. Nucleation of protein fibrillation by nanoparticles. *Proc Natl Acad Sci USA*, **104**(21), 8691 (2007). 38
- [120] Y. Negishi, K. Nobusada and T. Tsukuda. Glutathione-Protected Gold Clusters Revisited: Bridging the Gap between Gold(I)-Thiolate Complexes and Thiolate-Protected Gold Nanocrystals. *Journal of the American Chemical Society*, **127**(14), 5261 (2005). 40
- [121] U. Reinscheid. Accelerated Hydrolysis of Aspirin Using Alternating Magnetic Fields. *Nanoscale Research Letters*, **4**(8), 854 (2009). 42
- [122] H. Tada, T. Soejima, S. Ito and H. Kobayashi. Photoinduced Desorption of Sulfur from Gold Nanoparticles Loaded on Metal Oxide Surfaces. *Journal of the American Chemical Society*, **126**(49), 15952 (2004). 42
- [123] Y. Pan, A. Leifert, D. Ruau, S. Neuss, J. Bornemann, G. Schmid, W. Brandau, U. Simon and W. Jahnen-Dechent. Gold Nanoparticles of Diameter 1.4 nm Trigger Necrosis by Oxidative Stress and Mitochondrial Damage. *Small*, **5**(18), 2067 (2009). 46, 47, 49
- [124] M. Liu, V. Bandaru, J. P. Bond, P. Jaruga, X. Zhao, P. P. Christov, C. J. Burrows, C. J. Rizzo, M. Dizdaroglu and S. S. Wallace. The mouse ortholog of NEIL3 is a functional DNA glycosylase in vitro and in vivo. *Proceedings of the National Academy of Sciences*, **107**(11), 4925 (2010). 60
- [125] P. V. AshaRani, G. Low Kah Mun, M. P. Hande and S. Valiyaveetil. Cytotoxicity and Genotoxicity of Silver Nanoparticles in Human Cells. *ACS Nano*, **3**(2), 279 (2009). 62
- [126] G. H. Woehrle, L. O. Brown and J. E. Hutchison. Thiol-Functionalized, 1.5-nm Gold Nanoparticles through Ligand Exchange Reactions: Scope and Mechanism of Ligand Exchange. *Journal of the American Chemical Society*, **127**(7), 2172 (2005). 62
- [127] J. T. Milnes, O. Crociani, A. Arcangeli, J. C. Hancox and H. J. Witchel. Blockade of HERG potassium currents by fluvoxamine: incomplete attenuation by S6 mutations at F656 or Y652. *British Journal of Pharmacology*, **139**(5), 887 (2003). 70

-
- [128] C.-C. Kuo, W.-Y. Chen and Y.-C. Yang. Block of Tetrodotoxin-resistant Na^+ Channel Pore by Multivalent Cations. *J. Gen. Physiol.*, **124**(1), 27 (2004). 77, 78
- [129] S. Brownstein and A. E. Stillman. Proton Resonance Shifts of Acids in Liquid Sulfur Dioxide. *Journal of Physical Chemistry*, **63**(12), 2061 (1959). 80
- [130] J. P. Guthrie. Hydrolysis of esters of oxy acids: pK_a values for strong acids; Brønsted relationship for attack of water at methyl; free energies of hydrolysis of esters of oxy acids; and a linear relationship between free energy of hydrolysis and pK_a holding over a range of 20 pK units. *Canadian Journal of Chemistry*, **56**(17), 2342 (1978). 80
- [131] A. Hessler, O. Stelzer, H. Dibowski, K. Worm and F. P. Schmidtchen. Water Soluble Cationic Phosphine Ligands Containing m-Guanidinium Phenyl Moieties. Syntheses and Applications in Aqueous Heck Type Reactions. *The Journal of Organic Chemistry*, **62**(8), 2362 (1997). 81
- [132] C. Daguenet, R. Scopelliti and P. J. Dyson. Mechanistic Investigations on the Hydrogenation of Alkenes Using Ruthenium(II)-arene Diphosphine Complexes. *Organometallics*, **23**(21), 4849 (2004). 86
- [133] W. W. Weare, S. M. Reed, M. G. Warner and J. E. Hutchison. Improved Synthesis of Small ($d_{\text{CORE}} \approx 1.5 \text{ nm}$) Phosphine-Stabilized Gold Nanoparticles. *Journal of the American Chemical Society*, **122**(51), 12890 (2000). 90
- [134] N. L. Rosi, D. A. Giljohann, C. S. Thaxton, A. K. R. Lytton-Jean, M. S. Han and C. A. Mirkin. Oligonucleotide-Modified Gold Nanoparticles for Intracellular Gene Regulation. *Science*, **312**(5776), 1027 (2006). 93
- [135] F. Schiefer. *Synthese wasserlöslicher Diphosphin-stabilisierter Goldnanopartikel*. Diploma thesis, RWTH Aachen University (2010). 94
- [136] G. Löffler and P. E. Petrides. *Physiologische Chemie*. Springer-Verlag (1990). 4. Auflage, 1. korrigierter Nachdruck. 100
- [137] M. Semmler-Behnke, W. G. Kreyling, J. Lipka, S. Fertsch, A. Wenk, S. Takenaka, G. Schmid and W. Brandau. Biodistribution of 1.4- and 18-nm Gold Particles in Rats. *Small*, **4**(12), 2108 (2008). 116
- [138] S. Hirn, M. Semmler-Behnke, C. Schleh, A. Wenk, J. Lipka, M. Schäffler, S. Takenaka, W. Möller, G. Schmid, U. Simon and W. G. Kreyling. Particle size-dependent and surface charge-dependent biodistribution of gold nanoparticles after intravenous administration. *European Journal of Pharmaceutics and Biopharmaceutics*, **77**(3), 407 (2011). 116
- [139] C. Schleh, M. Semmler-Behnke, J. Lipka, A. Wenk, S. Hirn, M. Schäffler, G. Schmid, U. Simon and W. G. Kreyling. Size and surface charge of gold nanoparticles determine absorption across intestinal barriers and accumulation in secondary target organs after oral administration. *Nanotoxicology* (2011). Doi: 10.3109/17435390.2011.552811. 116
-

List of Figures

1.1	Control parameters for the cytotoxicity evaluation of AuNPs.	3
3.1	UV/Vis spectra of Au0.8MS, Au1.4MS and Au15MS.	34
3.2	STEM micrographs of 1.4 and 15 nm sized AuNPs.	35
3.3	Analytics of Au5.6MS.	35
3.4	IC ₅₀ values of different AuNPs (log. growth phase).	37
3.5	Analytics of Au1.1GSH.	40
3.6	IR spectra of Au1.4GSH and GSH.	41
3.7	STEM micrograph of Au1.4GSH.	41
3.8	Necrosis/Apoptosis investigation of Au1.2MS and Au1.4MS.	43
3.9	Gene chip results of Au1.4MS and Au15MS.	46
3.10	CM-H ₂ DCFDA and its fluorescent derivative.	47
3.11	Flow cytometry results after staining with CM-H ₂ DCFDA.	47
3.12	Four anti-oxidants tested for their inhibition potential of Au1.4MS toxicity. .	48
3.13	Effect of diverse anti-oxidants towards cytotoxicity of Au1.4MS.	49
3.14	Possible pathways related to oxidative stress induced by AuNPs.	51
3.15	Amino-TEMPO and Oxo-TEMPO.	51
3.16	EPR spectra of Amino-TEMPO solutions with Au15Citrate.	52
3.17	Time effect on EPR spectrum of Au15Citrate with Amino-TEMPO.	53
3.18	EPR spectra of samples of Amino-TEMPO with different AuNP species. . .	54
3.19	Scheme of sample preparation for genotoxicity studies.	56
3.20	DNA oxidation products (lesions) investigated at NIST.	57
3.21	Lesion concentrations from the first sample set (HeLa cells).	58
3.22	Second sample set (extracted DNA treated with AuNPs).	59
3.23	³¹ P-NMR spectrum of Au1.4MS in H ₂ O.	63
3.24	³¹ P-NMR spectrum of Au1.4MS after column chromatography.	64
3.25	Chemical structures of TPPMS, TPPMS=O and TPPMS-Au(I)-Cl.	64
3.26	³¹ P-NMR spectra of Au1.4MS with subsequent TPPMS addition.	66
3.27	Chemical shifts δ of the ³¹ P-NMR spectra of Au1.4MS plus TPPMS. . . .	66
3.28	Solid state ³¹ P-NMR spectra of Au1.4MS and TPPMS-Au(I)-Cl.	68

3.29	Dialysis experiment of Au1.4MS.	69
3.30	Schematic patch clamp setup.	70
3.31	Effect of Au1.4MS on hERG channel.	71
3.32	Concentration dependent response of hERG towards Au1.4MS	72
3.33	HERG response towards TPPMS.	73
3.34	Effect of Au1.4MS plus TPPMS on hERG.	74
3.35	Effect of subsequent TPPMS and Au1.4MS perfusion on hERG.	74
3.36	Effect of Au1.4MS plus GSH on hERG.	75
3.37	Effect of Au1.4MS plus FCS on hERG.	76
3.38	Thiol-stabilized AuNPs in patch clamp experiments.	76
3.39	Patch clamp experiment with a $\text{Na}_V1.5$ channel expressing CHO-K1 cell exposed to Au1.4MS.	78
3.40	Simulations of hERG in interaction with Au1.4MS with varying numbers of TPPMS ligands.	80
3.41	Reaction scheme of the Pd-catalyzed coupling reaction of diphenylphosphine with a iodo aryl species.	81
3.42	UV/Vis spectrum of Au1.4TPPMCMA.	83
3.43	STEM micrograph of Au1.4TPPMCMA.	83
3.44	UV/Vis spectrum of Au1.4TPPMC.	84
3.45	STEM micrograph of Au1.4TPPMC.	84
3.46	DPPETS, DPPPTS and DPPBTS.	86
3.47	Reaction scheme of the sulfonation reaction of diphosphines.	86
3.48	UV/Vis spectrum of Au1.4DPPETS.	87
3.49	STEM micrograph of Au1.4DPPETS.	88
3.50	Oxidative degradation of AuNPs in the presence of KCN.	89
3.51	Time-dependent plot from the UV/Vis spectra of the KCN degradation of Au1.4DPPETS and Au1.4MS.	90
3.52	DSC measurements of Au1.4DPPETS and Au1.4MS.	91
3.53	STEM micrograph of Au1.4DPPBTS.	92
3.54	Stability test of Au1.4DPPBTS with increasing concentrations of DTT.	93
3.55	UV/Vis spectra of Au13DPPETS, Au11DPPPTS and Au12DPPBTS.	95
3.56	STEM micrographs and histograms of DPPXTS gold colloids.	96
3.57	Histograms of DLS measurements (intensity weighted) of Au11Citrate, Au11DPPPTS and Au12DPPBTS.	97
3.58	Plots of time-dependently measured UV/Vis spectra at respective absorbance maxima during KCN degradation of diphosphine-stabilized gold colloids.	97
3.59	Coupling reaction scheme of a cell specific target molecule to Au1.4TPPMC.	98

3.60	EDC/sulfo-NHS coupling reaction of an amine R–NH ₂ , indicating bombesin or (Lys ³)-bombesin, to TPPMC.	99
3.61	DTT ligand exchange reaction with bombesin-functionalized AuNPs.	100
3.62	Bombesin and (Lys ³)-bombesin.	101
3.63	UV/Vis spectra of two batches of Au1.4MS/MC.	102
3.64	STEM micrograph of Au1.4MS/MC.	102
3.65	UV/Vis spectrum of Au1.4MS/MC-(Lys ³)-bombesin.	103
3.66	STEM micrograph of Au1.4MS/MC-(Lys ³)-bombesin.	103
3.67	IR spectra of Au1.4MS/MC and Au1.4MS/MC-(Lys ³)-bombesin.	104
3.68	GeneBLAzer GRPR-NFAT-bla CHO-K1 cells in fluorescence micrographs with Au1.4MS/MC-(Lys ³)-bombesin.	106
3.69	Chemical structure of the fluorophore 5-aminofluorescein.	108
3.70	5-Aminofluorescein, coupled to TPPMC <i>via</i> an amide bond.	108
3.71	UV/Vis spectra of Au1.4MS/MC-Aminofluorescein and 5-aminofluorescein.	109
3.72	STEM micrograph of Au1.4MS/MC-Aminofluorescein.	109
3.73	IR spectra of Au1.4MS/MC-Aminofluorescein and 5-aminofluorescein.	110
3.74	Fluorescence spectra of a Au1.4MS/MC-Aminofluorescein solution before and after reaction with DTT.	111
3.75	Fluorescence spectra of the washing supernatants from the coupling product Au1.4MS/MC-Aminofluorescein.	111

List of Tables

3.1	Results of EA of Au1.4TPPMC.	85
3.2	Results of EA of Au1.4DPPETS.	88
3.3	Results of EA of Au1.4DPPPTS.	91
3.4	Results of EA of Au1.4DPPBTS.	92
3.5	Two-phase ligand exchange reactions on Au1.4TPP.	94
5.1	Chemicals, solvents and suppliers.	119
5.2	AuNP concentrations for EPR spectroscopy.	137
5.3	TPPMS amounts for ^{31}P -NMR analysis.	139

Curriculum Vitae

Persönliche Daten

Name: Leifert

Vorname: Annika

Geburtstag: 18.07.1983

Geburtsort: Münster

Staatsangehörigkeit: deutsch

Qualifikationen

2001: Allgemeine Hochschulreife am Marie-Curie-Gymnasium Düsseldorf

2001 - 2007: Studium der Chemie zur Diplomchemikerin an der RWTH Aachen University

2007: Beginn der Promotion an der RWTH Aachen University